AD/A-002 141

PROJECT FM/CW ADAPTIVE MEASURE

J. E. Rice, et al

GTE Sylvania, Incorporated

Prepared for:

Rome Air Development Center

September 1974

REPORT DOCUMENTATION PAGE		READ INSTRUCTIONS BEFORE COMPLETING FORM
1. REPORT NUMBER RADC-TR-74-243	2. GOVT ACCESSION NO.	3. RECIPIENT'S CATALOG NUMBER AD/A-002141
4. TITLE (and Subtitle) PROJECT FM/CW ADAPTIVE MEASURE		5. TYPE OF REPORT & PERIOD COVERED Final Report 1 May 73 – 1 May 74
		6. PERFORMING ORG. REPORT NUMBER EDL-E214
7. AUTHOR(s) J. E. Rice R. G. Baender		8. CONTRACT OR GRANT NUMBER(s) F30602-73-C-0307
9. PERFORMING ORGANIZATION NAME AND ADDRESS GTE Sylvania, Incorporated Electronic Systems Group-Western Division Mountain View, California 94040		10. PROGRAM ELEMENT, PROJECT, TASK AREA & WORK UNIT NUMBERS PE 62702F JO 673A0151
11. CONTROLLING OFFICE NAME AND ADDRESS Rome Air Development Center/OCSL Griffiss Air Force Base, New York 13441		12. REPORT DATE September 1974
		13. NUMBER OF PAGES 155
14. MONITORING AGENCY NAME & ADDRESS(If different from Controlling Office) Same		15. SECURITY CLASS. (of this report) Unclassified
		15a. DECLASSIFICATION/DOWNGRADING SCHEDULE N/A

16. DISTRIBUTION STATEMENT (of this Report)

Approved for public release. Distribution unlimited.

17. DISTRIBUTION STATEMENT (of the abstract entered in Block 20, if different from Report)

Same

18. SUPPLEMENTARY NOTES

None

19. KEY WORDS (Continue on reverse side if necessary and identify by block number)

Hf Antenna   Broadside Array
Adaptive Arrays   Beamforming Network
Beverage Antenna

20. ABSTRACT (Continue on reverse side if necessary and identify by block number)

This report covers technical investigations and evaluation of system performances as well as the statistical design of large aperture, low sidelobe antenna arrays in the high frequency band of the radio frequency spectrum. The details covered include: (a) measurement and analysis of an existing receive array at Dexter, N.Y.; (b) modification of existing computer software to accept data from the array performance monitor; (c) design, development, and implementation of an array performance monitor for an existing array;

DD FORM 1473   EDITION OF 1 NOV 65 IS OBSOLETE

(d) analysis of the effect of using a finite radius in making flight checks of an array; (e) design study for a large aperture, low sidelobe array analysis and design including the statistical effect of errors in construction, design gain, system noise figure and aperture coefficients for constant beamwidth as a function of frequency.

PROJECT FM/CW ADAPTIVE MEASURE

J. E. Rice
R. G. Baender

GTE Sylvania, Incorporated

/

1 4-

FOREWORD

The work described in this Final Report was performed by GTE Sylvania, Incorporated, Electronic Systems Group - Western Division, P.O. Box 205, Mountain View, California. It was accomplished under the direction of Rome Air Development Center, Griffiss Air Force Base, New York, under Contract F30602-73-C-0307, Job Order 673A0151.

Numbered by the contractor, EDL-E214, the report covers the period 1 May 1973 to 1 May 1974.

Mr. John Clancy and Mr. Robert A. Mather, both of OCSL, were the RADC Contract Monitors.

The principal author was James E. Rice. Acknowledgement is given to Mr. C. Moore for his invaluable suggestions during the design and his flawless construction of the Performance Monitoring System. Acknowledgement is also given to Kathleen Santello and Warren Preston for their assistance in the preparation and publication of the report.

This report has been reviewed by the RADC Information Office (OI) and is releasable to the National Technical Information Service (NTIS).
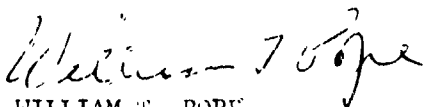
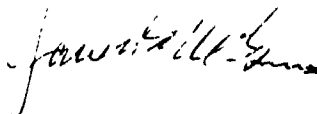This technical report has been reviewed and is approved.

APPROVED:

ROBERT A. MATHER
Project Engineer

APPROVED:

WILLIAM T. POPE
Assistant Chief
Surveillance and Control Division

FOR THE COMMANDER:

JAMES G. McGINNIS, Lt Col, USAF
Deputy Chief, Plans Office

ABSTRACT

From 1 May 1973 to 30 April 1974, GTE Sylvania Incorporated, Electronic Systems Group - Western Division, provided engineering field services in support of RADC's experimental HF FM/CW backscatter system at Dexter, New York. These services were primarily concerned with technical investigations and evaluation of system performance and with the statistical design of large aperture low sidelobe arrays. This report discusses the results from these detailed experimental/theoretical investigations.

EVALUATION

The work performed under this contract is
fundamental to the long range objectives of the ad-
vanced OTH technology program. The immediate goal
of this technology program is to develop a large
aperture, two dimensional adaptive array for opera-
tion in the High Frequency portion of the spectrum.
This report deals with the evaluation of existing
array design and operation as well as theoretical
investigations of more advanced concepts. The results
of this work increases the probability of success of
the work contemplated for the immediate future.

ROBERT A. MATHER
Project Engineer

-iv-

TABLE OF CONTENTS

TABLE OF CONTENTS -- Continued

ILLUSTRATIONS

ILLUSTRATIONS -- Continued

ILLUSTRATIONS -- Continued

1.0 INTRODUCTION

Since 1969, GTE Sylvania Incorporated has provided field-engineering services at RADC concerned with the investigation, development, and implementation of advanced data processing and analysis techniques directed toward the test and evaluation of RADC's experimental HF FM/CW backscatter system in upstate New York.[*] The research and development activities during the period 1 May 1973 to 30 April 1974 included:

(a) extensive measurement and limited analysis of the receiving antenna array located at Dexter, New York;

(b) modification of the computer software to accept data from the array performance monitor;

(c) design, development, and implementation of the array performance monitor for the Dexter array;

(d) analysis of the effect of using a finite radius in making flight checks of the Dexter array;

(e) extended trip to the RME overseas site to investigate the performance of the RME equipment;

(f) beamforming network analysis of the RECAP III array both before and after modifications and repair;

(g) design study for large aperture low sidelobe array analysis and design, including the statistical effect of errors in construction, design gain, system noise figure, and aperture coefficients for constant beamwidth as a function of frequency.

These activities are described in detail in the following sections.

---

[*] A working knowledge and understanding of the experimental FM/CW system at RADC is assumed. Also, it should be noted that some of the results presented in this report are preliminary or transitory since the system has not attained final operational status.

2.0 ENGINEERING SERVICES

2.1 BEAM-FORMING NETWORK PERFORMANCE MONITOR

The manual tests performed on the Dexter receiving antenna array beam-former corrected many problems, but they showed a need for automatic, or at least semi-automatic, measuring equipment. As a result, the Beam-forming Network Performance Monitor was designed, constructed, tested, and employed. It consists of a control unit, a beam selector, an element selector, amplitude and phase measuring equipment, and a display section.

2.1.1 Element Selector

The element selector is designed to provide a signal to a selected element either sequentially under automatic control, individually at random under manual control, or simultaneously to all elements.

These functions are directed and monitored by the control unit. The outputs of this unit are relay contact closures which are sensed by the element selector. The input is a binary word containing the element number and function. After sensing and reacting to the input, the element selector in turn then returns to the control unit the detected and performed commands. These commands are then compared to verify that the element selector has completed the desired operation.

Since simultaneous signals are required, the 64 RF outputs are derived from a two-way power splitter and two 32-way power splitters.

2.1.2 Beam Selector

The beam selector is designed to provide a single RF signal to the amplitude and phase measuring equipment. The selection is controlled by a binary word containing the desired beam number (1 through 49). The beam selector is also designed to return a binary number indicating the beam decoded and selected for comparison of completion and accuracy.

2.1.3 Amplitude and Phase Measuring Equipment

Amplitude and phase are measured by an HP 656A amplitude and phase detector, modified by Hewlett-Packard to accept an external tuning signal 100 kHz above the frequency to be measured.

(2)

The normal analog outputs (phase and amplitude difference) were multiplexed for analog to digital conversion. The conversion is done by a 12 bit ADC for output to a digital computer and display section.

2.1.4 Display Section

The display section accepts the digital information from the beam selector, element selector, and the A/D converter and multiplexer. The binary information is converted to BCD coding for display. The displays are:

(a) beam selected (either transmitted or received),

(b) element selected (either transmitted or received),

(c) error indication if transmitted and received do not compare,

(d) mode of operation (manual, sequential, or external),

(e) amplitude difference (0 - 80 dB) in 0.1 dB steps, and

(f) phase difference (0 - 360°) in 0.1° steps.

2.1.5 Control Unit

The control unit is designed to control the element selector, beam selector, displays, and data acquisition from one of three sources: externally from a computer simulator (as is presently used as no computer is available), internally generated sequence control with outputs for a computer, or internally from manual controls.

The control unit was designed to provide self-timing as well as monitoring accuracy of operation. Since the units contained numerous and various types of relays, no set period could be defined as switching times depended upon the number of units being switched (element or beam number) and the relative response time of each. The feedback feature was incorporated to monitor the operation and also to indicate the completion of an operation, since the beam selector, element selector, and control unit can be separated by as much as 1000 feet.

A block diagram of the control unit is shown in Figure 1. Figure 2 is a flow chart of the logic. The detailed circuit diagrams and descriptions were furnished to RADC Dexter site personnel and are not included in this report.

The unit was installed and tested at the Dexter site. The self-timing feature of the system performed as expected to provide the maximum switching rate consistent with relays and coaxial switches.

(3)
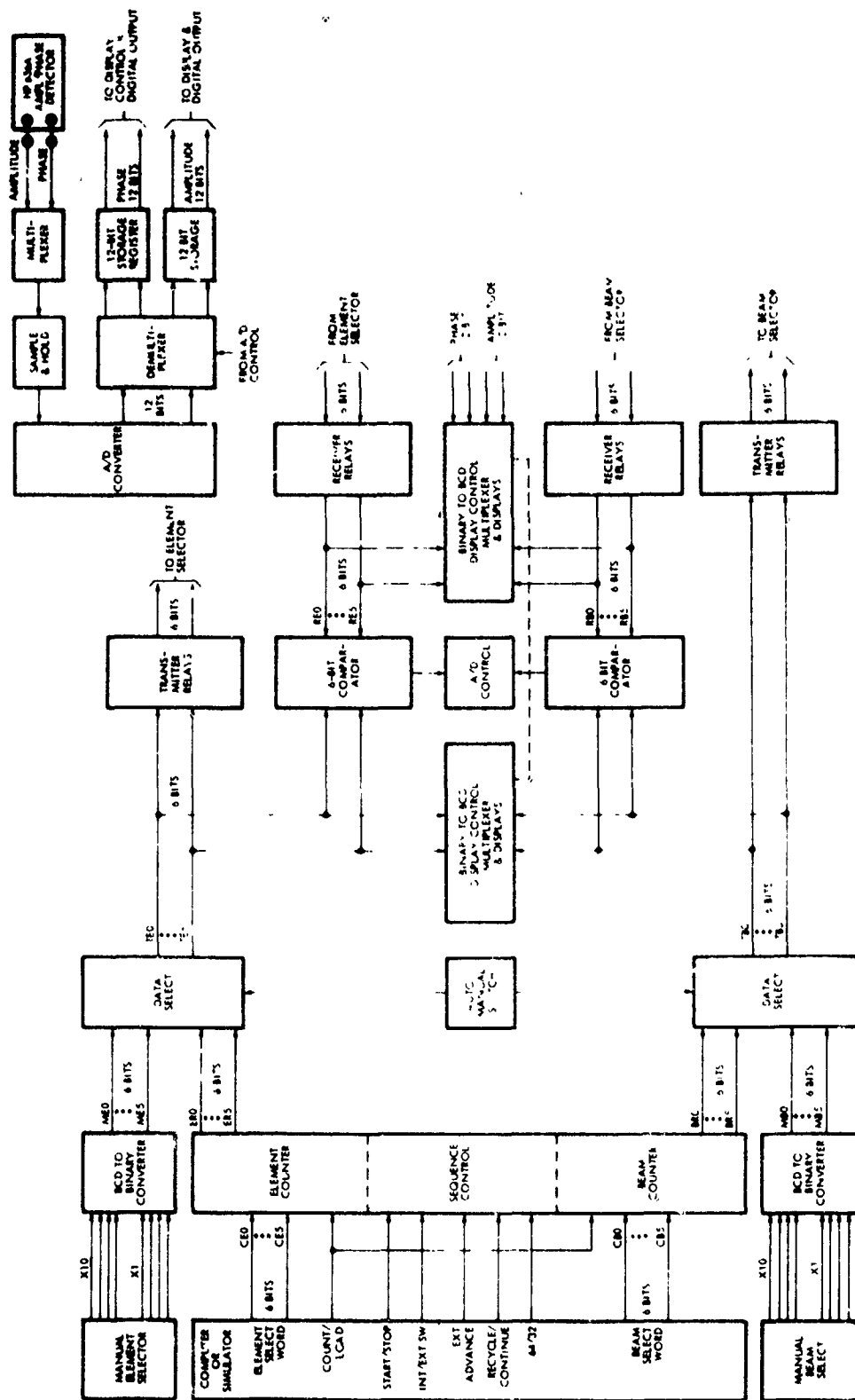
Figure 1. Beamforming Network Performance Monitor.
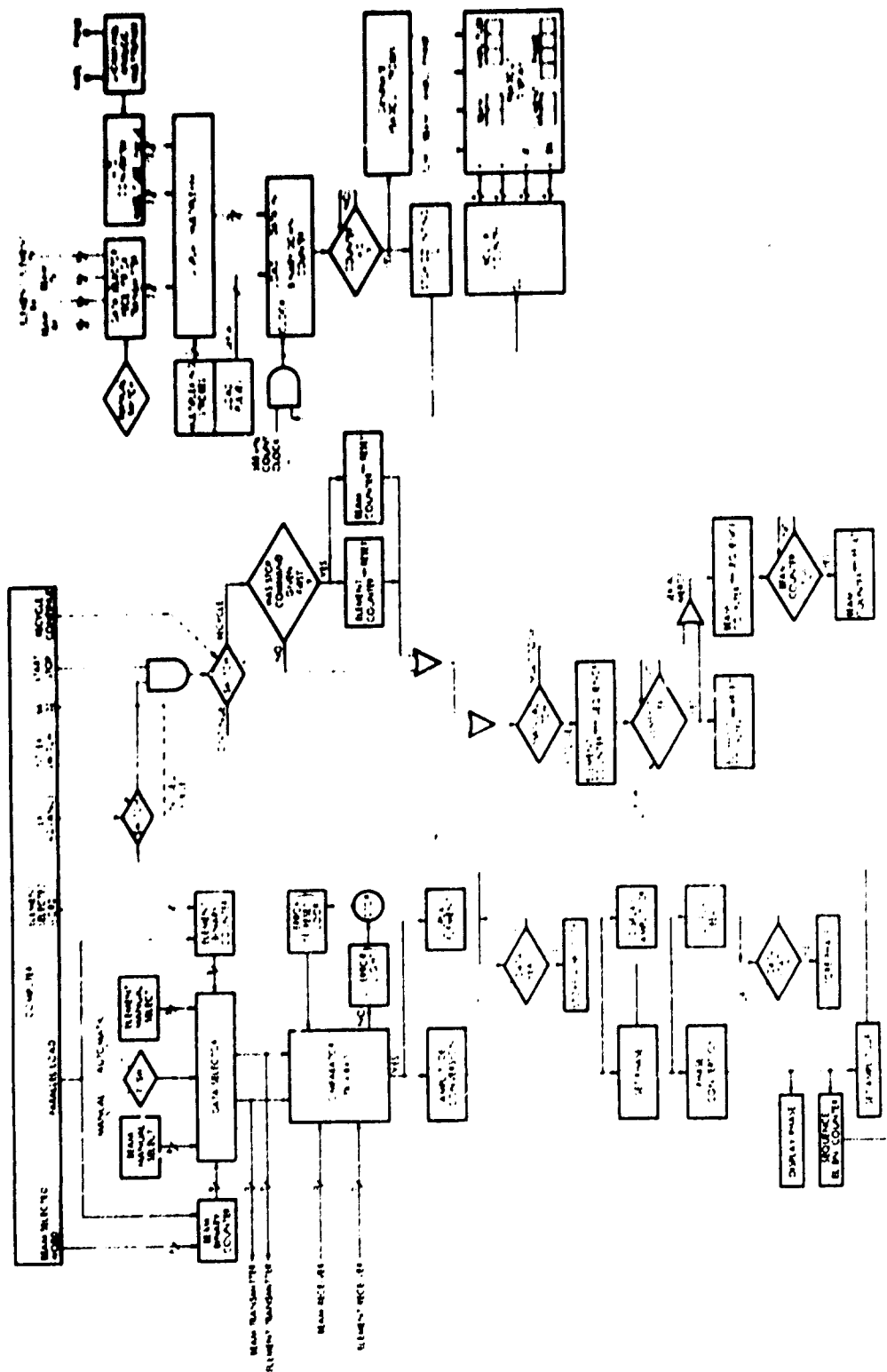
Figure 2. Beamforming Network Performance Monitor Flow and Logic Chart

(5)

2.2 BEAM FORMER PREINSPECTION

Prior to making extensive measurements on the beam-forming network, a preliminary inspection was made to eliminate obvious errors or faults.

2.2.1 Delay Cables

The delay cables cut and phased as per computer printouts, were found to be installed incorrectly. These cables provide the steering delay for combining the two 32-element E/W arrays into one 64 element array and also the phasing for multiple beam summation. The steering cables and phasing cables were found to be interchanged within the array.

To determine the possible effects that this error could have had on the experiments which had already used the system in the erroneous configuration, ideal patterns using the interchanged values were calculated. The calculated patterns are shown in Figures 3 and 4 for 10 and 20 MHz, respectively. In the ideal case (no random errors) there is a loss of approximately 36 dB in sidelobe level and a 5 dB loss in power between the relative patterns at the peak of the beam.

This condition was corrected for the one combined beam in use, and further corrections were postponed until the permanent installation was made.

Further checking of these cables showed that they had been trimmed incorrectly. While the computer printouts listed the required measured values for three frequencies, the lower frequency checks had been skipped for several cables, which were found to be one wavelength (at 30 MHz) short. In addition, the spread of the tolerance increased directly with the number of cables trimmed, probably as a result of longer periods between instrumentation calibrations.

The cables were retrimmed in accordance with the design data and new cables made to replace the shortened ones.

2.2.2 VSWR Sources

Checks of the voltage standing wave ratio (VSWR) at various points internal to the main beam-forming network showed several high VSWRs within the unit. The major sources of these high readings were as follows:
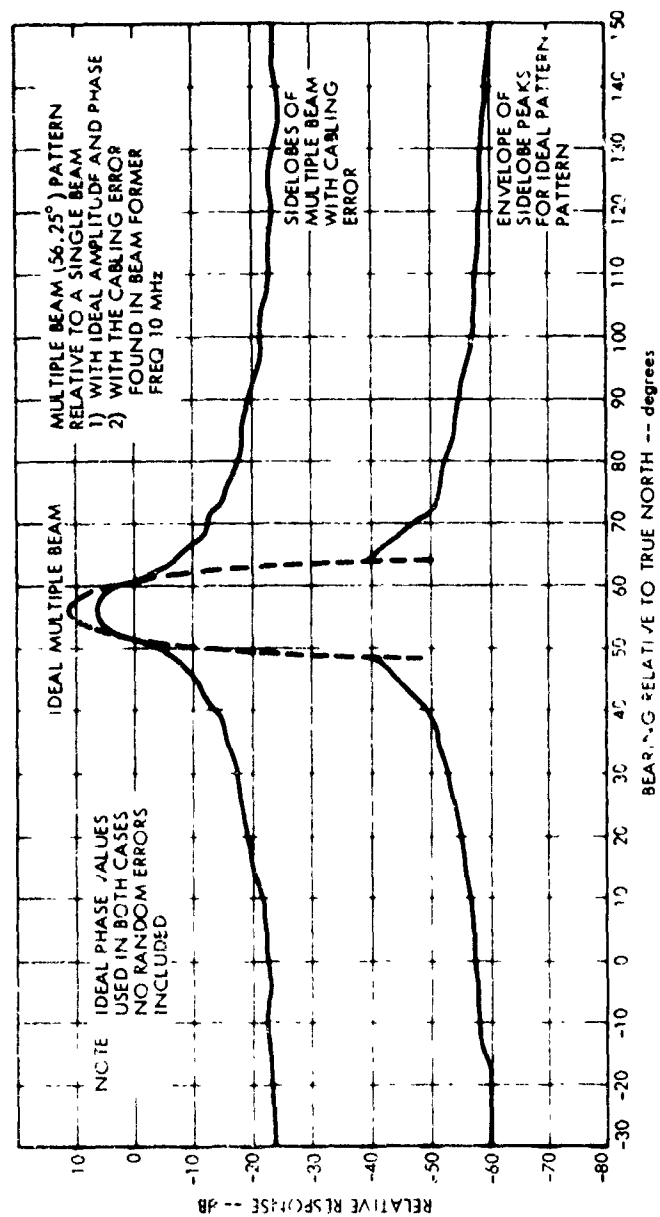
Figure 3. Dexter Antenna Array (64 Elements)

(7)
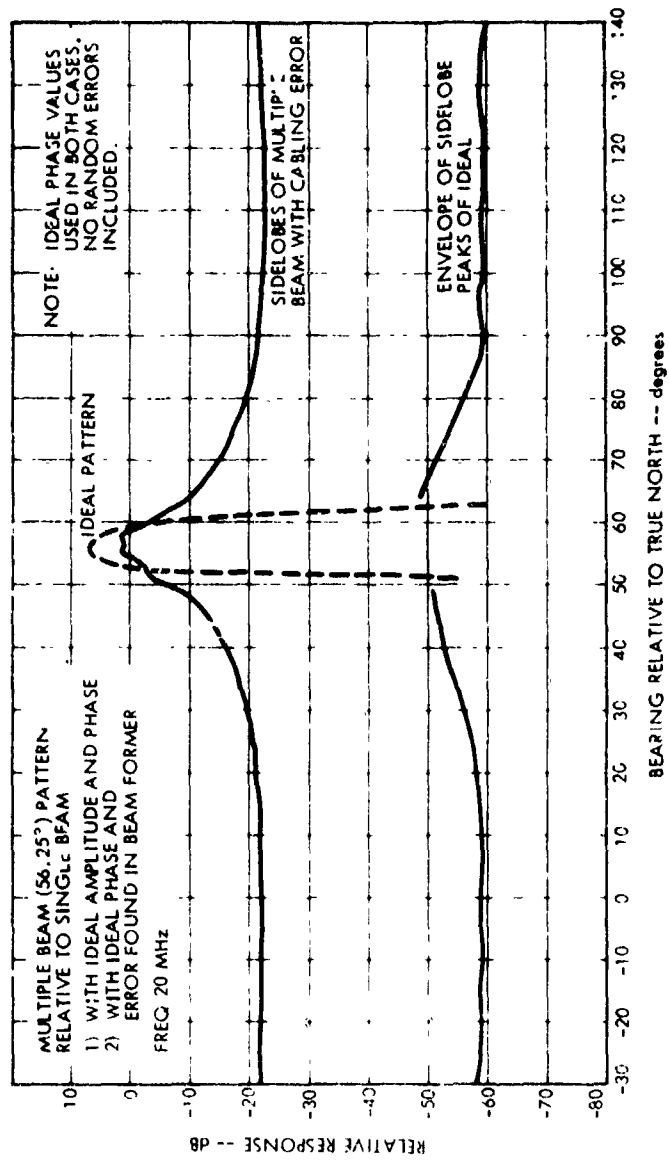
Figure 4. Dexter Antenna Array (64 Elements).

(a) Loose ground connections to the printed circuit boards which carried the amplifiers and the Taylor weighting coefficient attenuators. Since the ground connections are purely mechanical, tightening the retaining screws reduced the VSWRs to acceptable levels.

(b) Broken or sheared connectors and loose BNC connectors. These were replaced and/or locked in place.

(c) Bad hybrids (5 way) with one or more ports inoperative. These were replaced where required or feasible.

(d) Open cables, with no apparent association with the connector but internal to the cable.

(e) Faulty 50 ohm loads. Apparently due to mechanical damage, the loads were repaired or replaced as required.

The preinspection pointed up the need to rotate the tedious and repetitious task of trimming cables or to provide for automatic test and calibration to prevent costly short cuts. Also, reducing the number of mechanical connections required reduces the probability of bad connections. (This includes cable connectors where not absolutely necessary.) Where connectors are required, they should be protected from mechanical damage and indiscriminate disconnecting and reconnecting (or lack thereof).

2.3 BEAM FORMER MEASUREMENTS

Following the installation of the Beam-forming Network Performance Monitor, preinspection, and repairs, extensive measurements of the Dexter beam former were performed by site personnel.

2.3.1 Test Plans

The tests were designed to allow the measurement of the major components of the beam former, including field preamplifiers and cables. A block diagram of a typical element installation is shown in Figure 5. The test setup used to measure the amplitude and phase of the field units is shown in Figure 6.

For the field components tests, only the amplitude and phase measuring portion of the Beam-forming Network Performance Monitor was used as there was no calibration system in the field.

(9)

MAIN
BEAM FORMING
NETWORK

BEAM FORMING
TRAILER-PATCH
PANELS AND
DISTRIBUTION

APPROX
1000'
COAX
CABLE

50Ω
LOAD

JUMPER
CABLES

BEV
ELEMENT

180° COAX CABLE
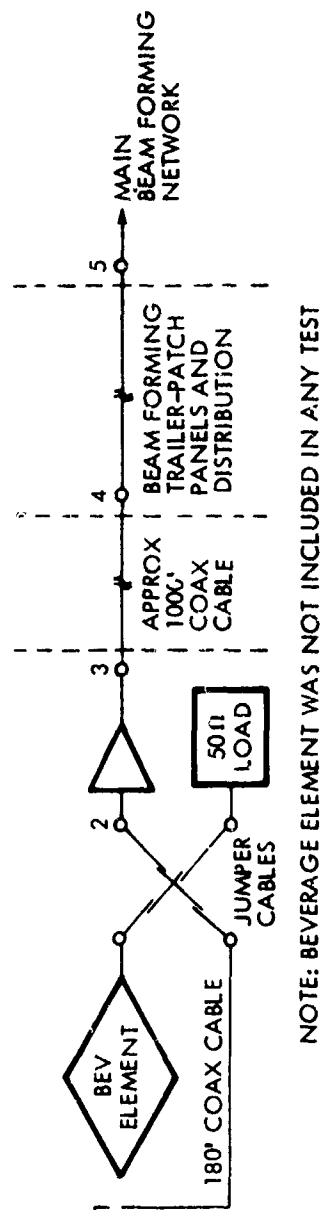
NOTE: BEVERAGE ELEMENT WAS NOT INCLUDED IN ANY TEST

Figure 5.   Block Diagram of a Typical Element Installation at Dexter, New York.
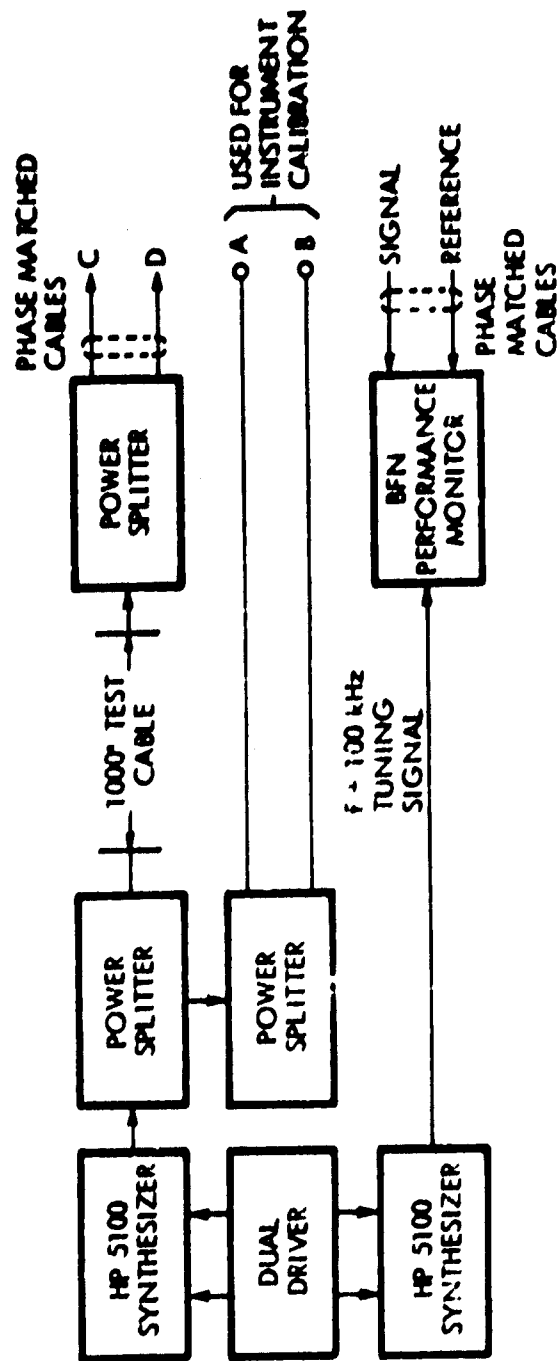
Figure 6. Block diagram of the test set-up used to measure the field components of the Dexter beamforming network.

(11)

The four tests performed were made on element pairs (comparison test). The signals were injected into the system using the kth and k+1 elements and the output measured using the kth element as reference and k+1 as data. For tests, signals from C and D (Fig. 6) were injected at location 3 (Fig. 5), which is the input to the 1000 ft cable, and the output was measured at location 4. The test was repeated with the output measured at location 5. Signals from C and D were then injected at location 1 with the 180 ft cable patched into the amplifier, and output measured at location 5. The test was repeated, measuring the output at location 4.

Before each measurement, the equipment was checked for calibration. Each time the measurements advanced one element, the signals C and D were interchanged to allow any mismatch of the cables and power splitter to average out.

The tests were designed to allow the separation of the various parts and obtain a check on the measurements.

The beam former was then measured from the main input location 5 (Fig. 5) through the output of the line driver of the individual beams using the Beam-forming Network Performance Monitor in the standard configuration.

2.3.2 Modification to Beam-Former Analysis Programs

It was necessary to modify the computer programs used on the CDC 1700 located at the RADC Data Reduction Center to accept the new data. There were three major modifications:

(a) the ±180° ambiguity of the vector voltmeter was changed to the 0-360° data from the Beam-forming Network Performance Monitor.

(b) programs were added to analyze the field component tests.

(c) programs were added to use the field component data in pattern calculations.

2.3.3 Beam Former Analysis

The analysis of the beam-forming measurements was not completed due to problems in the CDC 1700 software. Difficulties were encountered in the data analysis programs (written in Fortran for the CDC 1700), and debugging showed the problem to be in the CDC 1700 system software. Numerous attempts by RADC and the resident DRC contractor to obtain help from CDC on this problem were unsuccessful. Subsequently the DRC resident programmer in researching for another purpose

(12)

located the source to be the CDC 1700 floating point package: "Numerical inaccuracies are generated by the loss of at least the two low order bits in the floating point package. During extensive calculation this error could increase rapidly."[*]

The limited analysis output was for the field components only.

2.3.3.1 Analysis Procedures

The tests were of a comparison nature, i.e., only relative measures were made between two adjacent pairs. These data were then reduced to an absolute measurement against an arbitrary standard. The standard chosen was the average or mean value of all the readings so that each element could be plus or minus.

The tests were conducted in this manner and were then combined to separate the components and check the validity of the tests.

(a)   Test 1 contained only the 1000 ft cables from the element to the beam former trailer.

(b)   Test 4 contained the 1000 ft cables plus the 180 ft cables and amplifiers. Therefore, the difference between test 4 and test 1 by element should contain only the 180 ft cables and amplifiers for an element.

(c)   Test 2 contains the 1000 ft cables plus the internal distribution cables and amplifiers. Therefore, the difference between test 2 and test 1 by element should contain only the internal distribution cables and amplifiers for an element.

(d)   Test 3 contains all the components. Therefore, the difference between test 3 and test 1 (the results of (b) and (c) above) should contain only residue caused by errors. These errors an be cable connections improperly made during the course of the test, VSWR reflections from improper terminations, or measurement and recording errors.

2.3.3.2 Field Component Analysis Results

The results of the N/S 32 element array field components indicated that:

(a)   the 1000 ft cables are within ±1.2 ft and ±0.8 dB limits (with one cable showing -1.5 dB only at higher frequencies);

[*]1700 Systems Bulletin #10, dated 12 January 1968.

(b) the internal distribution system is within ±0.7 ft and ± 1.8 dB limits;

(c) the 180 ft cables and amplifiers are within ±2.6 ft and ±1.9 dB limits;

(d) the residual after all components are subtracted showed a variation between ± 0.8 ft and ± 1.8 dB limits, which indicates that there were errors in the measurements on the order of magnitude of the calculated errors for the components.

The results of the E/W 64 element array field components indicated that:

(a) the 1000 ft cables are within ±4.7 ft and ± 0.9 dB limits;

(b) the internal distribution system is within ±1.7 ft and ±2.5 dB limits with one bad connection (probably improperly attached at time of measurements as there is a large residue for this element indicating a bad series of measurements);

(c) the 180 ft cables and amplifiers are within ±3.1 ft and ±1.3 dB limits;

(d) the residual data indicate errors in measurements on the order of magnitude of the calculated errors, with several ports indicating measurement error or connector problems between measurements.

2.3.3.3 Examples

An example of a probable reading or recording error is shown in Table 1 for element 10 of the N/S array from the residual data (which should be zero for an ideal system and perfect measurements).

Table 1. Extract of Reduced Residual Data for N/S Array Element 10
(cable velocity factor = 0.66).

Frequency (MHz)	Amplitude (dB)	Cable (ft)
4.9	0.61	0.67
10.1	-0.04	0.22
21.1	-2.71	0.17
29.8	-0.76	-0.03

An example of a probable cable connector not fully mated either because of loose fit or corrosion is shown in Table 2. The increasing of amplitude and decreasing of phase angle approximates that of a RC high pass filter due to the lack of a solid metal to metal connection.

Table 2. Extract of Reduced Internal Distribution System
Data Reductions for Element 40 (cable velocity
factor = 0.66).

Frequency (MHz)	Amplitude (dB)	Cable (ft)
4.9	-4.4	-7.99
10.1	-1.8	-4.21
21.1	-0.4	-0.14
29.8	-0.4	-0.11

2.3.3.4 Conclusions

From the measurements of the field components for which the analysis could be completed, the following conclusions were drawn.

(a) From the results of the residual data (which would be zero for an ideal system and perfect measurements) it becomes apparent that the measurements should be made numerous times. From several measurements, the data points could be averaged for a better estimation of the actual conditions.

(b) The data should be taken fully automatically, thereby eliminating the human error factor associated with repetitious tasks and increasing the repeatibility of such measurements.

(c) A permanently installed calibration system is required if numerous measurements are to be made. The manual method requires several days and places a severe strain on equipment calibration and personnel.

2.4 ORBITS AND PATTERNS

The standard orbit used by the RADC flight check aircraft is a 10 nm radius. The calculated patterns for the Dexter site (and most other arrays in general) assume an orbit of infinite radius (plane wave fronts). To determine the degradation for the Dexter site caused by 10 nm orbits, ideal (no random errors) patterns were calculated. These calculations assumed that the signal source was small compared to the distance and that the wave fronts were spherical.

In Figure 7, two values, 10 and 100 nm, were selected as the orbit radii. It is seen that at an aperture equal to 57.6 wavelengths, the first three nulls are obscurred when a 10 nm orbit is used and even the first null is lost with a 100 nm orbit. The patterns shown on Figure 8 have an aperture of only 9.6 wavelengths, and the 10 nm orbit only obscures the first null. It should be noted, however, that the 3 dB beamwidth remains identical in either case. Yet the 10 nm orbit at 30 MHz has spread the 6 dB beamwidth, but less than the probable error made during actual flight checks.

To compare the calculated patterns to an actual flight check, the pattern for 11.64 MHz was calculated. Seven points from the main beam pattern are shown in Figure 9 plotted relative to the main beam peak values. It is seen that the 10 nm orbits cause distortion in the measured pattern through spherical distortion of the wave fronts.

The aircraft is normally held in orbit by the autopilot and an X band beacon at the site. Since the beacon is not located at the array center, the apparent shift of the main beam is approximately 0.25°. This error is within experimental error and should not be considered at this time.

(16)
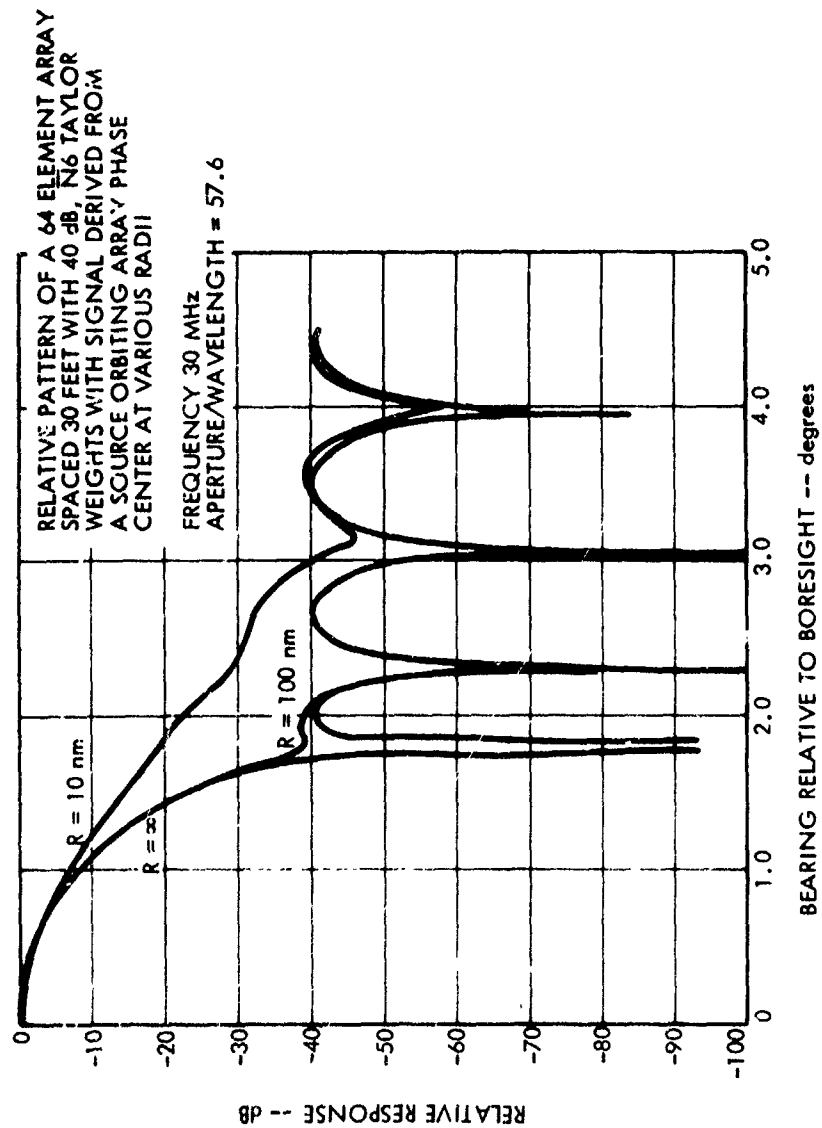
Figure 7. Relative Response of 64 Element Array.

(17)
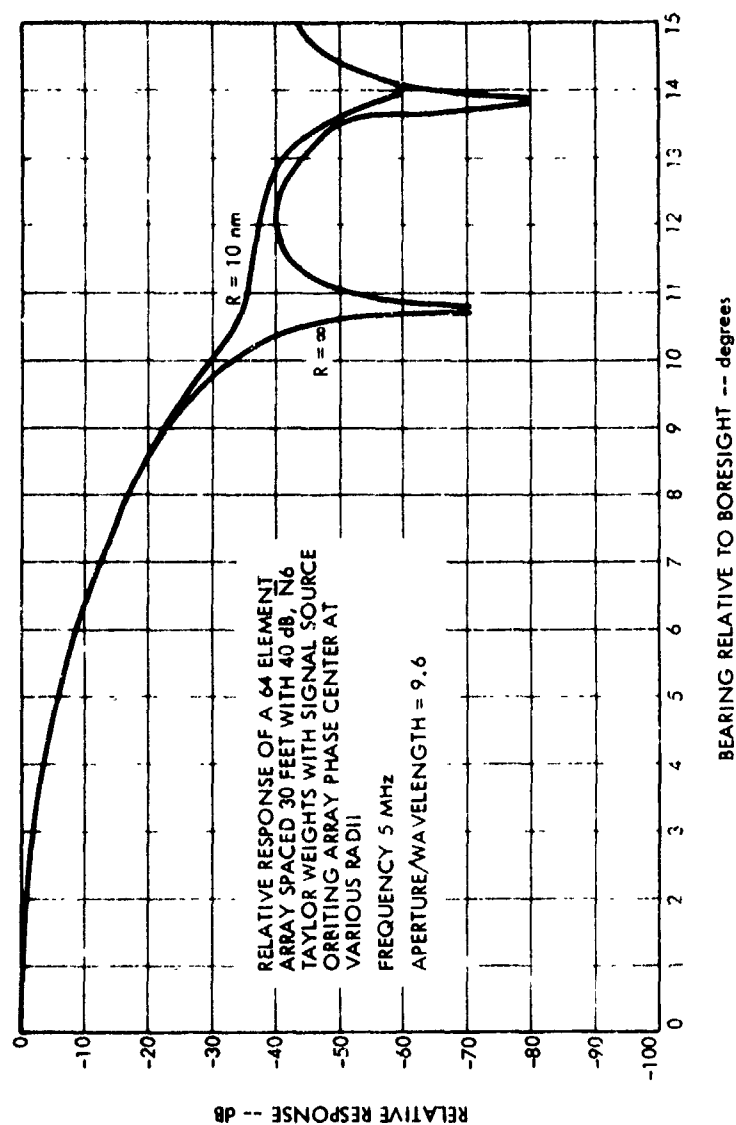
Figure 8. Relative Response of 64 Element Array.

RELATIVE RESPONSE OF A 64 ELEMENT
ARRAY SPACED 30 FEET WITH 40 dB, N̄6
TAYLOR WEIGHTS WITH SIGNAL SOURCE
ORBITING ARRAY PHASE CENTER AT
VARIOUS RADII

FREQUENCY 5 MHz

APERTURE/WAVELENGTH = 9.6

BEARING RELATIVE TO BORESIGHT -- degrees

RELATIVE RESPONSE -- dB

R = 10 nm

R = 8

(18)

Figure 9. Comparison of Measured and Calculated Responses.

(19)

2.5 RME OVERSEAS SITE INVESTIGATION

The trip to RME overseas site was made during the period of 14 July to 9 August 1973. The complete trip report is contained in Appendix A and is summarized below.

The trip was made primarily to investigate two problem areas: the cause of the high minimum discernible signal (MDS) experienced by the RME system, and the cause of the synchronization problem between the receiver and transmitter sites with the apparent loss of accurate timing with respect to world time standards. Four other problem and general areas were to be observed: the "connector problem", general maintenance procedures and level of performance, general operational procedures, and any general areas where system performance could be improved.

Because of limited time available, it was stipulated that no maintenance or repairs of the RME system or tests of auxiliary equipment would be performed unless directly related to the definition of the immediate problems.

To accomplish these tasks, the investigation was to be carried out in two phases.

(a) Complete tests of the RME receiver system and auxiliary receiving equipment used by the system (e. g., multicouplers, amplifiers) and the transmitter equipment were to be conducted to determine if the MDS problem was hardware induced.

(b) If no hardware problems were found, on-air tests were to be conducted to observe the noise sources causing high MDS readings and if any were found, to determine whether they were independent or signal related.

2.5.1 Conclusions

From this trip it was evident that all unit personnel are making a dedicated and professional effort to operate, analyze/report, and maintain the system for peak performance. The following specific conclusions cover the areas of interest.

2.5.1.1 High MDS

(a) The equipment is in generally good to excellent condition and is now operating with specified or better performance (with one major and some minor reservations, none of which directly relate to the MDS problem).

(20)

(b) The ground wave at the receiver site can limit system performance simply by rising to a level which exceeds the available receiver dynamic range. In addition, it presently increases the probability of inter-modulation distortion and cross-modulation products. The ground wave averages approximately -50 dBm, with recorded peaks of -30 dBm in the summer. Since the transmitted broadband noise floor is 100 dB or more below the transmitted signal, the inband noise floor at operational ranges is set by the receiver to approximately 102 dB below the strongest received signal in the preselector bandwidth. Therefore, under normal operating conditions the average value (-50 dBm) would limit the MDS to -152 dBm. While the peak value (-30 dBm) would limit the MDS to -132 dBm, the previous data collected on ground wave strength would indicate that this peak level is rarely attained.

(c) An external, non system related noise which could limit the system performance was observed at -130 to -135 dBm signal levels. No statistical data other than the limited numbers below were collected during the short time available. The source of the noise is unknown. However, it appears to be an OTH noise source, since it has a short term cyclic period of 0.5 to 2 minutes with a much longer period superimposed upon this (period not identified) and was not observed on frequencies which were 8 to 10 MHz above the 3000 km MUF. During the on-air testing performed, this noise restricted the MDS to values above -140 dBm.

(d) A signal related noise was observed with a relative time delay centered at 150 km, which, in conjunction with a large ground wave signal, could cause problems within the receiver. However, there was no evidence that this noise caused problems at operational ranges during the limited testing.

(e) A further source of noise which could set a lower limit in achievable MDS is the spurious responses generated in the transmitter due to blower motors and the like. These spurious signals are not at integer values of 50 Hz and thus tend to cause a peaking of the noise between PRF lines which, since the fax recorder responds to peak values, results in a

(21)

corresponding increase in displayed noise. However, the measured level of these spurious signals is such that they are not considered to be the cause of the high MDS values reported.

(f) Local noise may become a problem in the near future, as new construction indicates the city is expanding in the direction of the site. Since local noise is generated in the near vicinity of the receiving antenna, the noise signal is propagated as a surface wave. The effect of the ground is to reduce the received signal strength below free space propagation loss. This reduction becomes negligible and independent of polarization as the height of the two antenna approaches one wavelength above the ground. The present antenna system is two to four wavelengths above ground and will be more susceptible to this threat than a low profile antenna.

2.5.1.2 Synchronization Problem

(a) The severity of the problem was not found to be as great as pretrip briefings had indicated. These estimates were that the time code generator was typically in error as much as several seconds with respect to world time standards. Presently, each operating shift checks the time code generator against a world standard time signal. The maximum deviation observed was 40 msec (one PRT period at 25 Hz operation).

(b) There is a hardware problem which at present requires a small slewing of the time code generator to compensate. However, the action of the advance/retard controls on the time code generator is somewhat misleading and operators under pressure to complete QSYs quickly, occasionally slew the clock the wrong way, thereby compounding the synchronization problem. Standardized operating procedure, and modifying the advance/retard controls should do much to alleviate the problem.

2.5.1.3 General Areas

(a) No connector problems were encountered during this trip. Site personnel indicated that only three connectors had exhibited the described symptoms. It was recommended that cold solder joints be considered as a possible problem before extensive connector relocation or replacement is undertaken.

(22)

(b) No observations of the general maintenance procedures were made, as the testing disrupted normal maintenance schedules. However, the fact that receiver oscillations below 15 MHz were found indicates that the system has not been periodically checked. The discovered receiver IF instability suggest that checks in addition to off-air MDS readings, are required to verify the more subtle system parameters (e. g. , IMD product levels).

(c) The general operating procedures were not observed, as the testing disturbed the normal operating schedules. The one operational and maintenance procedure observed (and tested) was reliance on the Lorch receiver to check clear channels, detect interference on the operational frequency, and in conjunction with the Saicor analyzer and a fax recorder test the antenna for IMD and cross-modulation. However, due to the Lorch receiver performance degradation, this procedure resulted in many unnecessary and time consuming QSYs and also extensive antenna maintenance which may not have been necessary.

2.5.2 Recommendations

2.5.2.1 High MDS

(a) The large ground wave signal level present, with all the attendant problems, should be reduced by further decoupling the sites. This greater decoupling could be achieved either by moving one site or through antenna design.

(b) To reduce the OTH noise, the receiver site must be capable of discriminating against unwanted signals. This can only be accomplished by reducing the antenna sidelobe structure to an acceptable level, provided the noise source is not located in the target area. Assuming the noise is entering the system through the sidelobe structure of the array, the sidelobes will require at least a 20 dB reduction from the present levels.

(c) Further identification and characterization in terms of amplitude, spectrum and frequency of occurrence of the signal related noise should be performed.

(d) The spurious lines in the transmitters should be reduced, at least to the levels found during the original acceptance tests on the equipment. Additional on-air spectrum tests should be made at various carrier frequencies to verify the results obtained at the single frequency tested.

(23)

2.5.2.2 Synchronization Problem

(a) An investigation to determine the source of the hardware problem is under-way.

(b) Different synchronization procedures should be instituted to reduce the effects of the hardware problem until it is found. Such procedures were started by the unit, but some diligence will be required until these become routine.

(c) To alleviate some operator confusion, a minor modification to the time code generator should be made to standardize the function of the advance/retard controls. In the demodulator controller, the advance switch, for example, advances the local oscillator timing in range. In the time code generator, however, the advance switch retards the time code generator. (This is standard TCG Logic, the theory being that the World Time Standard Pulse, as seen by an oscilloscope synchronized to the TCG 1 PPS output, is advanced by retarding the TCG; hence, the inverse logic.)

2.5.2.3 General Areas

(a) The three connectors should be inspected for loose or cold solder joint con-nections. This will require removing the insulation from the connection and the wire from the connector to install new insulation. It would be a minor operation to determine whether changing or relocating the connectors is actually required.

(b) After the receiver IF is realigned, the tests made during this trip should be repeated and curves (see system test) generated. These curves would then become a base line reference to which periodic tests could be compared. In this manner gain, noise figure and IMD performance degradation could easily be identified.

(c) Greater reliance should be placed on the MDS readings and RME fax display, in conjunction with the interference monitor (the Lorch receiver should be deemphasized) before starting a QSY. In addition, the Lorch receiver should be repaired or replaced before being used for any further antenna testing.

(24)

(d) The Rockland synthesizer should be returned for repair of the design flaw. The site has developed a reasonable substitute for the calibrator. By adjusting the level of the dis.   parameter in the system software to obtain a uniform shade of grey, a close correlation to MDS can be made. This technique can be used until the synthesizer is returned.

(e) Some provision should be made to cool the preamplifier in summe₁. The temperature was high during the tests, which apparently degraded the preamplifier performance. If the performance were to deteriorate even further during hotter days, this could present a problem with intermodulation and cross-modulation products.

(f) The RF switch and directional coupler on the calibrator chassis should be relocated. The new location should be in the vicinity of the receiver input. This would have the additional advantage that the RF input cable is not routed through an extra cabinet.

(g) The patch panel connections for the various systems should be tested for cross-coupling on critical cables.

2.6 POLAR RECAP III ARRAY

During the planning of Polar Recap III, it was necessary to determine the performance of the array of 32 beverage elements available on the site. The plan view and schematic drawing of the beam-forming network are shown in Figure 10.

2.6.1 Ideal Patterns

To provide a more realistic pattern for the antenna array system, the pattern of the wire was included in all array system patterns. The wire pattern for the elements was taken from the SWRI work done on beverage antennas. The wire patterns used for 5 and 10 MHz are shown in Figures 11 and 12. The array designer , based upon limited flight checks of the wire, felt that 14 dB sidelobes would have been a closer approximation.

Referring to Figure 10, it is seen that the element spacing is 133.37 feet, which corresponds to a filled array up to 7.3 MHz if no steering is provided. However, steering is available in 1° increments up to ±5°. Unfortunately, the steering is accomplished by summing the elements in blocks of four and then steering these

Figure 10. Plan View and Combining Schematic of the Polar Recap III Beverage Array.

Pattern Not Symmetrically
Placed About Boresight ≈5° Shift

RELATIVE RESPONSE -- dB

BEARING RELATIVE TO BORESIGHT -- degrees
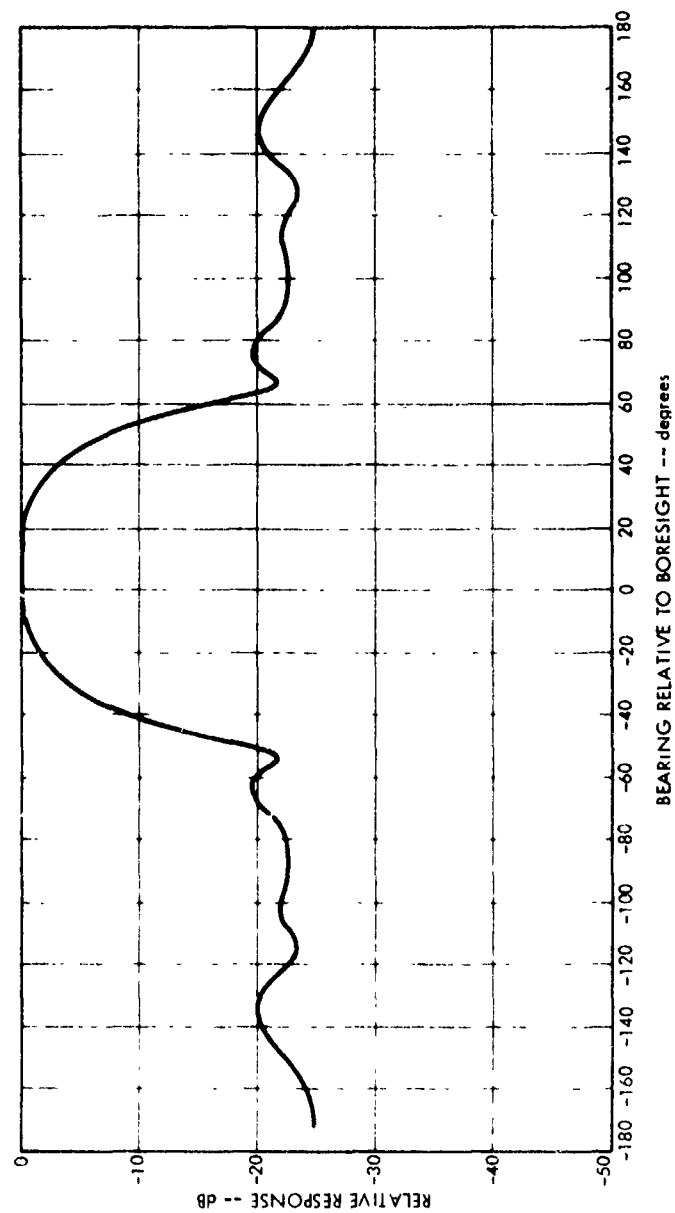
Figure 11.   Polar Recap III Beverage Array Assumed Wire Pattern at 5 MHz.

(27)
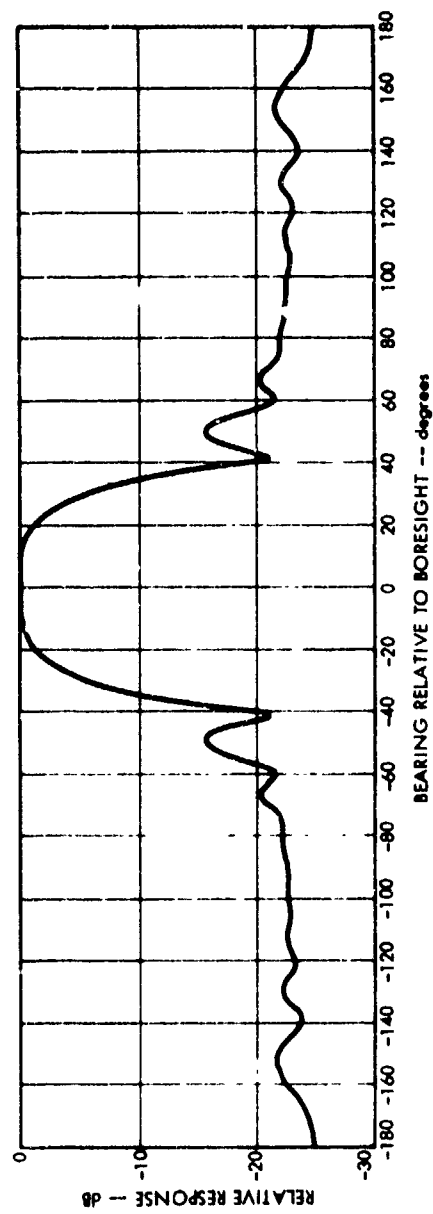
Figure 12. Polar Recap III Beverage Array Assumed Wire Pattern at 10 MHz.

(28)

blocks. Hence, the steering aperture is 533.49 feet, which is a filled aperture up to 1.84 MHz. Therefore, steering above 1.84 MHz causes grating lobes to become visible.

Figure 13, an ideal pattern of the array system, clearly shows that no grating lobes are visible with 0° of steer. However, in Figure 14, which is 6° of steer at 5 MHz, the grating lobes are plainly visible.

The grating lobes are more pronounced at 10 MHz as shown in Figure 15, where they are visible even with 0° steer since these lobes are suppressed by the wire pattern only. In Figure 16, 10 MHz with 6° of steer, the grating lobes are so numerous that the main lobe should be considered to be located at -4°.

This effect is not controlled by the wire but by the pattern of the four element block which is in reality the element pattern of the steered array. This pattern, which is only approximately 11° wide, has attenuated the 6° lobe greater than the -4° lobe.

To assess the effect of using Taylor weighting, the patterns were recalculated using 40 dB, $\overline{N}6$ Taylor weights. These patterns are shown in Figures 17 through 20. As would be expected, the weighting had no effect upon the grating lobes (except broadening, as was the main lobe). In Figures 17 and 19, the sidelobes are down 40 dB in accordance with the weighting function used, while in Figures 18 and 20 they are not. This effect is the interaction of the sidelobes from the blocks of four elements and the nonfilled steered aperture.

From the results of these patterns, it was decided to install the 40 dB, $\overline{N}6$ Taylor weighting. Since only eight ports (blocks of four elements) are steered, six attenuators were sufficient (center two steering ports were 0 dB attenuation). The values for these six attenuators were calculated and given to RADC personnel for implementation.

2.6.2 Measured Amplitude Patterns

Upon arriving at the site, the RADC personnel measured the amplitude performance of the array as it was found. The amplitude performance was again measured after the installation of the attenuators and repairs were completed. The values as measured by RADC of relative amplitude are shown in Table 3.
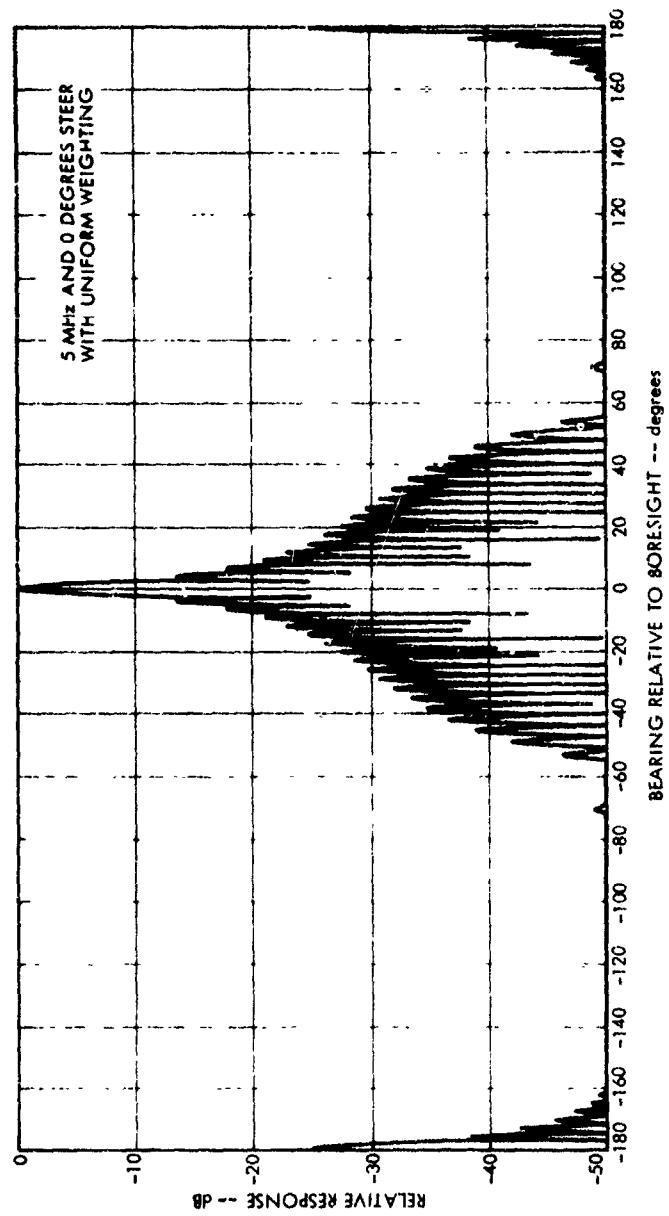
Figure 13. Ideal Relative Pattern of the Polar Recap III Beverage Array.

(30)
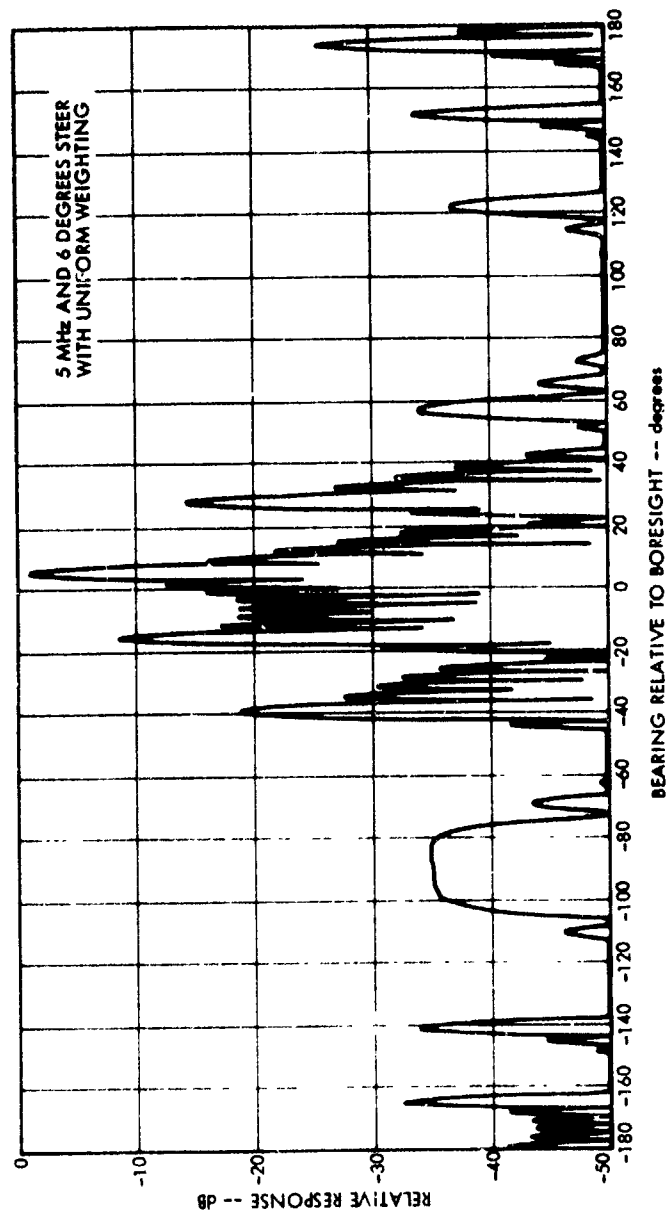
Figure 14. Ideal Relative Pattern of Polar Recap III Beverage Array.

(31)
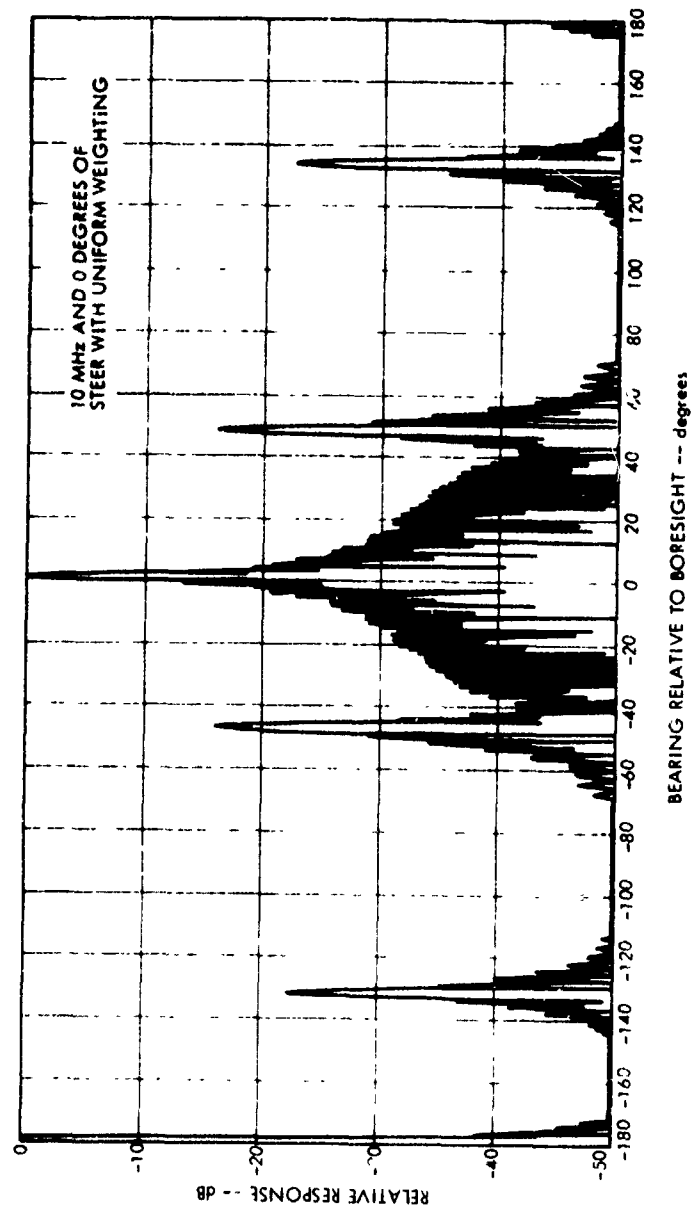
Figure 15.   Ideal Relative Pattern of the Polar Recap III Beverage Array.

(32)
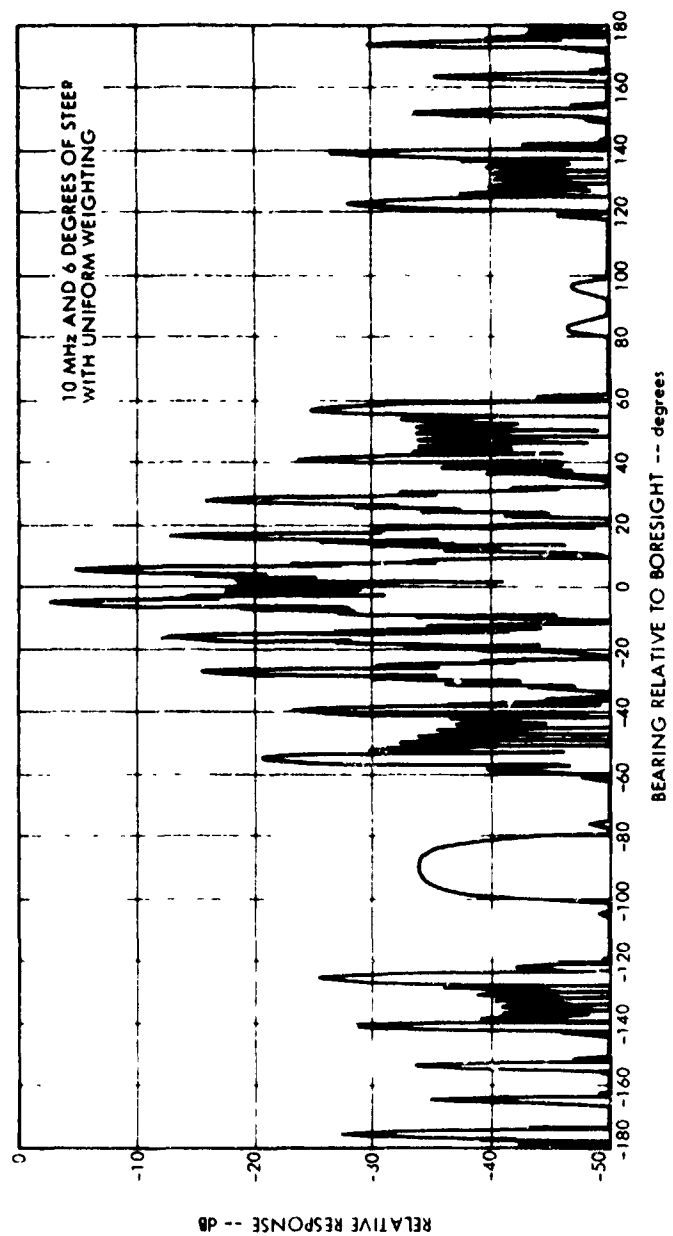
Figure 16.   Ideal Relative Pattern of the Polar Recap III Beverage Array.

(33)

IDEAL RELATIVE PATTERN OF THE
POLAR RECAP III BEVERAGE ARRAY
AT 5 MHz AND 0 DEGREES OF STEER
WITH 40 dB R̄6 TAYLOR WEIGHTING

BEARING RELATIVE TO BORESIGHT -- degrees

RELATIVE RESPONSE -- dB
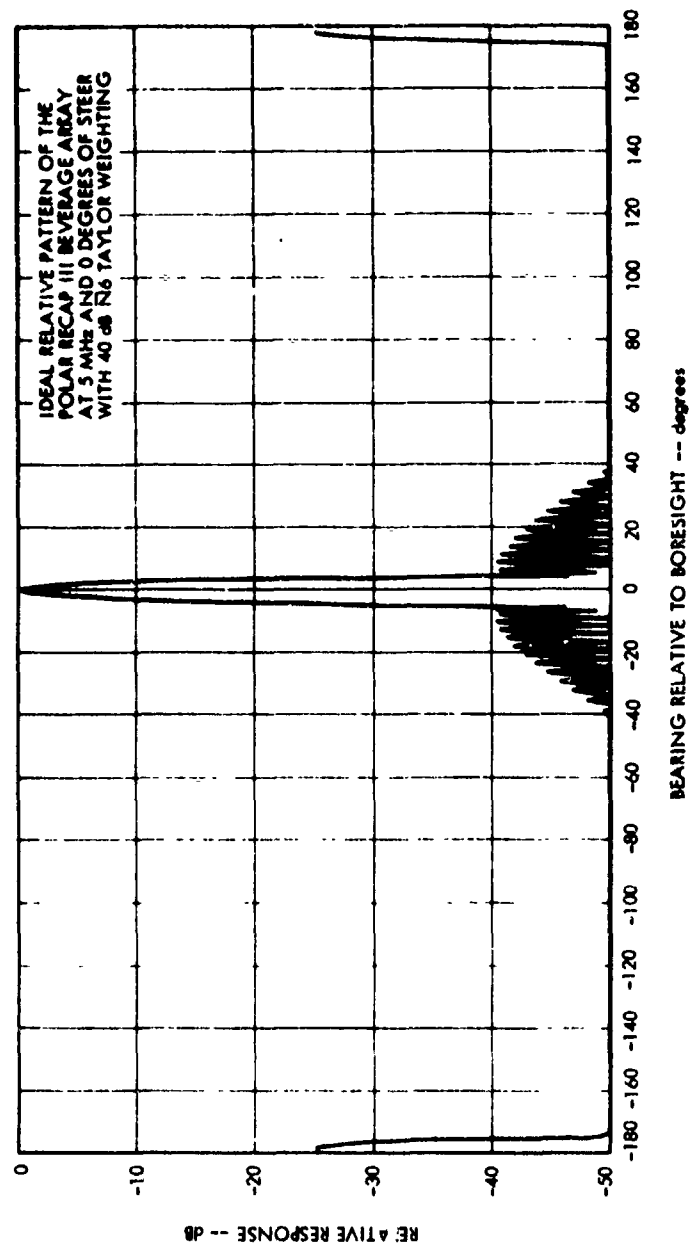
Figure 17.   Ideal Pattern of Polar Recap III Beverage Array.

(34)
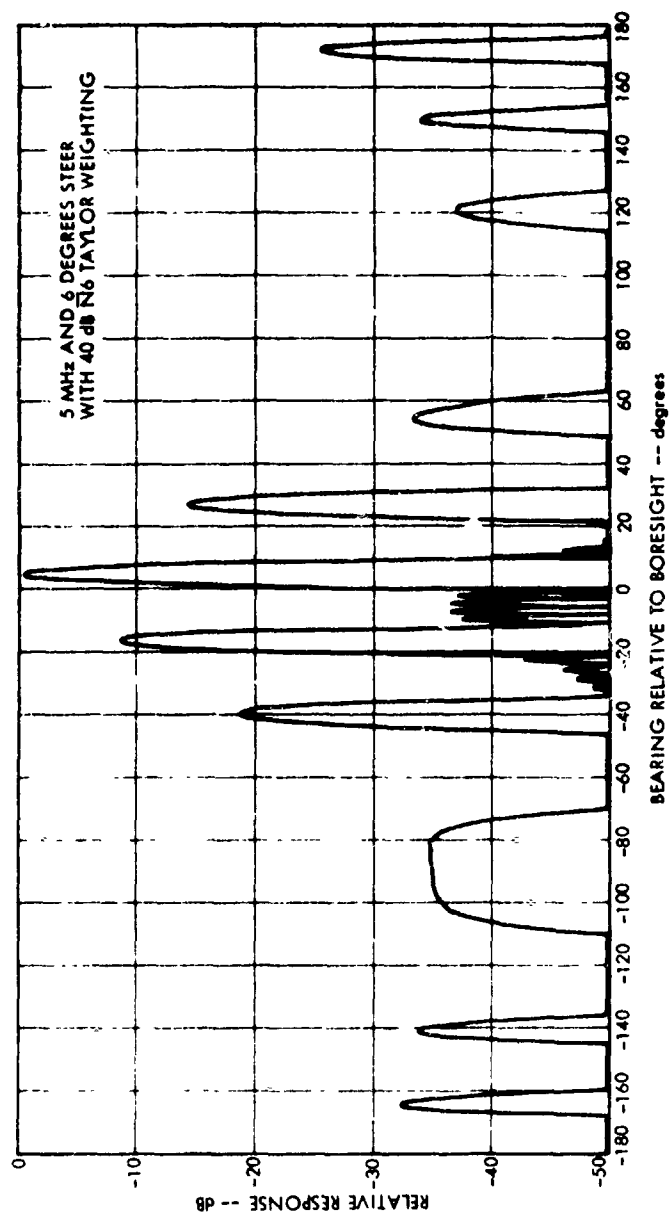
Figure 18.   Ideal Relative Pattern of the Polar Recap III Beverage Array.

(35)

IDEAL RELATIVE PATTERN OF THE
POLAR RECAP III BEVERAGE ARRAY
AT 10 MHz AND 0 DEGREES OF STEER
WITH 40 dB N̄6 TAYLOR WEIGHTING
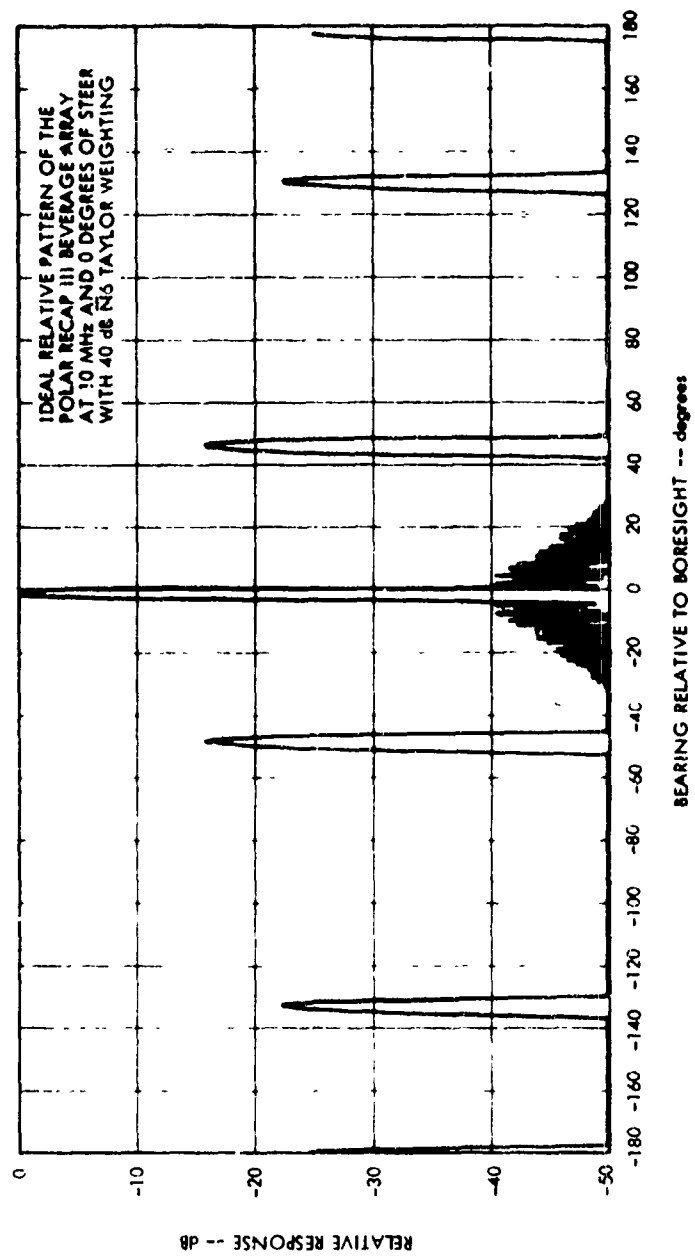
Figure 19.   Ideal Relative Pattern for Polar Recap III Beverage Array.

(36)
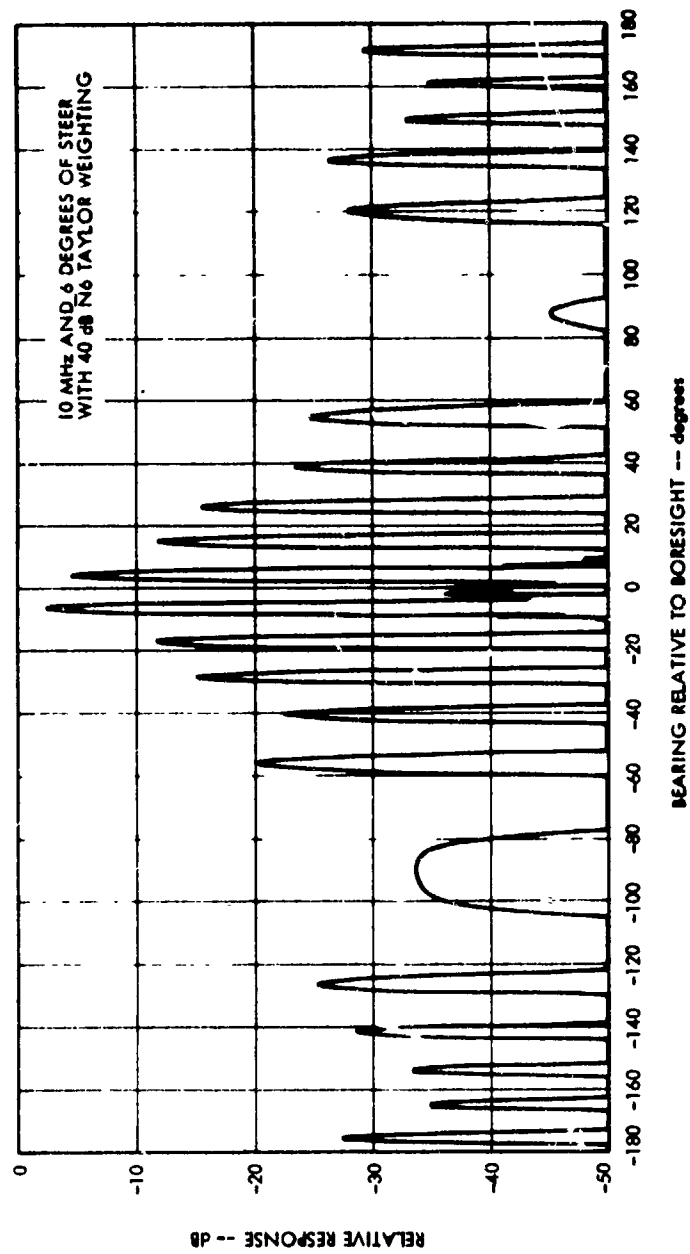
Figure 20.   Ideal Relative Pattern of the Polar Recap III Beverage Array.

(37)

Table 3. Relative Amplitude (in dB) of Polar Recap III
Beverage Array Elements Before and After
Repairs and Attenuator Installation (Element
20 used as reference)

ELEMENT	BEFORE	AFTER
1	2.5	-14.5
2	2.5	-14.5
3	0.5	-16.5
4	2.5	-14.5
5	- 2.0	- 9.5
6	0	- 7.5
7	- 1.5	- 9.0
8	- 3.0	-10.5
9	- 8.5	- 2.0
10	- 8.0	- 1.5
11	- 8.0	- 1.5
12	- 9.0	- 2.5
13	- 2.0	- 1.5
14	- 0.5	- 5.5
15	- 0.5	0
16	0	0.5
17	1.0	1.0
18	0.5	0.5
19	0	0
20	0	0
21	2.0	- 0.5
22	1.5	- 1.0
23	2.0	- 0.5
24	0.5	- 2.0
25	0.5	- 6.0
26	0	- 6.5
27	- 0.5	- 7.0
28	- 1.0	- 7.5
29	-23.0	-16.0
30	-22.5	-15.5
31	-22.0	-15.0
32	-22.0	-15.0

Using the amplitude values in Table 3, patterns were calculated for the array.
Since no realistic estimate could be made concerning the phasing cables, these
patterns were calculated using ideal phase for the beam-forming network. No definite
data were obtained as to even the phasing procedure except that a time domain re-
flectometer (TDR) was used. There was no information concerning the TDR settings
and conditions. Hence, the ideal phase was used which results in patterns which are
optimistic at least.

(38)

The series of patterns were calculated for boresight (0° steer) and 3° steer as it was decided not to use 6° steer. The patterns are shown in Figures 21 through 28. Figures 21 and 25 shown the power gain factor with respect to an ideal uniformly illuminated array. From the values it is seen that repairing the array restored approximately the same gain as the Taylor weighting required.

2.7 BEAM-FORMING NETWORK ERRORS

The array pattern shown in Figure 9, the measured pattern, and the calculated patterns shown in Figures 21 through 28, illustrate that the ideal calculated patterns are difficult to achieve in practice. The errors in phase and amplitude, which are inevitable in any real system, will reduce the ideal to the achievable.

In the past and in the above examples, the arrays were constructed, the errors measured, and the patterns calculated. This procedure certainly allows the designer to determine what he has constructed. However, it is desirable to be able to predict the results of a design, within given limits, so that it will be neither over nor under specified.

Because of errors in cable construction and other factors, the amplitudes and phases of the signals present at the several input ports of the beam-forming network will not be the ideal values for which the summing network was designed. This will result in higher sidelobe levels than could be obtained with ideal signals. In the following paragraphs it will be assumed that these amplitude and phase errors can be kept within specified tolerance levels. It will then be assumed that the errors introduced can be considered random variables, the statistics for which are determined by the specified tolerance levels. Finally the expected sidelobe level will be calculated in terms of the root-mean-square (rms) values of the random input phase and amplitude errors.

(39)
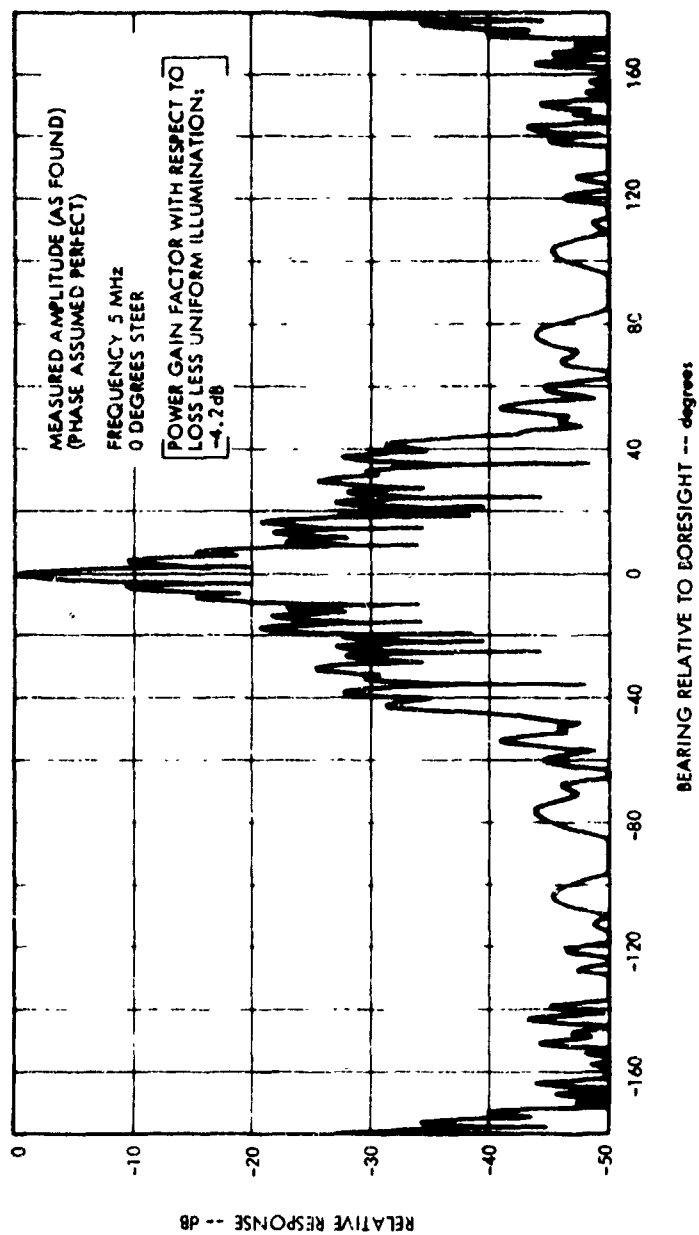
Figure 21. Polar Recap III Beverage Array.

(40)
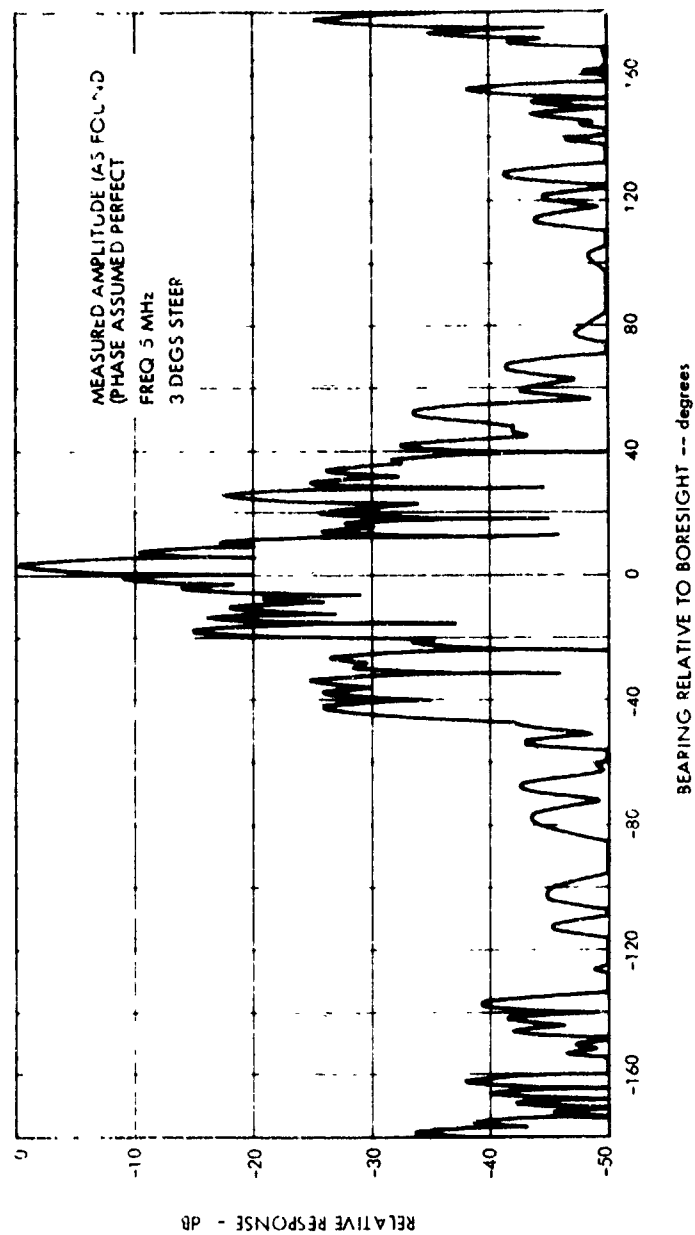
Figure 22. Polar Recap III Beverage Array.

(41)
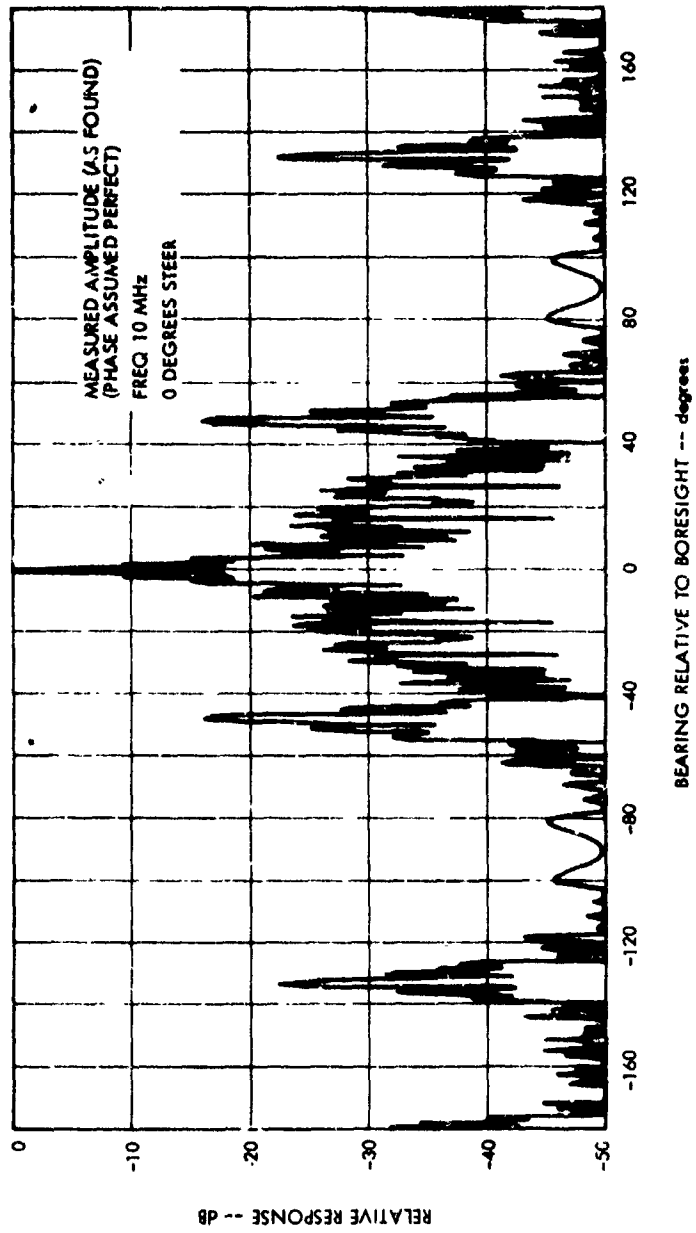
Figure 23. Polar Recap III Beverage Array.

(42)
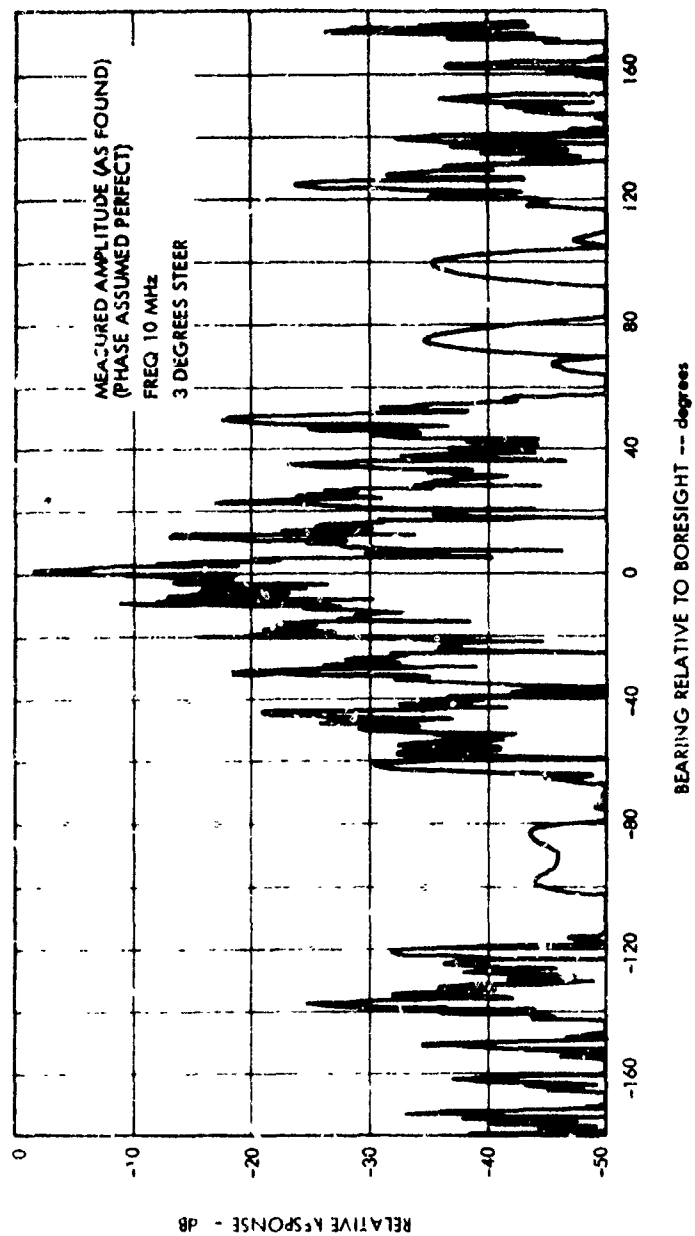
Figure 24. Polar Recap III Beverage Array.

(43)
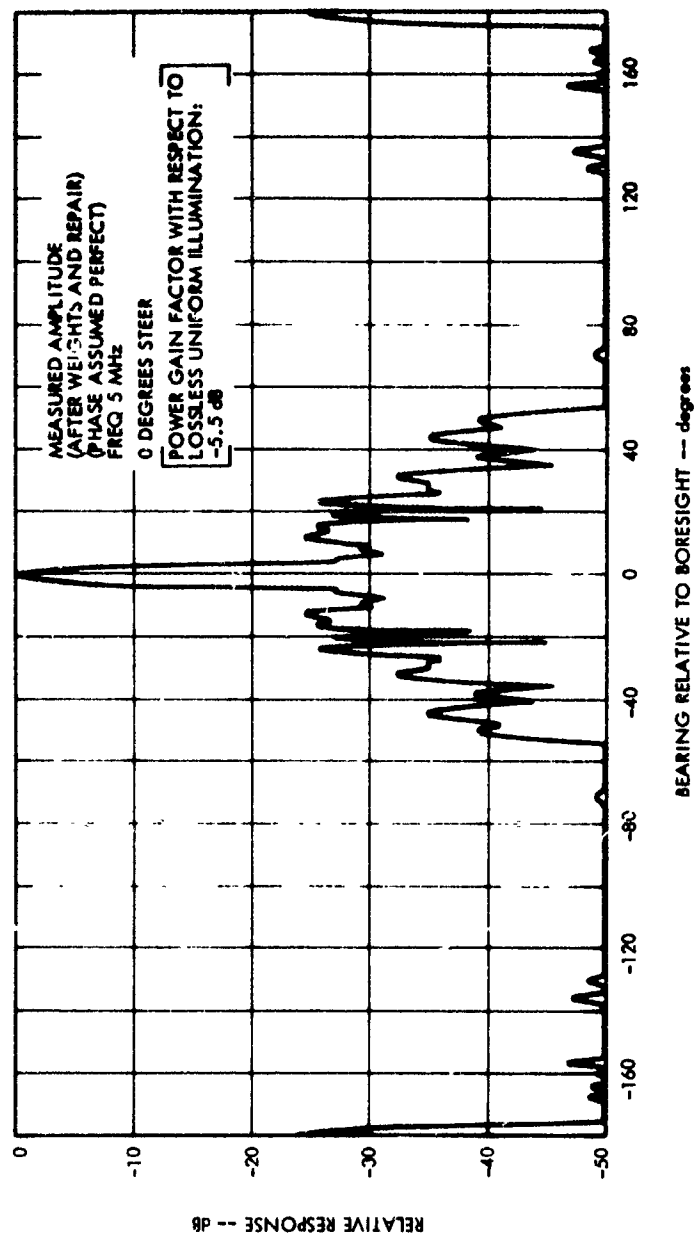
Figure 25. Polar Recap III Beverage Array.

(44)
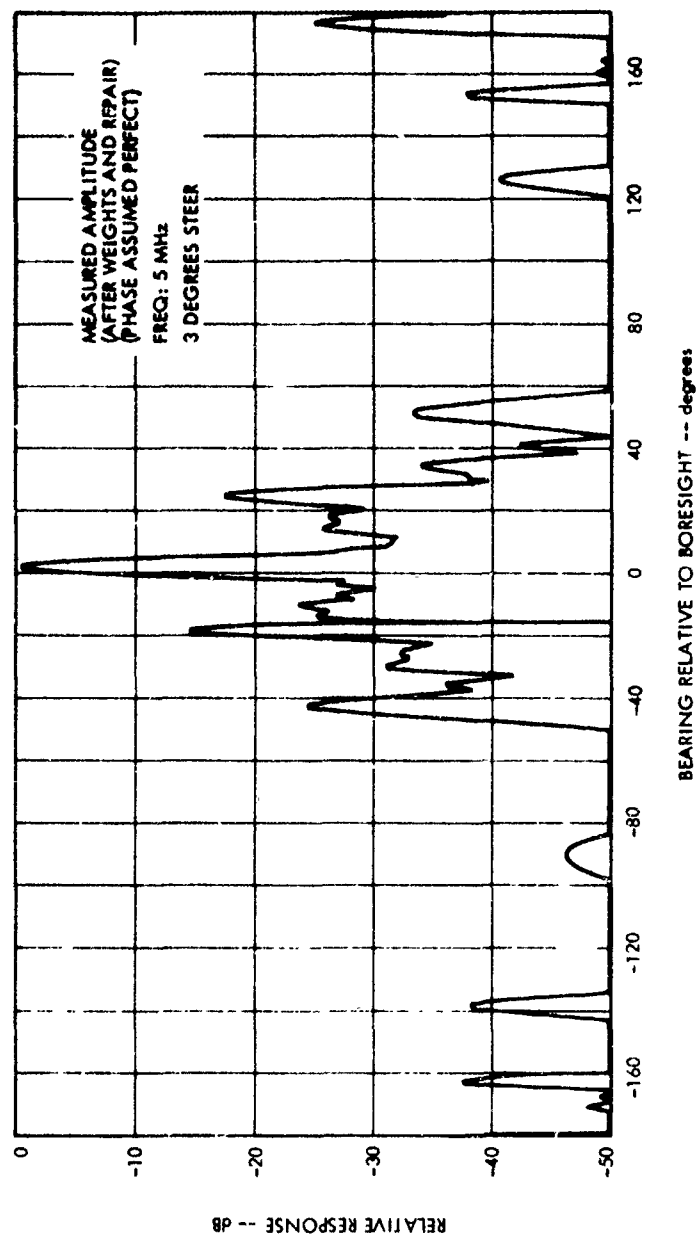
Figure 26. Polar Recap III Beverage Array.

(45)
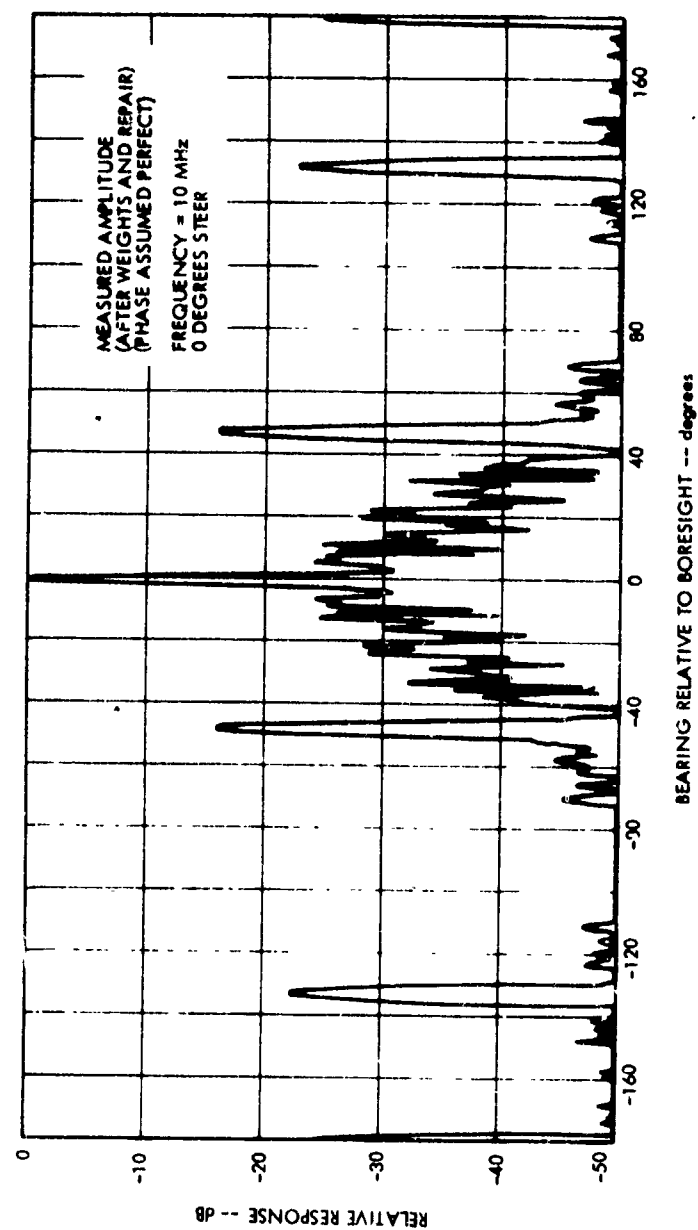
Figure 27.   Polar Recap III Beverage Array.

(46)
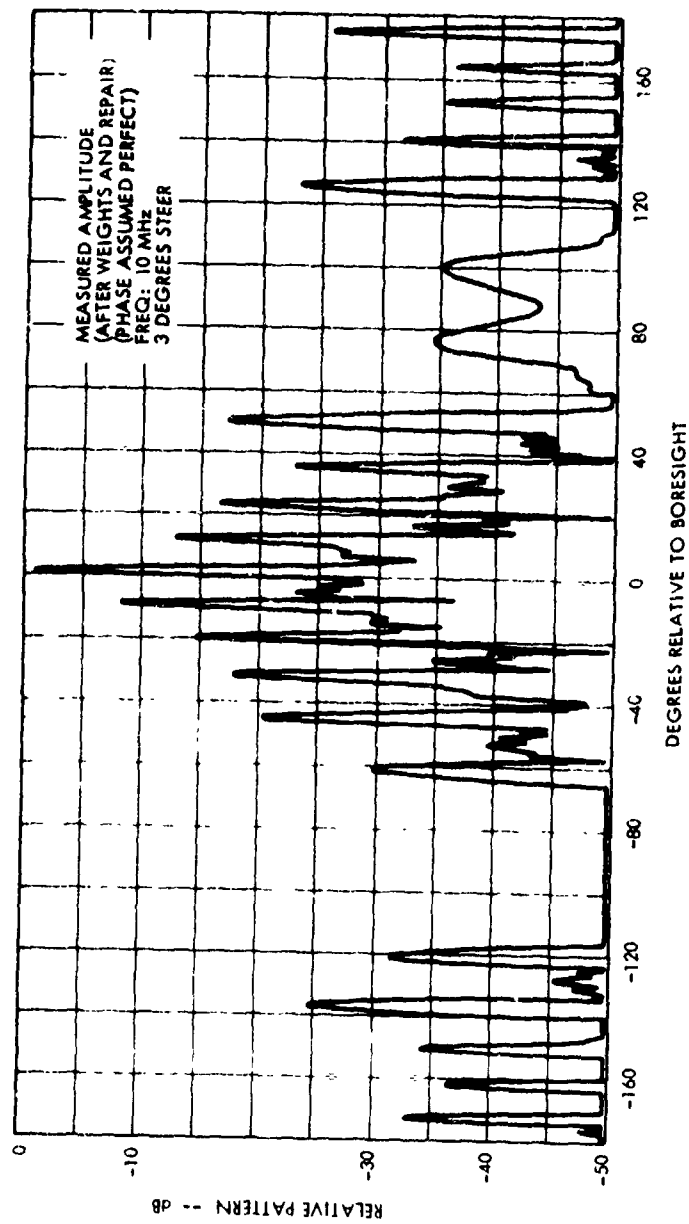
Figure 28. Polar Recap III Beverage Array.

(47)

2.7.1 Sidelobe Analysis

It is assumed that the signal S_k present at the kth input port of the beam-forming network (summing network) is of the form

$$S_k = A_k (1+a_k)e^{i(\varphi_k + \epsilon_k)} \tag{1}$$

where

A_k = the amplitude of the ideal signal at the kth input port

φ_k = the phase angle of the ideal signal at the kth input port (determined by array geometry and the direction of arrival of the incoming radio wave)

a_k = the random amplitude error at the kth input port

ϵ_k = the random phase error at the kth input port.

If there are N input ports to the summing network, there will be 2N random variates a_k, ϵ_k, $k = 1, \ldots, N$. It is assumed that the a_k are independent, identically distributed random variates with zero mean and rms value σ_a. Similarly, the ϵ_k are assumed to be independent, identically distributed random variates with zero mean and rms value σ_ϵ.[*] It is further assumed that the angle variates ϵ_k are uncorrelated with the amplitude variates a_k.

The summing network multiplies each input signal by a weighting coefficient C_k and produces an output sum, the squared amplitude of which is

$$\left| \text{Output} \right|^2 = \left| \sum_k c_k A_k (1+a_k)e^{i(\varphi_k + \epsilon_k)} \right|^2 . \tag{2}$$

For an ideal antenna array, the ideal amplitudes A_k would have a common value at all input ports. For simplicity, it will be assumed that common value is unity, in which case the A_k may be dropped from equation 2, which may then be rewritten as

[*]The effect of non-zero means would be to merely introduce a constant multiplicative factor common to all input ports. This would have no effect on the calculated sidelobes. On the other hand, violation of the assumption that the several random variables are independent (therefore uncorrelated) would introduce additional distortions not included in this present analysis. A more detailed analysis would allow for off-diagonal elements in the correlation matrix of the random variates.

(48)

$$\left|\text{Output}\right|^2 = \left[\sum_k c_k (1+a_k)e^{i(\varphi_k + \epsilon_k)}\right]\left[\sum_l c_l (1+a_l)e^{-i(\varphi_l + \epsilon_l)}\right] \tag{3}$$

$$= \sum_k c_k^2 (1+2a_k + a_k^2) + 2\sum_{k>l} c_k c_l (1+a_k + a_l + a_k a_l) \cos\left[(\varphi_k - \varphi_l) + (\epsilon_k - \epsilon_l)\right].$$

The assumption is now made that the error angle term ($\epsilon_k - \epsilon_l$) which appears in equation 3 is small compared to 1 radian. This yields approximately

$$\cos\left[(\varphi_k - \varphi_l) + (\epsilon_k - \epsilon_l)\right] = \left[1 - \frac{(\epsilon_k - \epsilon_l)^2}{2}\right]\cos(\varphi_k - \varphi_l) - (\epsilon_k - \epsilon_l) \tag{4}$$
$$\sin(\varphi_k - \varphi_l).$$

Averaging equation 3 and using equation 4 obtains for the expected (average) value of the squared output amplitude

$$\overline{\left|\text{Output}\right|^2} = \sum_k (1 + \sigma_a^2) c_k^2 + 2\sum_{k>l} (1 - \sigma_\epsilon^2) c_k c_l \cos(\varphi_k - \varphi_l)$$
$$= (\sigma_a^2 + \sigma_\epsilon^2)\sum_k c_k^2 + (1 - \sigma_\epsilon^2)\left[\sum_k c_k^2 + 2\sum_{k>l} c_k c_l \cos(\varphi_k - \varphi_l)\right]$$
$$= (\sigma_a^2 + \sigma_\epsilon^2)\sum_k c_k^2 + (1 - \sigma_\epsilon^2)\left|\sum_k c_k e^{i\varphi_k}\right|^2, \tag{5}$$

where the bar over a quantity denotes "expected value" and where the previous assumptions of uncorrelated random variates with zero mean has been used.

The last factor on the righthand side of equation 5 is recognized as the value that would be present at the output of the summing network if only ideal signals (no errors) were present at the input ports. It has been further assumed that the rms value of the angle errors is small compared to unity; it is seen then from equation 5 that the principal effect of the random amplitude and phase errors is to add a term $(\sigma_a^2 + \sigma_\epsilon^2)\sum c_k^2$ to the output of the summing network. This is equivalent to injecting noise into the system at the output of the beamforming network.

The ideal output attains its maximum value when the ideal phase angles φ_k are all zero (incoming radio wave on boresight):

$$\left|\text{Max ideal output}\right|^2 = \left|\sum c_k\right|^2. \tag{6}$$

Dividing equation 5 by equation 6 yields (assuming $\sigma_\epsilon < 1$).

$$\frac{\left|\text{Output}\right|^2}{\left|\text{Maximum ideal output}\right|^2} = \frac{\left|\text{Ideal Output}\right|^2}{\left|\text{Max ideal output}\right|^2} + \frac{\sigma_a^2 + \sigma_e^2}{I} \qquad (7)$$

where $\qquad \left|\text{Ideal Output}\right|^2 = \left|\sum_k c_k e^{i\varphi_k}\right|^2$

$$I = \left|\sum_k c_k\right|^2 / \sum c_k^2 \qquad\qquad \begin{array}{l}= \text{integration (or summing) gain} \\ \text{of beam-forming network.}\end{array}$$

We will call the quantity $\left|\text{Ideal Output}\right|^2 / \left|\text{Max ideal output}\right|^2$ the ideal arraying factor (IAF). It has a maximum value of unity. For a linear array, IAF will depend on the angle δ ($0 \leq \delta \leq 180°$) which the direction of the incident plane radio wave makes with the (directed) axis of the linear array, the axis being the straight line along which the individual elements are placed. The three dimensional representation of IAF(δ) is a figure of revolution about the array axis. For an unsteered array, the plane which is normal to the axis and which passes through the mid-point of the axis is a plane of symmetry: IAF(δ) = IAF($180°-\delta$). The boresight of the array lies some-where in this plane of symmetry*, the angle δ for which is $\delta = 90°$. The function IAF(δ) gives the shape of the "arraying pattern", and the main lobe** of the arraying pattern occurs in a relatively small angular region centered at $\delta = 90°$. If the angle δ is in the region of the main lobe it will be called a main lobe angle, ortherwise it will be called a sidelobe angle.

For angles δ in the sidelobe region (that is outside of the main beam region), ideal sidelobe level is as defined.

*   The presence of phase errors in a real system will destroy the symmetry of the real arraying pattern, and real boresight need no longer be at $\delta=90°$. However the presence of amplitude errors (not accompanied by phase errors) would not destroy the symmetry.

** If the array is steered an angle α ($-90° \leq \alpha \leq 90°$) away from boresight, there will be no plane of symmetry for the array. The main lobe will then occur in a conical region (the axis of the cone being the same as the axis of the array) centered on the angle $\delta=90°-\alpha$.

$$SL_{ideal} = \frac{\left|\text{Ideal Output from sidelobe angle } \delta\right|^2}{\left|\text{Max Ideal output}\right|^2} = IAF \tag{8a}$$

Similarly, the expected (or averaged) sidelobe level (where the average is to be taken over the phase and amplitude errors at the input ports) is defined as

$$SL_{av} = \frac{\overline{\left|\text{Output from sidelobe angle } \delta\right|^2}}{\left|\text{Max ideal output}\right|^2} \tag{8b}$$

With these definitions it is at once obtained from equation 7:

$$SL_{av} = SL_{ideal} + (\sigma_a^2 + \sigma_\epsilon^2)/L \tag{9}$$

A eraging equation 9 over all sidelobe angles, the desired practical formula is obtained:

$$\overline{SL_{av}} = \overline{SL_{ideal}} + \frac{\sigma^2}{I}, \tag{10}$$

where

$$\sigma = \sqrt{\sigma_a^2 + \sigma_\epsilon^2} = \text{total rms input error} \tag{10a}$$

and the bar over a quantity again denotes averaged value. It should be noted that the average (or expected) sidelobe level $\overline{SL_{av}}$ has been obtained by averaging over all sidelobe angles and also over the amplitude and phase errors at the input ports.

In the above derivation, all angles were expressed in radians and σ_ϵ is the rms angle error also expressed in radians, which is a dimensionless quantity. The amplitude errors a_k were also expressed in dimensinless form

$$a_k = \frac{\text{Amplitude at } k^{th} \text{ port - Ideal amplitude at } k^{th} \text{ port}}{\text{Ideal amplitude at } k^{th} \text{ port}}.$$

The rms amplitude error σ_a is then also dimensionless. The total rms input error σ as given by equation 10a is then also dimensionless.

To express the amplitude error in logarithmic form (that is, in terms of dB), use is made of the logarithmic amplitude error LAE defined as

$$LAE = 20 \log_{10}(1+a) \simeq 8.68 a \text{ (for small "a")}$$

(51)

where a is the dimensionless amplitude error defined above and LAE is the amplitude error expressed in decibels. To keep LAE within ± 0.2 dB, "a" must be kept within ± 0.023.

All of the above discussion is independent of the precise statistical distributions of the random errors. They may be gaussian, uniform, or any other. However, for the purposes of specifying tolerances, it is desirable to connect the rms values σ_a and σ_ϵ of the random errors to a maximum permissible error, or tolerance, which the system designer might then use to "spec" the system. To do this, it becomes necessary to assume some convenient statistical distribution for the anticipated errors. For this purpose, it will be assumed that the errors are uniformly distributed between $\pm t$, where t is the tolerance value. For a uniform distribution, the tolerance t is related to the rms value σ by

$$t = \sqrt{3}\ \sigma.$$

Applying this formula yields for the phase error tolerance t_ϵ (degrees) expressed in degrees

$$t_\epsilon(\text{degrees}) \ = \ \frac{180}{\pi} \sqrt{3}\ \sigma_\epsilon \approx 100\ \sigma_\epsilon, \tag{10b}$$

and for the logarithmic amplitude error (expressed in dB)

$$t_{LAE} \ = \ 8.68 \sqrt{3}\ \sigma_a \approx 15\ \sigma_a \tag{10c}$$

where σ_ϵ and σ_a are the dimensionless rms errors defined above.

It should be stressed that the rms values σ_a, σ_ϵ are the physically important quantities. The tolerance levels given by these last two equations merely express the σ on a different scale. However these tolerance levels are of value in that they are suggestive of some maximum error, namely the maximum error associated with given σ if the errors were uniformly distributed. The conservative system engineer might wish to assume that the statistical distribution for the random errors were more like

(52)

$$\text{error} = \begin{cases} t \text{ with probability } 1/2 \\ -t \text{ with probability } 1/2. \end{cases}$$

The rms value σ for this distribution is $\sigma = t$. With this more conservative viewpoint, the system engineer would choose his tolerances to be a factor of $\sqrt{3}$ smaller than those given by equations 10b and 10c.

The expected sidelobe levels were calculated from equation 10 for:

(a) 50 dB, $\overline{N}6$ and 60 dB, $\overline{N}7$ Taylor weighting of the aperture;

(b) apertures of 10, 20, 40, and 80 wavelengths; and

(c) numbers of ports 32, 64, 128, and 256.

These values were plotted as a function of the total rms input error σ and are shown in Figures 29 and 30.

2.8 CONSTANT BEAMWIDTH COEFFICIENTS

The use of multiple beams to form beams of nearly constant beamwidth has been previously reported. The present RADC beverage array at Dexter forms the individual beams and then sums five natural beams to form a combined beam. The concept of element NESTS was also previously reported to accomplish the same purpose. With the use of an element NEST, the multiple beam is formed and the remaining beam-forming network is required to steer only the wider beam.

The element NEST essentially generates an additional set of aperture weighting coefficients of $\sin(x)/(x)$ distribution to give a square response in the spatial domain. These coefficients are frequency dependent. However, the NESTS will provide the current coefficient distribution according to the frequency of the signal, thereby providing a frequency independent beam-forming network.

Through the use of the NEST, the coefficients can be calculated at a frequency for evaluation of the beam-forming network performance at the selected frequency. The parameters which can then be evaluated include:

(a) Power gain factor (PGF)

$$\frac{\left[\sum_{1}^{N} C_n \right]^2}{N^2} \tag{11}$$

(53)
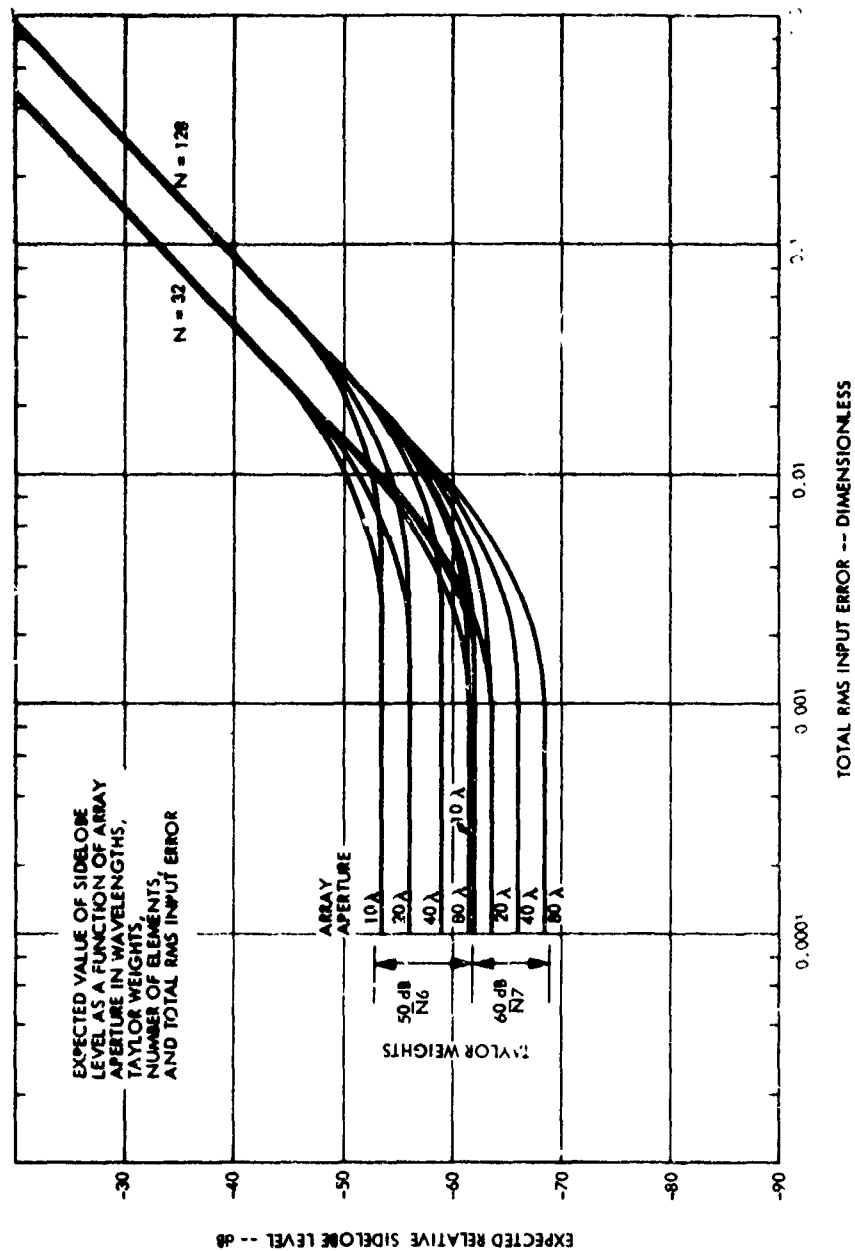
Figure 29. Expected Value of Sidelobe Level.

(54)
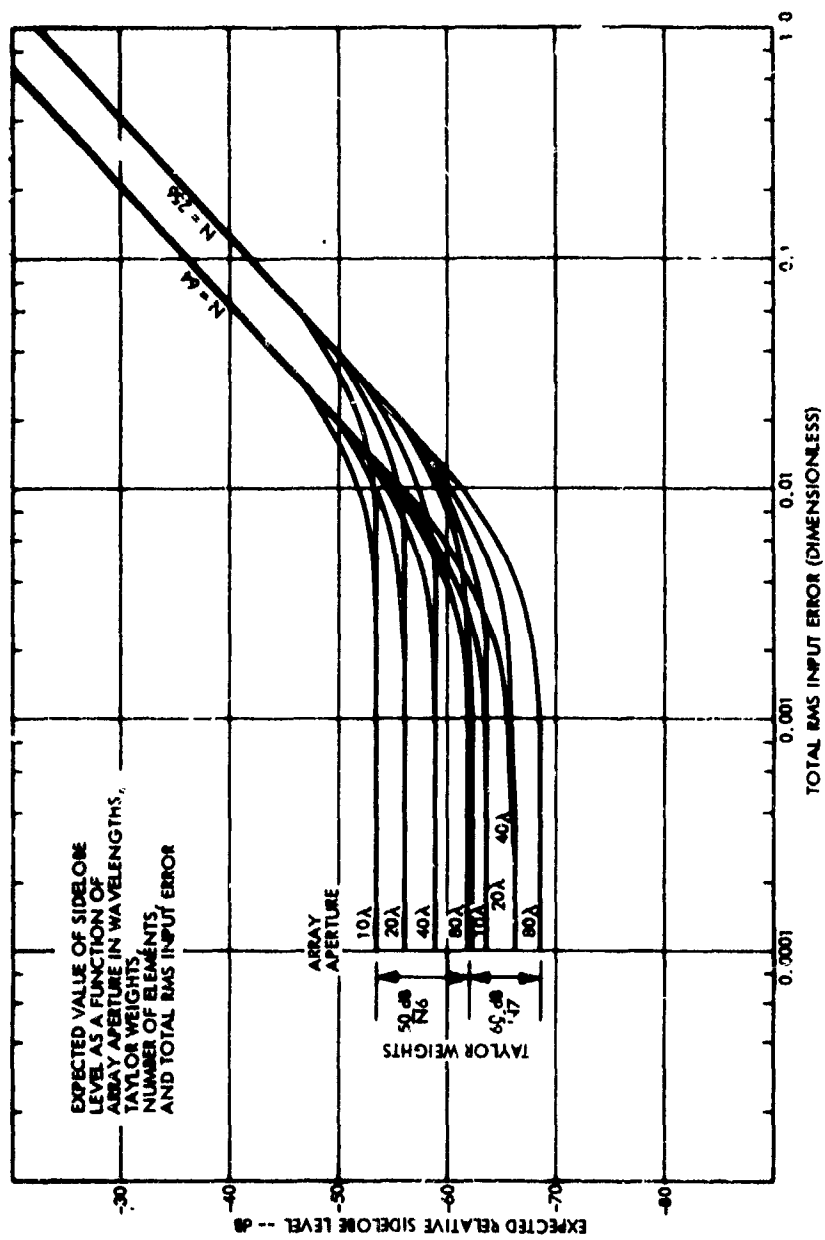
Figure 30. Expected Value of Sidelobe Level.

(55)

(b) Signal to noise ratio factor (SNRF)

$$\frac{\left[\sum\limits_{1}^{N} C_n\right]^2}{N \sum\limits_{1}^{N} C_n^2} \qquad\qquad (12)$$

(c) Expected sidelobe level (SL)

$$\overline{SL_{av}} = \overline{SL_{ideal}} + \frac{(\text{Total rms input Error})^2}{N(\text{SNRF})} \qquad (13)$$

The approximate values for the power gain factor of the array (PGFA) and SNR factor of the array (SNRFA) in dB can be found by using the following empirical approximations:

$$PGFA = 20 \log \left\{ \frac{BA_{(6\ dB)}}{BN_{(6\ dB)}} \right\} + PGLW \qquad (14)$$

$$SNRFA = 10 \log \left\{ \frac{BA_{(3\ dB)}}{BN_{(3\ dB)}} \right\} + SNRLW \qquad (15)$$

where:

BA_{3dB} and BA_{6dB} are the 3 and 6 dB beamwidths of the final array;

BN_{3dB} and BN_{6dB} are the 3 and 6 dB beamwidths of the natural array with the aperture weighting used;

PGFW is the power gain factor of the aperture weighting used; and

SNRFW is the SNR factor of the aperture weighting used.

The minimum number of beams to use in a NEST is

$$\text{minimum beams} = \text{integer value of } \left\{ \frac{(\text{desired beamwidth})}{BN_{(3\ dB)}} + .5 \right\} \qquad (16)$$

The maximum number of beams to use in the NEST is the designer's choice, as the array performance varies only slightly with the number of beams used once the minimum beam criterion is met. The beam positioning (for the purpose of NEST design) is found as follows:

(a) $BN_{(3dB)}$ as previously defined, at the highest frequency,

(b) K as the number of beams used in NEST equal to or greater than the minimum found above,

(c) $BA_{(3dB)}$ as previously defined,

(d) A as the "beam" aperture required to obtain the desired $BA_{(3dB)}$ and $A > BA_{(3dB)}$.

The positions of the two outside beams are such that the difference between the lower (in bearing) 3 dB point of one beam and the upper (in bearing) 3 dB of the other beam is equal to A, as shown in Figure 31.

$$\text{Beam Spacing} = \frac{(A - BN (3_{db}))}{K - 1} ; \tag{17}$$

and the beam bearing of the kth beam becomes,

$$\text{Bearing (k)} = (A - BN_{3 \, dB}) \left[\left(\frac{k - 1}{k - 1} \right) - 0.5 \right] , \tag{18}$$

where: $1 \le k \le K$.

For an array of N elements, the length (L) of the NEST cable for the nth element and k^{th} beam becomes,

$$L (n, k) = L_{ref} + \left[n - \frac{N+1}{2} \right] (S) \text{Sin (Bearing (k))} \tag{19}$$

where: $L_{rel} = \left[\frac{N-1}{2} \right] (S) \text{Sin (Bearking (K)}$ and $\tag{20}$

S = element spacing in feet for L(n, k) in feet.
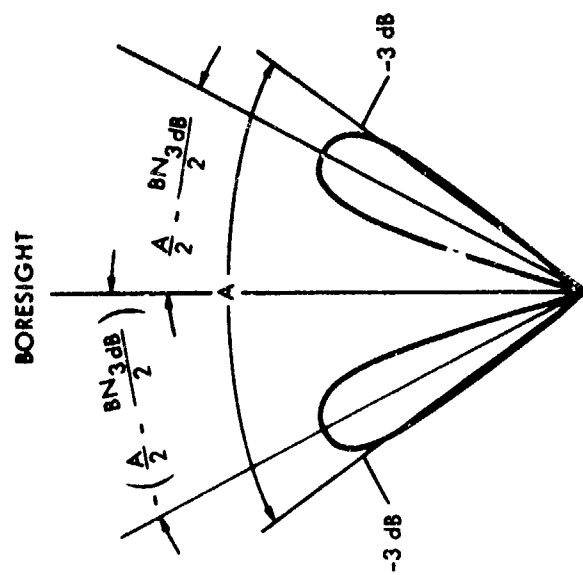
Figure 31. Positioning of the Two Outermost Natural Beams for a Nest Design.

(58)

2.8.1 Array Example 1

An array design, having the following parameters was selected.

Frequency Range	8 - 30 MHz
Number of Elements	96
Nominal Design Beamwidth	5°
Element Spacing	23 ft
Aperture Weighting	50 dB $\overline{N}5$ Taylor Weighting
Power gain factor	-5.77 dB
Signal-to-noise ratio factor	-1.53 dB
Natural 3 dB Beamwidth	1.14° at 30 MHz
Minimum number of Beams	4

The array synthesis was performed using four, six, eight, and ten beams in the NEST calculations. The 3 dB beamwidth of the design (minimum number of beams) is shown in Figure 32 and the power gain factor and SNR factor are shown in Figure 33.

The power gain factor is always less than unity and represents the reduction (relative to a uniformly illuminated aperture, i.e. one for which all weighting co-efficients are unity) in output power caused by the weighting coefficient. Similarly, the SNR factor is always less than unity and represents the reduction (relative to a uniformly illuminated aperture) in SNR caused by the weighting coefficients. If uniformly illuminated, the aperture considered for this example would yield a beamwidth of approximately 0.8° at 30 MHz. Such a narrow beam would not be suitable for covering a 5° sector. Since the beamwidth is inversely proportional to the aperture length, in order to produce a 5° beamwidth with uniform illumination, it would be necessary to reduce the aperture by a factor of 6.25. This would cause an approximate 8 dB reduction in SNR (relative to a uniformly illuminated aperture of the full assumed length), also 13 dB sidelobes, and also would require a new aperture for each frequency used. From Fig. 33, it can be seen that at 30 MHz, the use of NESTS causes a similar 8 dB reduction in SNR relative to a uniformly illuminated aperture of the full assumed length. It can be concluded that the NESTS with Taylor weights do not reduce the system SNR below that which would be produced by a uniformly illuminated aperture of the same 5° beamwidth. In addition, the NESTS provide (a) a beamwidth which is relatively independent of frequency, (b) low side-
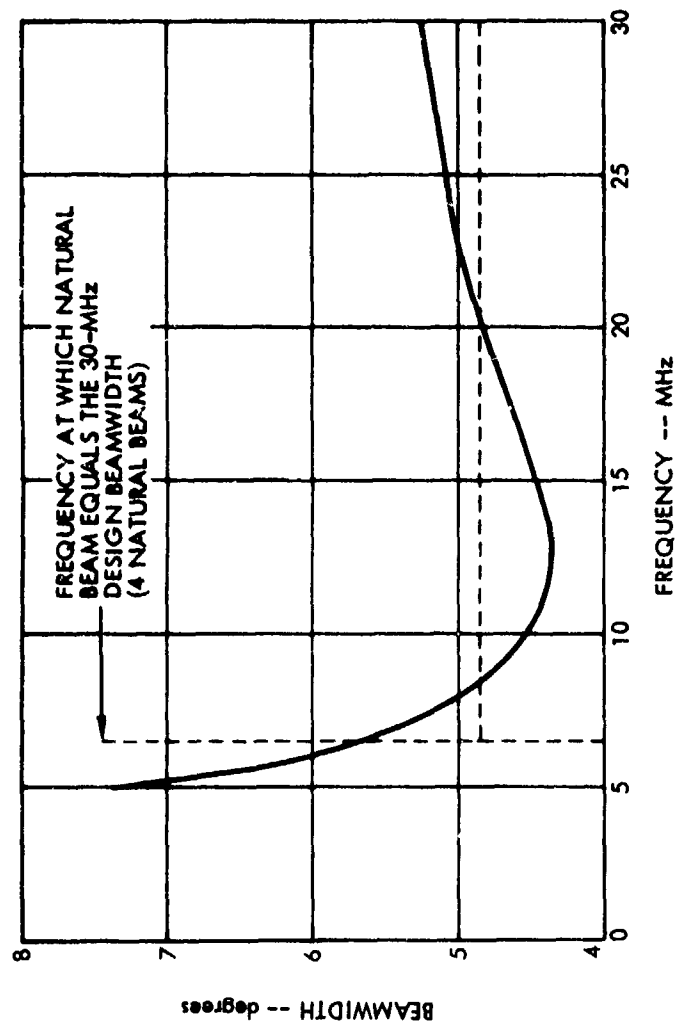
Figure 32.   Beam Width as a Function of Frequency for a Nominal 5 Degree Design.

(60)
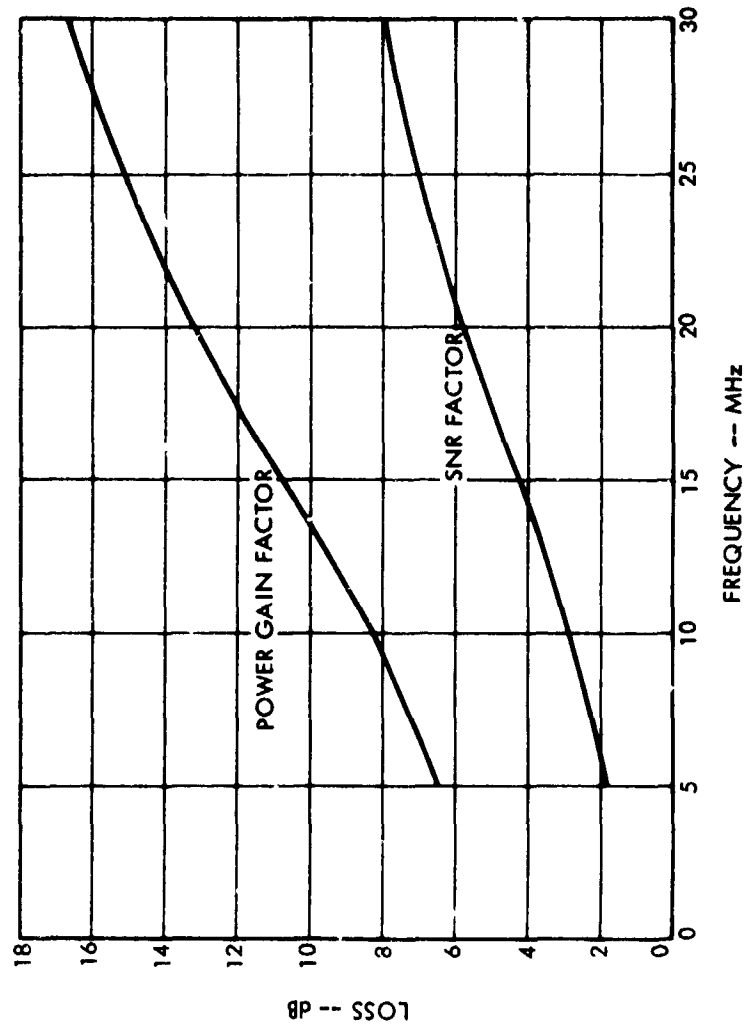
Figure 33. Power Gain Factor and SNR Factor as a Function of Frequency for a Nominal 5 Degree Design.

(61)

lobes (to be discussed shortly) for the rejection of interference and noise, (c) a large number of antenna elements so as to reduce the effects of construction errors.

The shape of the 3 dB beamwidth for all four designs varied only in very minor differences. The results are shown below for the 8 - 30 MHz frequency range.

No. of Beams	3 dB Beamwidth	6 dB Beamwidth
4	4.87° ± 0.39°	6.09° ± 0.27°
6	4.90° ± 0.36°	6.22° ± 0.28°
8	4.91° ± 0.35°	6.25° ± 0.30°
10	4.91° ± 0.35°	6.21° ± 0.27°

The SNR factor and the power gain factor are summarized in Tables 4 and 5.

Table 4. Summary of the SNR Factor Calculated
as a Function of Number of Beams and Frequency

| Frequency (MHz) | SNR Factor (- dB) | | | |
	4 Beams	6 Beams	8 Beams	10 Beams
10	2.74	2.83	2.87	2.77
15	4.25	4.32	4.34	4.24
20	5.84	5.85	5.86	5.76
25	7.01	7.02	7.02	6.92
30	7.92	7.93	7.93	7.83

Table 5. Summary of the Power Gain Factor Calculated
as a Function of Number of Beams and Frequency

| Frequency (MHz) | Power Gain Factor (- dB) | | | |
	4 Beams	6 Beams	8 Beams	10 Beams
10	8.20	8.43	8.49	8.39
15	10.72	10.93	10.98	10.94
20	13.22	13.37	13.41	13.38
25	15.12	15.32	15.35	15.32
30	16.68	16.88	16.92	16.90

The design parameters for array example 1 were used with five beams to design the NESTS and complete patterns calculated and plotted. The ideal patterns are shown in Figures 34, 35, and 36 for 8, 16, and 30 MHz, respectively. These figures show that the sidelobes of the ideal patterns are much lower than the 50 dB Taylor weights used for the aperture weighting. Also, the main beam response has a flat top response at 30 MHz, where the synthesis was referenced. The 22 MHz pattern (not shown) continues to have the flat top response, while at 16 MHz very little flat top response is left. At 8 MHz, the response resembles that of the natural beam which has increased to 4.275°.

2.8.2 Array Example 2

An additional array was selected having the parameters shown below.

Frequency Range	12 - 30 MHz
Number of Elements	128
Element Spacing	20 ft
Nominal Design Bandwidth	6°
Aperture Weighting	50 dB $\overline{N}6$ Taylor Weighting
Power gain factor	-5.77 dB
SNR factor	-1.53 dB
Natural 3 dB Beamwidth	0.98° at 30 MHz
Minimum Number of Beams	6

The NESTS for this array were calculated on the basis of six beams. The ideal patterns were calculated and integrated to obtain the average ideal sidelobe level for three frequencies.

    12.29392 MHz (element spacing = 0.25λ),

    19.67028 MHz (element spacing = 0.4λ), and

    29.50542 MHz (element spacing = 0.6λ).

Using the data calculated from the ideal patterns (average ideal sidelobe level and the SNR factor) and equation 13, the expected sidelobes were calculated as a function of total rms input error for the three frequencies. The expected sidelobes were plotted and are shown in Figure 37.

96 ELEMENTS 23 FEET SPACING
ILLUMINATION: 50 dB N6 TAYLOR

SUMMATION: 5 BEAMS
POWER GAIN FACTOR -7.36 dB
SNR FACTOR -2.28 dB

FREQUENCY = 8 MHz
0 DEGREES STEER
(VERTICAL ANGLE 0 DEG)

BEARING RELATIVE TO BORESIGHT -- degrees

RELATIVE RESPONSE - dB
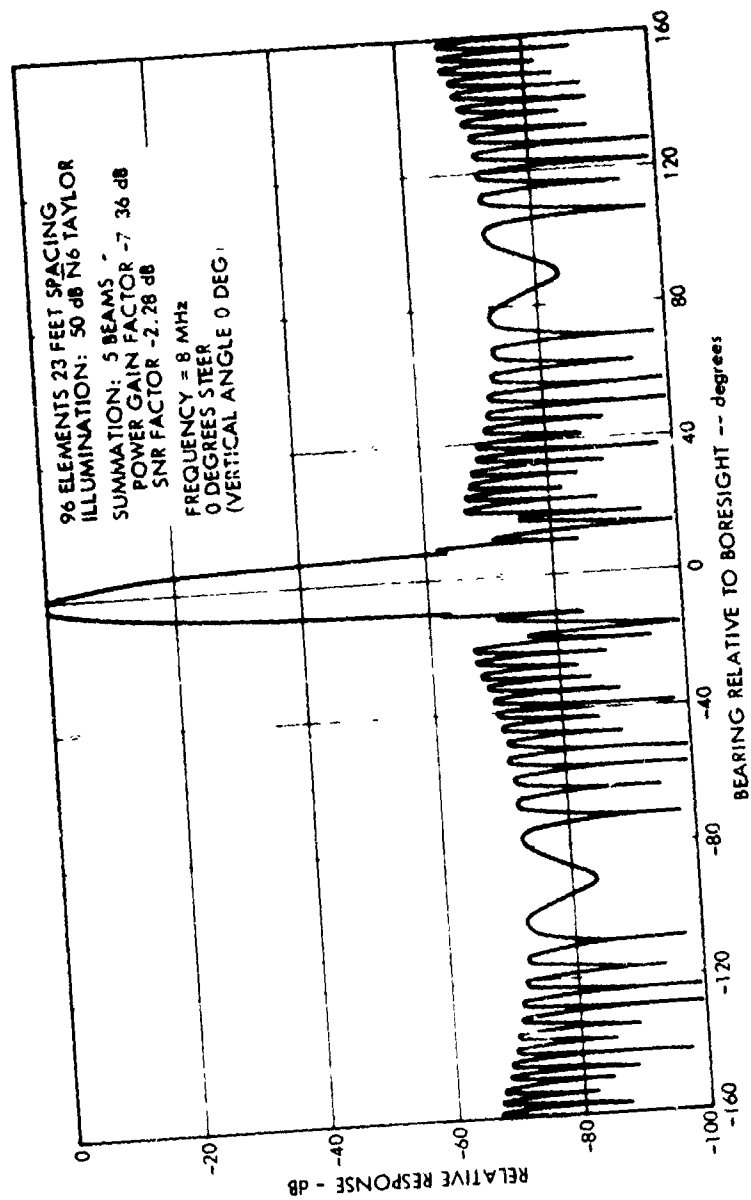
Figure 34. Broadside Pattern.

(64)

96 ELEMENTS 23 FEET SPACING
ILLUMINATION: 50dB, N6 TAYLOR

SUMMATION: 5 BEAMS
POWER GAIN FACTOR -11.16 dB
SNR FACTOR -4.5 dB

FREQUENCY = 16 MHz
0 DEGREES STEER
(VERTICAL ANGLE 0 DEG.)
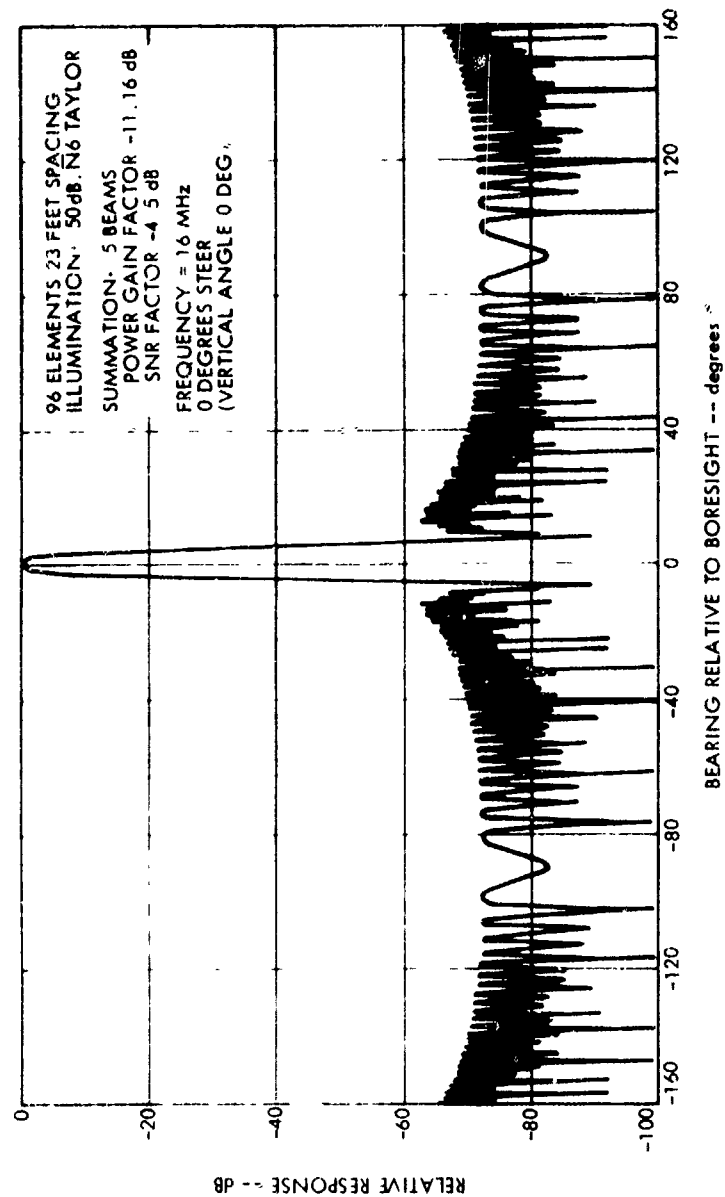
Figure 35.   Broadside Pattern.

(65)

96 ELEMENTS 23 FEET SPACING
ILLUMINATION: 50 dB N̄6 TAYLOR
SUMMATION: 5 BEAMS
POWER GAIN FACTOR -13.94 dB
SNR FACTOR -6.25 dB

FREQUENCY = 30 MHz
0 DEGREES STEER
(VERTICAL ANGLE 0 DEG)

BEARING RELATIVE TO BORESIGHT -- degrees

RELATIVE RESPONSE -- dB
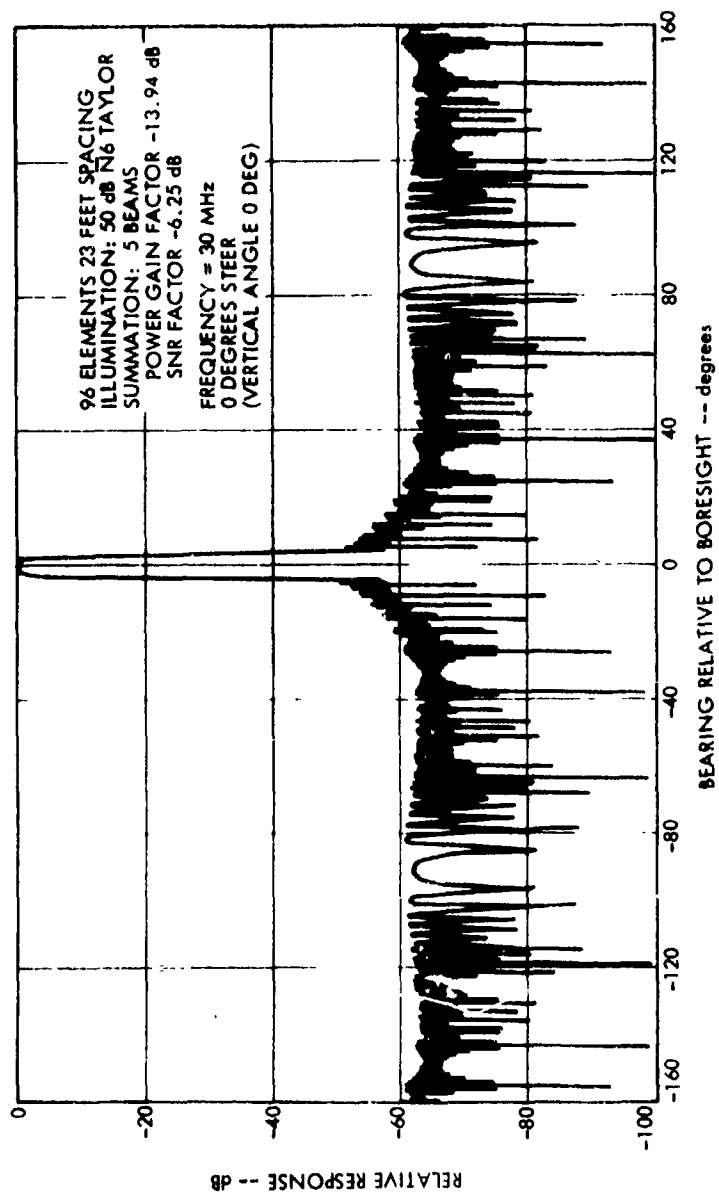
Figure 36. Broadside Pattern.

(66)
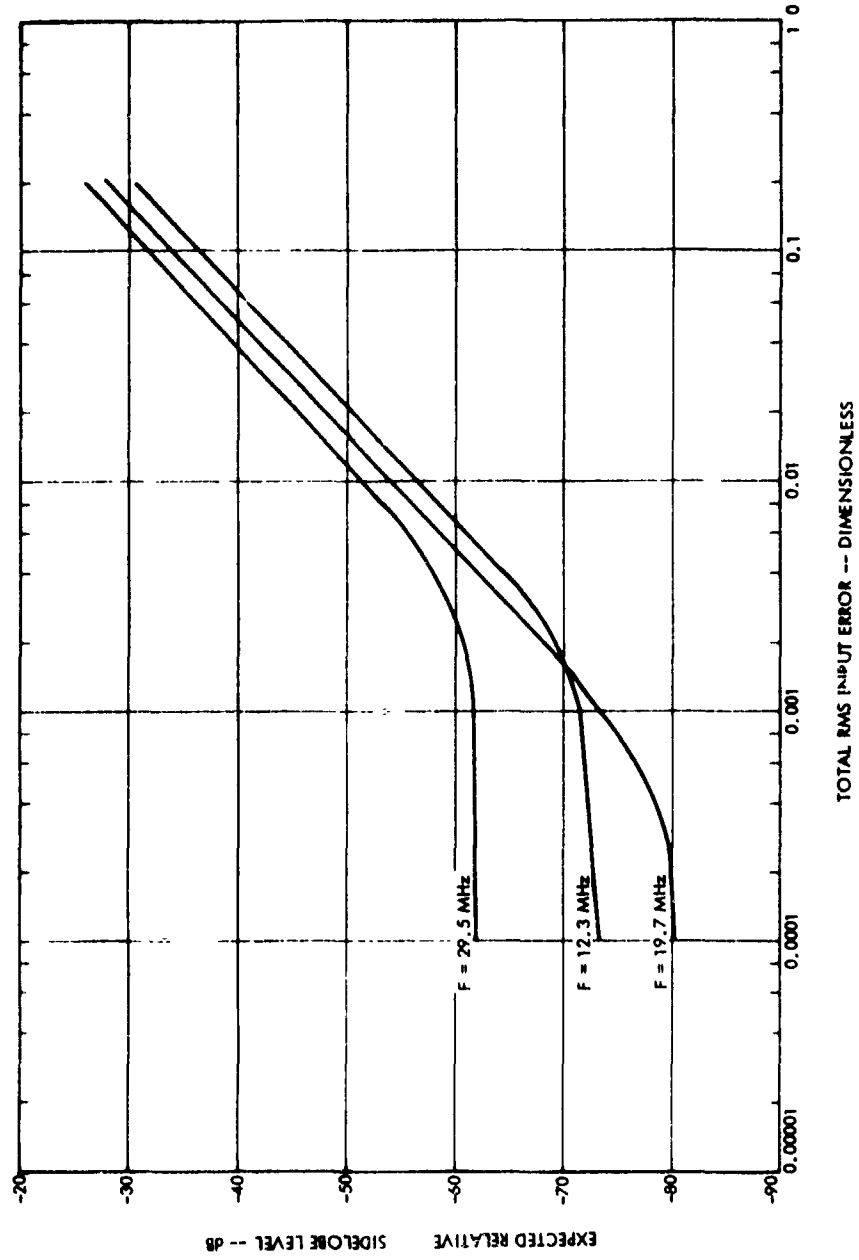
Figure 37. Expected Sidelobe Level as a Function of Frequency and Total RMS Error for Array Parameters of Example 2.

(67)

As a further check on the above calculations, an additional Monte Carlo calculation was undertaken. At each frequency, amplitude and phase errors were selected from a uniform distribution and were used to modify the array coefficients so as to simulate an actual array.

It should be noted that the errors cannot be added directly to the final set of coefficients as would be done with a natural beam. The NEST coefficients are calculated as separate beam-forming networks (which they are) and resulting coefficients are calculated, which are then combined with the remaining beam-forming networks to arrive at a final set of coefficients used to calculate the pattern.

The errors used in the simulation were chosen randomly from a uniform distribution using the following tolerance limits (as defined in Section 2.4.1).

(a)   the phase error was restricted to ±1.5° at 30 MHz and reduced linearly with the frequency ratio;

(b)   the amplitude error was restricted to ±0.2 dB at all frequencies.

For each frequency, one set of errors was chosen randomly, the array coefficients were modified, and the patterns were calculated, plotted, and integrated so as to obtain the average sidelobe level for that particular choice of errors. The plotted ideal patterns and the patterns with the selected errors are shown in Figures 38 through 43 for the three frequencies.

Figure 44 is the error pattern at 29.5 MHz multiplied by a seven element endfire pattern. The endfire element spacing is 106 feet, making a planar array of 128 by 7 elements and spacing of 20 by 106 feet. The reduction of average sidelobe level is readily apparent, even with the endfire grating lobes. A further reduction would be expected if the element pattern is directive.

A summary comparison of the results shown in Figure 37 which are based on equation 13 with the results obtained from these Monte Carlo calculations is given in Table 6. Based on this rather limited number of three comparisons, it can be concluded that the simple formula of equation 13 gives a reasonably accurate (within 2.1 dB for these three comparisons) method for anticipating the average sidelobe level once the rms values for the phase and amplitude errors have been established.

(68)
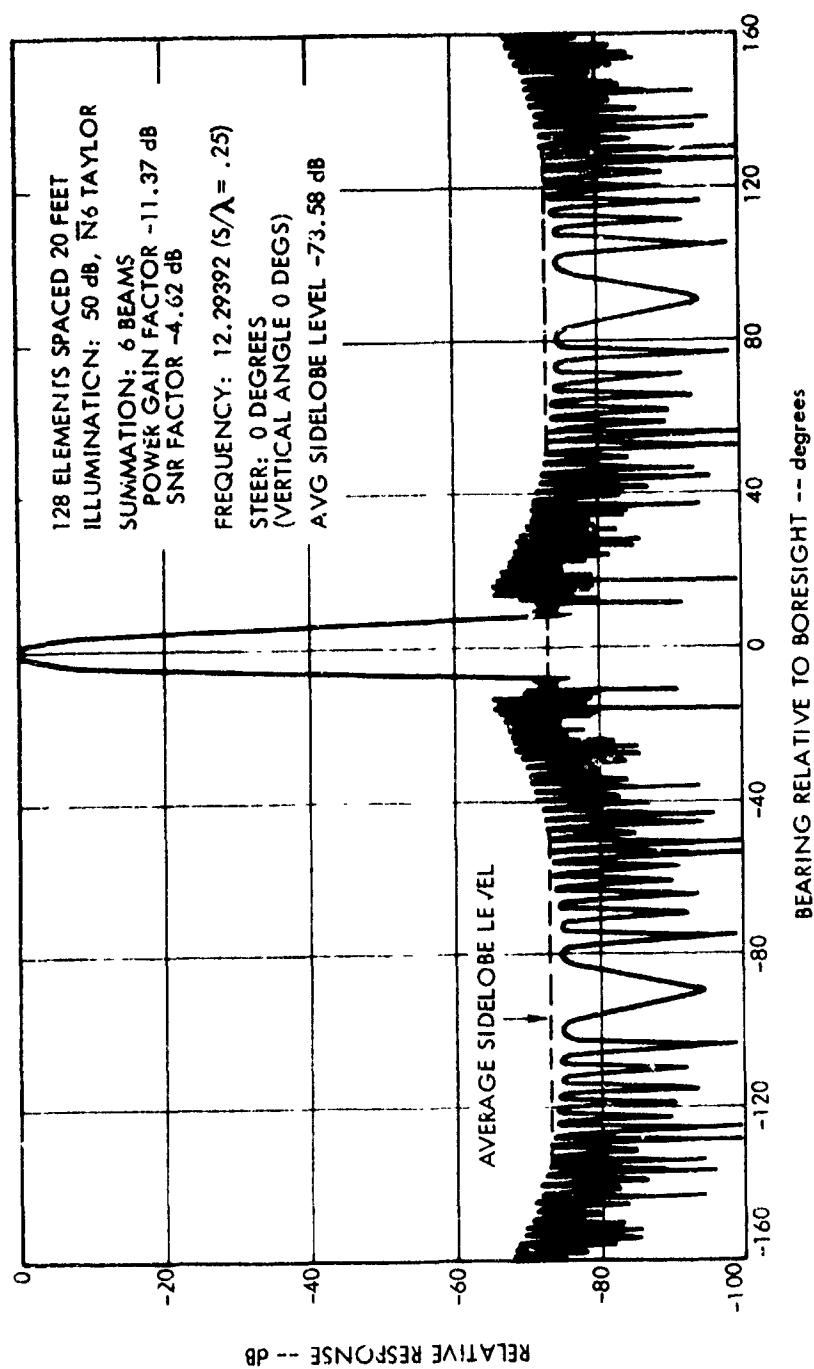
Figure 38. Broadside Pattern.

(69)
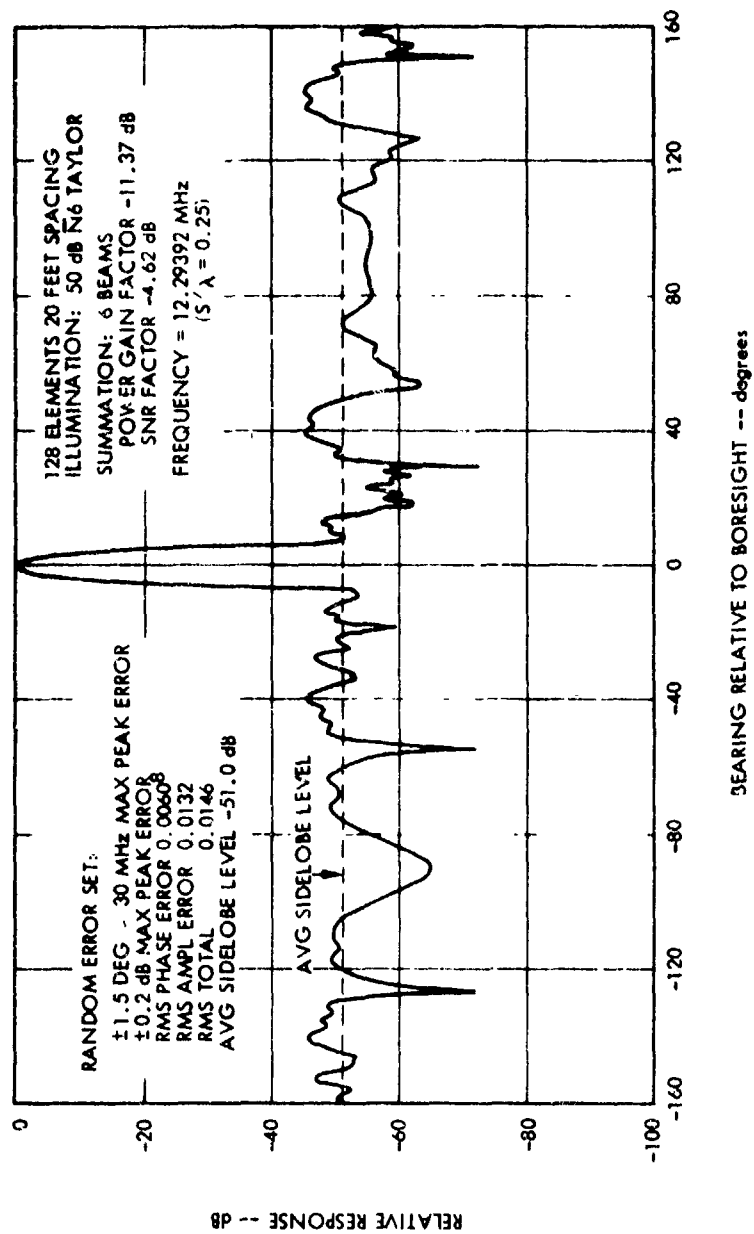
Figure 39. Broadside Array With Errors.

(70)

128 ELEMENTS SPACED 20 FEET
ILLUMINATION: 50 dB N6 TAYLOR

SUMMATION: 6 BEAMS
POWER GAIN FACTOR -15.44 dB
SNR FACTOR -7.72 dB

FREQUENCY = 19.67028 mHz
(S/λ = 0.4)

0 DEGREES STEER
(VERTICAL ANGLE 0 DEG)

AVG SIDELOBE LEVEL -81.59 dB
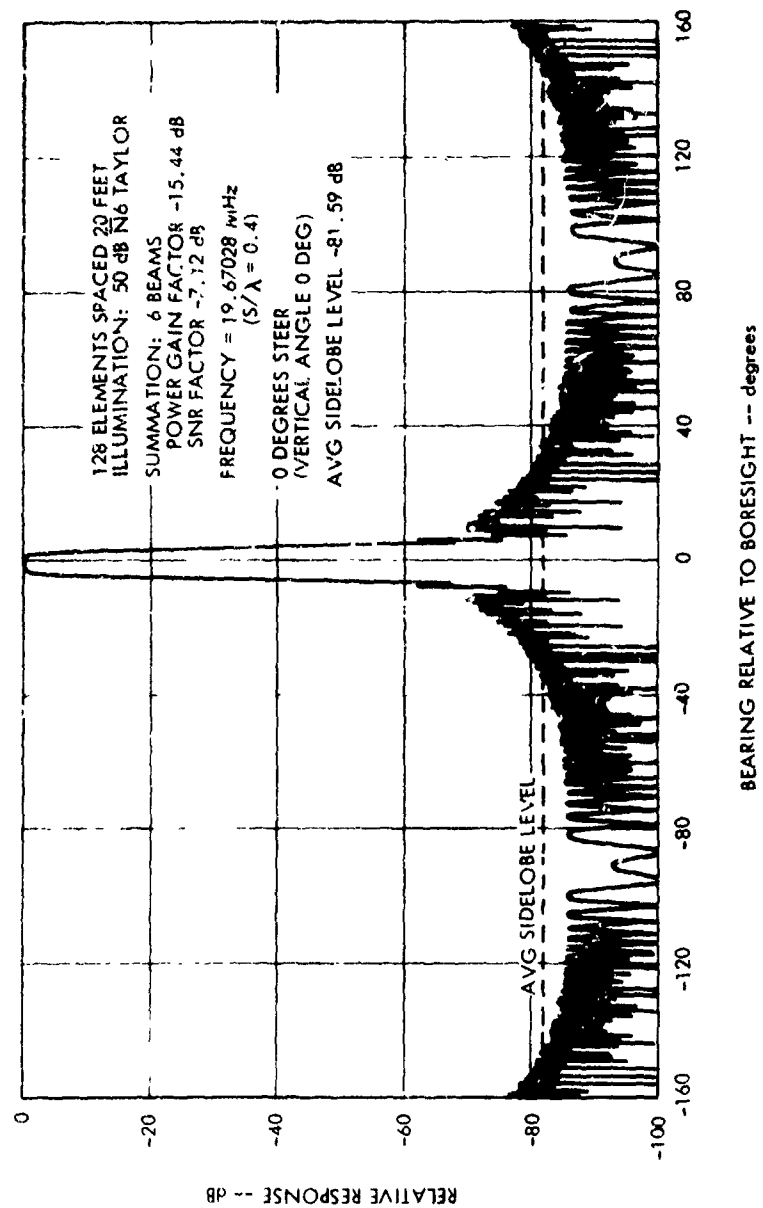
Figure 40.   Broadside Pattern.

(71)

128 ELEMENTS 20 FEET SPACING
ILLUMINATION: 50 dB N̄6 TAYLOR
SUMMATION: 6 BEAMS
POWER GAIN FACTOR -15.44 dB
SNR FACTOR -7.12 dB

FREQUENCY = 19.67028 MHz
(S'/λ = 0.4)

RANDOM ERROR SET:
±1.5 DEG -- 30 MHz MAX PEAK ERROR
±0.2 dB MAX PEAK ERROR
RMS PHASE ERROR 0.0097
RMS AMPL ERROR 0.0133
RMS TOTAL 0.0164
AVG SIDELOBE LEVEL -49.2 dB

AVG SIDELOBE LEVEL

BEARING RELATIVE TO BORESIGHT -- degrees

RELATIVE RESPONSE -- dB

Figure 41. Broadside Array with Errors.

(72)

128 ELEMENTS SPACED 20 FEET
ILLUMINATION: 50 dB N̄6 TAYLOR

SUMMATION: 6 BEAMS
POWER GAIN FACTOR -18.98 dB
SNR FACTOR -9.15 dB

FREQUENCY = 29.50542 MHz
(S/λ = 0.6

0 DEGREES STEER
(VERTICAL ANGLE 0 DEG)

AVG SIDELOBE LEVEL -63.08 dB

BEARING RELATIVE TO BORESIGHT -- degrees

RELATIVE RESPONSE -- dB
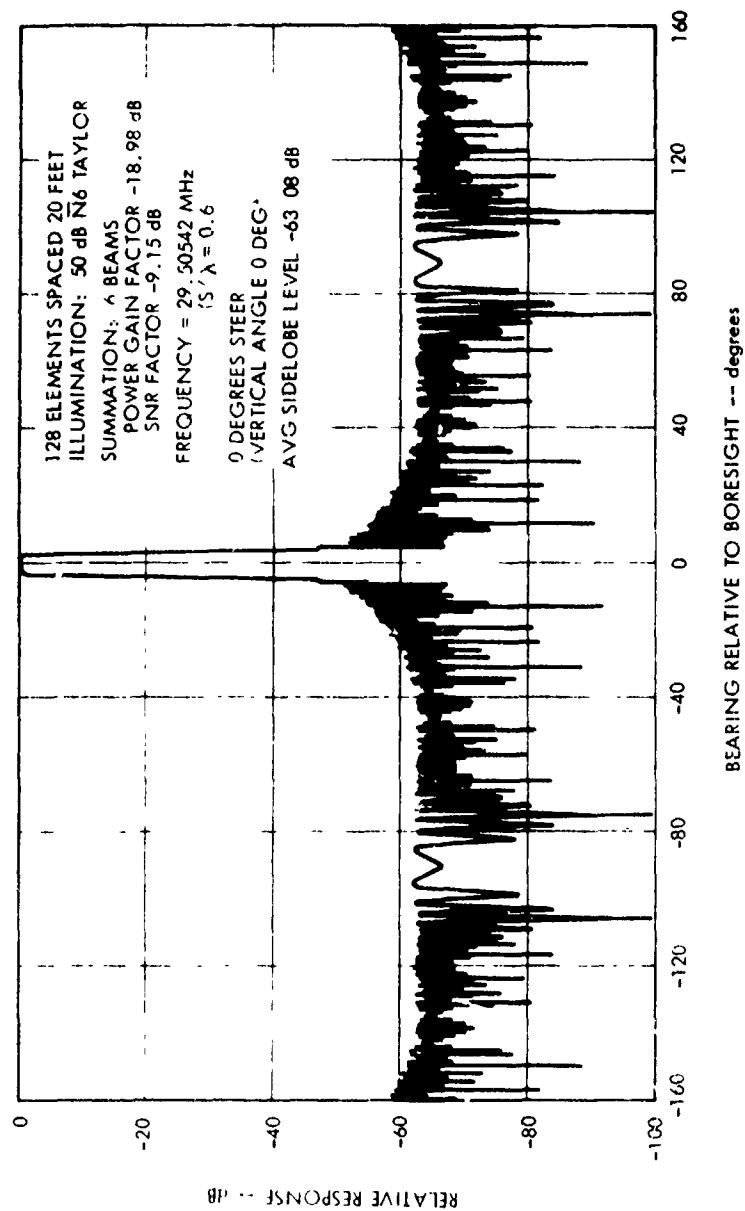
Figure 42. Broadside Pattern.

(73)
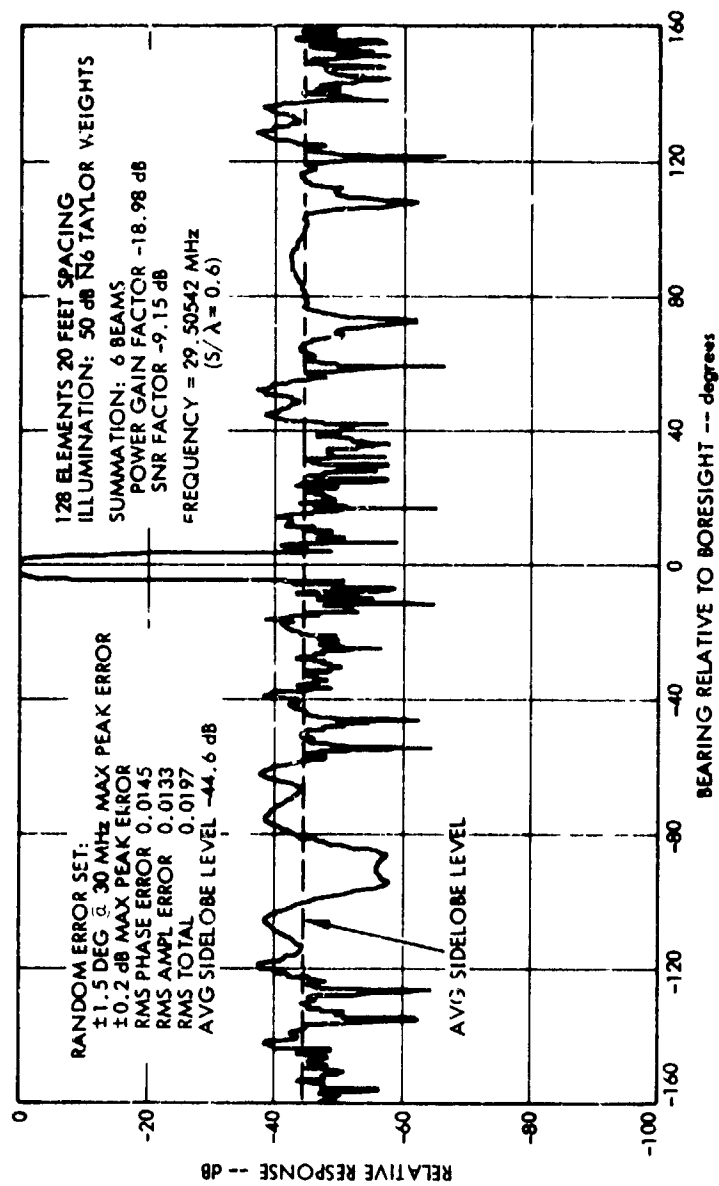
Figure 43.　Broadside Array with Errors.

(74)
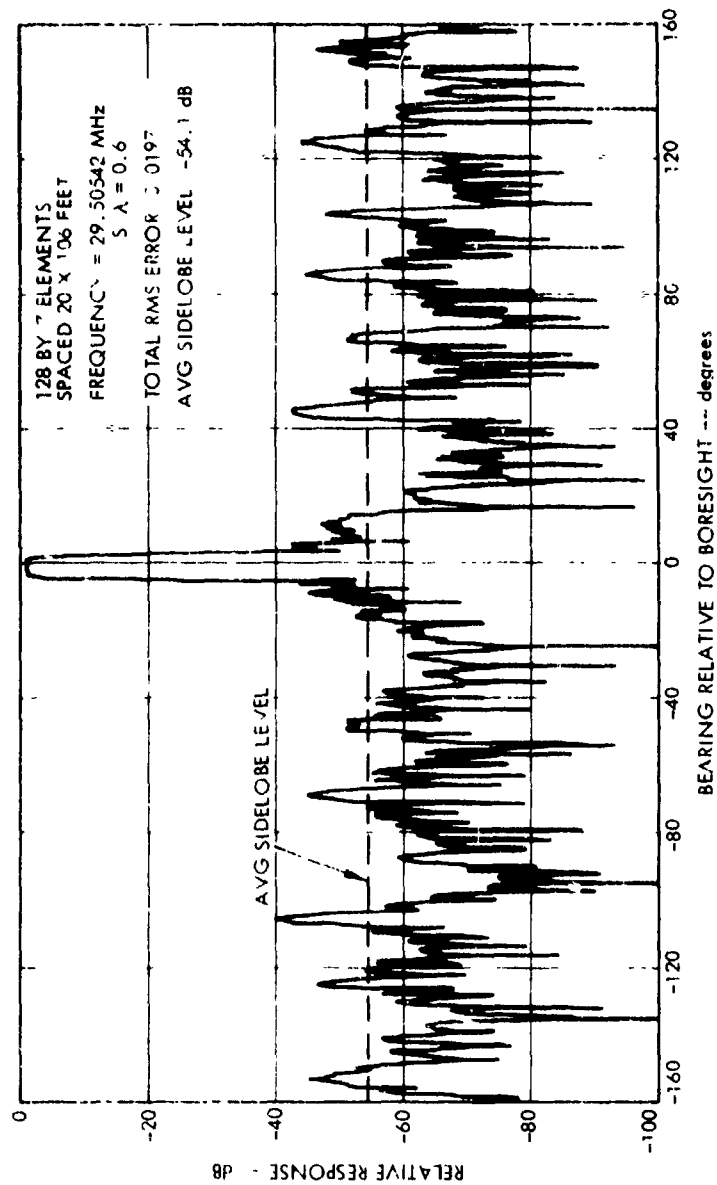
Figure 44. Planar Array with Errors.

(75)

Table 6. Comparison of the Simple Formula (Equation 13) with the Results obtained from the Monte Carlo Calculations

Method	Freq. (MHz)	Total rms Phase and Amplitude Error	Average Sidelobe Level (dB)
Formula 13	12.3	.0147	-53.1
Monte Carlo	12.3	.0146	-51.0
Formula 13	19.7	.0166	-49.5
Monte Carlo	19.7	.0164	-49.2
Formula 13	29.5	.0200	-45.5
Monte Carlo	29.5	.0197	-44.6

2.9 BEVERAGE ELEMENT

During the array work, the need for a computer program to predict the relative pattern of the RADC beverage element became evident. The program was decided not to be a complete predictor but an approximation which could be compared to the flight test data taken at Dexter. The basis for the model is taken from the SWRI work, which consisted of a single wire, which therefore only approximates the patterns for the RADC multiple wire configuration.

(a) The basic model includes a planar array of isotropic elements (modified by the directional vector of the signal with respect to the wire).

(b) The elements are assumed to be interconnected by delay lines (the wires) for which the propagation constant has been found.

(c) The launcher sections are used as summing junctions and for impedance transformation, as well as for secondary elements.

(d) The impedance matches of the elements to the output ports are used to determine the coefficients of reflection.

(e) The ground reflection constants and the image of the array are assumed to be known.

2.9.1 Geometry

The geometry of the planar array is based upon the element configuration shown in Figures 45 and 46. Assuming the element to consist of J wires with each wire segmented into N equivalent ports, the array contains NJ total ports.

(76)
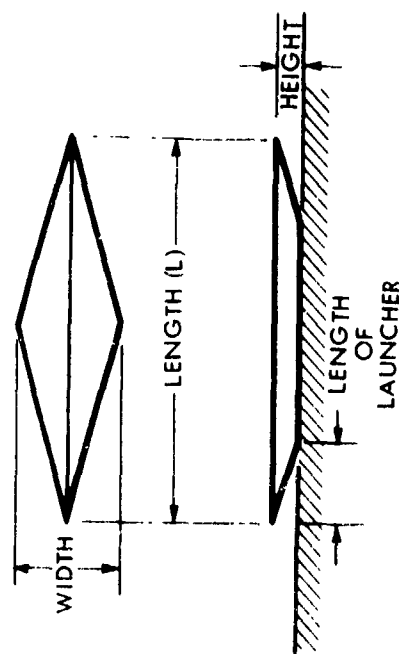
Figure 45. Plan and Sideview of Beverage Element Showing Major Dimension Required for Calculations.
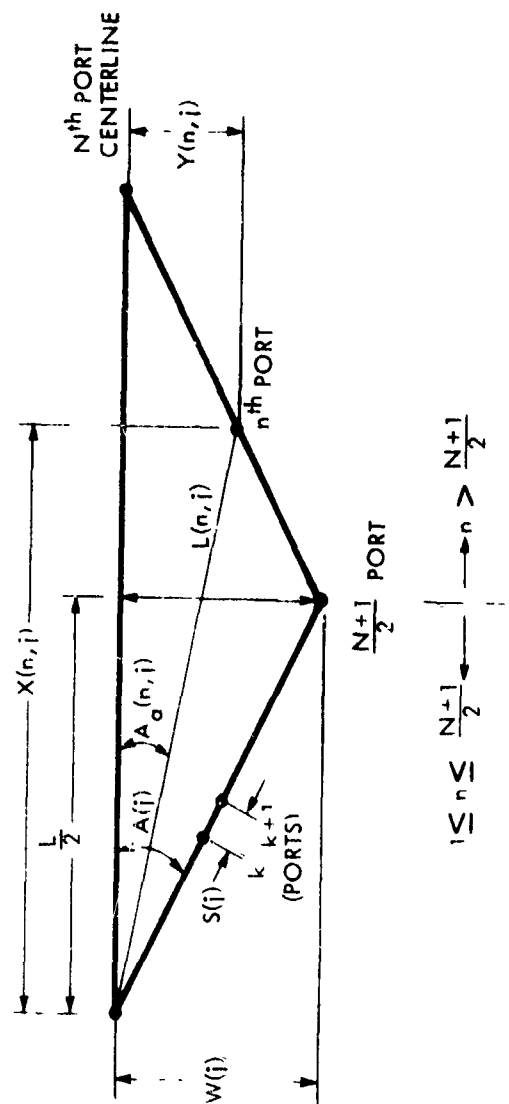
Figure 46. Plan View of the jth Wire in the Beverage Element Indicating the Physical Parameters used in the Calculation.

(78)

The reference phase is taken at the common junction of the several wires with the launcher. Therefore, the signal phase is determined by the distance between element one and element (n,j) less the launcher length of the jth wire and is designated as L(n,j) in Figure 46. The delay of the received signal is the length of the wire from element (n,j) to either launcher (forward and back traveling waves).

The spacing between equivalent ports is determined by the frequency such that the spacing does not exceed 0.1 wavelength for the longest wire or less than 21 ports.

From Figure 46 the physical parameters required during calculations are

$$W(j) \; = \; (\text{Width}) \; \left[\frac{j-1}{J-1} \; - \; \frac{1}{2} \right], \tag{21}$$

$$A(j) \; = \; \text{ARCTAN} \left(\frac{2W(j)}{L} \right), \tag{22}$$

$$S(j) \; = \; \frac{\left[\left(\frac{L}{2} \right)^2 \; + \; W^2(j) \right]^{1/2}}{\left(\frac{N-1}{2} \right)} \tag{23}$$

(Note: N is always chosen odd to ensure an equivalent port at the element apex.)

For $\quad 1 \le n \le \left(\frac{N+1}{2} \right)$

$$L(n,j) \; = \; (n-1) \, S(j) \quad \text{and} \tag{24}$$

$$A_a(n,j) \; = \; A(j) \tag{25}$$

For $\quad \frac{N+1}{2} < n \le N$

$$X(n,j) \; = \; \frac{L}{2} \; + \; S(j) \left[n - \left[\frac{N+1}{2} \right] \right] \cos(A(j)) \tag{26}$$

$$Y(n,j) \; = \; W(j) - S(j) \left[n - \left[\frac{N+1}{2} \right] \right] \sin(A(j)) \tag{27}$$

$$L(n,j) \; = \; \left(X^2(n,j) \; + \; Y^2(n,j) \right)^{1/2} \quad \text{and} \tag{28}$$

$$A_a(n,j) \; = \; \text{Arctan} \left(\frac{Y(n,j)}{X(n,j)} \right) \tag{29}$$

(79)

2.8 2 Electrical Constants

The constants for the wire in the beverage element are:

(a) γ the propagation constant where

$\gamma = \alpha + \beta i$,

α = the attenuation in nepers/meter,

β = the phase constant in radians/meter.

(b) Z_o is the impedance of a single wire at the input to the summing junction (launcher area).

(c) Z_T is the transformed and parallel impedance at the output of the summing junction.

(d) K is the reflection coefficient of the termination end of the element,

(e) VSWR is the voltage standing wave ratio seen looking into the element.

The above constants are found by

$$\gamma = \left\{ \left[\frac{0.832/f}{b} + j\, 2\omega \ln\left(\frac{2h}{b}\right) + 4\omega\,(P+jQ) \right] \frac{j\omega\, 2\pi\epsilon_o 10^{-7}}{\ln\left(\frac{2h}{b}\right)} \right\}^{1/2} \qquad (30)$$

and

$$Z_o = \left\{ \left[\frac{0.832/f}{b} + j\, 2\omega \ln\left(\frac{2h}{b}\right) + 4\omega\,(P+jQ) \right] \frac{\ln\left(\frac{2h}{b}\right) 10^{-7}}{\omega\, 2\pi\epsilon_o} \right\}^{1/2}, \qquad (31)$$

where:

f = frequency in Hz

b = the wire diameter in meters

h = wire height above ground

$\epsilon_o = 8.854(10^{-12})$

$\omega = 2\pi f$

The value of P and Q are found as follows

$$r_c = .00317 \, h \, \sqrt{\sigma_g f} \qquad (\sigma_g = \text{ground conductivity in} \atop \text{MHOS/meter}) \qquad (32)$$

if:

$$0 \leq r_c \leq 6 \quad P = [2.54 + 1.34 \, r_c]^{-1} \qquad (33)$$

$$r_c > 6 \qquad P = \frac{(.707 \, r_c - 1)}{r_c^2} \qquad (34)$$

$$0 \leq r_c \leq 0.5 \quad Q = -0.0368 + 1/2 \, \ln \left(\frac{2}{r_c}\right) + \frac{r_c}{4.24} \qquad (35)$$

$$.5 < r_c \leq 6 \quad Q = [0.56 + 1.42 \, r_c]^{-1} \qquad (36)$$

$$r_c > 6 \quad Q = \frac{.707}{r_c} \qquad (37)$$

From which,

$$\alpha = R_e \, [\gamma] \text{ in nepers/meter}$$

$$\beta = I_m \, [\gamma] \text{ in radians/meter}$$

and

$$R_o = R_e \, [Z_o] \text{ in ohms}$$

$$I_o = I_m \, [Z_o] \text{ in ohms,}$$

which represent the characteristics of the pseudo-delay lines for the equivalent ports. The impedance at the termination end would be the parallel impedance of the wires, or

(81)

$$Z = \frac{Z_0}{J} \tag{38}$$

if it were not for the mutual coupling between wires. The empirical relationship below provides a reasonable value for the physical configuration used

$$Z_T = \frac{Z_0}{(J)^{\sqrt{\frac{1}{J}}}} \quad \text{ohms} \tag{39}$$

The reflection coefficient for the line and the ground reflection terms for vertical and horizontal polarizations can then be calculated using the equations available in any standard reference.

The launchers are treated as separate antennas interconnected by the wires forming a standing wave pattern with an amplitude decreased by the ratio of the launcher length/element length.

The currents for the basic array, the reflected wave from the terminated end, and the launcher are then summed and the vertical and horizontal ground reflection constants used to form a two port (antenna and reflection) array spaced twice the height.

2.9.3 Results

The development was not completed during this time period. The preliminary results indicate excellent agreement with the main lobe compared to flight test data. The sidelobe levels are predicted within reasonable limits, however, the sidelobe structure does not compare primarily in location of nulls.

In addition, before the total program can be used it must be converted to the AN/GYK-26, as the HIS 6000 Timeshare System will not accept the entire program.

2.10 ARRAY PERFORMANCE

One important measure of an antenna's performance is the ratio of the antenna output relative to an isotropic antenna, namely the power gain, usually expressed in dBi. When the antenna is used with a system, the system performance is normally defined by a noise figure and any other parameters vital to the designer (such as the

$$Z = \frac{Z_0}{J} \qquad (38)$$

if it were not for the mutual coupling between wires. The empirical relationship below provides a reasonable value for the physical configuration used

$$Z_T = \frac{Z_0}{(J)^{\sqrt{\frac{1}{J}}}} \quad \text{ohms} \qquad (39)$$

The reflection coefficient for the line and the ground reflection terms for vertical and horizontal polarizations can then be calculated using the equations available in any standard reference.

The launchers are treated as separate antennas interconnected by the wires forming a standing wave pattern with an amplitude decreased by the ratio of the launcher length/element length.

The currents for the basic array, the reflected wave from the terminated end, and the launcher are then summed and the vertical and horizontal ground reflection constants used to form a two port (antenna and reflection) array spaced twice the height.

2.9.3 Results

The development was not completed during this time period. The preliminary results indicate excellent agreement with the main lobe compared to flight test data. The sidelobe levels are predicted within reasonable limits, however, the sidelobe structure does not compare primarily in location of nulls.

In addition, before the total program can be used it must be converted to the AN/GYK-26, as the HIS 6000 Timeshare System will not accept the entire program.

2.10 ARRAY PERFORMANCE

One important measure of an antenna's performance is the ratio of the antenna output relative to an isotropic antenna, namely the power gain, usually expressed in dBi. When the antenna is used with a system, the system performance is normally defined by a noise figure and any other parameters vital to the designer (such as the

(82)

If each antenna element is one of N identical units, the total power input to the system is N times the power delivered by a single input. Thus, the "antenna system" must be considered to have a gain over an isotropic antenna of N times the gain of the element as found above.

Any further losses, gains, or SNR deterioration is correctly and properly assigned to the receiving system. Thus, the beamforming network becomes a part of the receiving system and it now only becomes necessary to find the system noise figure.

2.10.2 System Noise Figure

For the purpose of this analysis, two assumptions are made: (a) the noise sources are random, and independent; and (b) the losses, weighting coefficients, etc., attenuate the signal and only the excess noise available from the preamplifiers.

To comply with assumption (b), the normally accepted definition of noise power available at an amplifier output

$$P_N = (KTB) \; F_a \, G_a \, , \tag{41}$$

where F_a is the amplifier noise factor, G_a is the power gain of the amplifier, and KTB is the thermal noise power, will be rewritten to express the excess noise available above thermal:

$$P_N = (KTB) \; (1 + R_e), \tag{42}$$

$$\text{where:} \qquad R_e = (G_a F_a \cdot \tag{43}$$

From assumption (b), only the noise R_e KTB can be attenuated by the coefficients. This ensures that with high attenuations the resulting noise power is not reduced below thermal noise power.

The general array block diagram is shown in Figure 47.
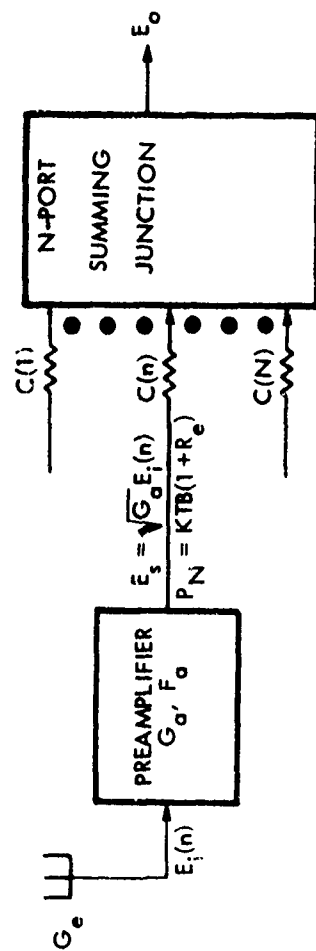
Figure 47. Block Diagram of General Array with Preamplifiers.

Referring to Figure 47, and assuming all signals $E_{i(n)}$ to have the same amplitude and phase the output signal voltage is found as,

$$E_O = \frac{E_s}{\sqrt{N}} \sum_1^N C(n)$$

(44)

and the output signal power is

$$P_O = E_O^2 = \frac{E_s^2}{N} \left[\sum_1^N C(n) \right]^2$$

(45)

where the summation junction is assumed constant impedance, and C(n) are weighting coefficients which contain all losses which might exist between the preamplifier and the summing junction, such as cable attenuation, mismatch losses, insertion losses, aperture weighting losses, and power splitting loss (more than one beam). (These losses do not contain the (1/N) loss of the constant impedance summing junction).

Since the coefficients C(n) only attenuate the excess noise, the output noise power N_O is found to be,

$$N_O = KTB \left[1 + \frac{R_e \sum_1^N C(n)^2}{N} \right].$$

(46)

Thus, the output signal-to-noise ratio (SNR_O) is,

$$SNR_O = \frac{E_s^2 \left[\sum_1^N C(n) \right]^2}{KTB \left[1 + \frac{R_e}{N} \sum_1^N C(n)^2 \right] N}$$

(47)

To determine the noise factor of the system the value

$$E_S^2 = E_i^2 G_a$$

(48)

is substituted into equation (47 and the output SNR becomes

$$SNR_O = \frac{G_a E_i^2 \left[\sum_1^N C(n) \right]^2}{N KTB \left[1 + \frac{R_e}{N} \sum_1^N C(n)^2 \right]}$$

(49)

(86)

The definition of noise factor is given as

$$F = (N_o/N_i)(P_o/P_i)^{-1} = \frac{SNR_i}{SNR_o} \qquad (50)$$

From Figure 47 it is seen that the total input power to the N port system would be,

$$P_i = NE_i^2 \qquad (51)$$

and the noise power input is KTB (thermal noise), thus,

$$SNR_i = \frac{NE_i^2}{KTB} \qquad (52)$$

Substituting equations 49 and 52 into equation 50 the array noise factor $'F_R)$ becomes

$$F_R = \frac{N^2\left[1 + \frac{R_e}{N}\sum_1^N C(n)^2\right]}{G_a\left[\sum_1^N C(n)\right]^2} \qquad (53)$$

Solving equation 43 for Ga and substituting into equation 53 yields

$$F_R = \frac{N^2\left[1 + \frac{R_e}{N}\sum_1^N C(n)^2\right]}{(R_e + 1)\left[\sum_1^N C(n)\right]^2} F_a \qquad (54)$$

To determine the noise factor of the system the equation for cascaded noise factors ,

$$F_s = F_R + \frac{F_b - 1}{G_R} \qquad (55)$$

can be used where F_b is the noise factor of the circuits following the summing junction and G_R is the available power gain of the array. The value of G_R is found,

(87)

using equations 45 and 51 as

$$G_R = \frac{P_o}{P_1} = G_a \frac{\left[\sum\limits_1^N C(n)\right]^2}{N^2} .$$ (56)

Substituting equations 54 and 56 into equation 55 the system noise factor (F_s) becomes

$$F_s = \frac{N^2}{\left[\sum\limits_1^N C(n)\right]^2} \left\{ \frac{\left(1 + \frac{R_e}{N} \sum\limits_1^N C(n)^2\right)}{R_e + 1} F_a + \frac{F_b - 1}{C_a} \right\}$$ (57)

Equation 57 shows that the system noise factor is reduced by the gain of the pre-amplifiers, regardless of the losses associated with the values of $C(n)$ or N.

Using the assumption that

$$\frac{\left(1 + \frac{R_e}{N} \sum\limits_1^N C(n)^2\right)}{(R_e + 1)} \quad F_a \gg \frac{F_b - 1}{C_a} .$$ (58)

as would be the case in a well designed system, the system noise factor (F_s) becomes

$$F_s = \frac{N^2 \left[1 + \frac{R_e}{N} \sum\limits_1^N C(n)^2\right] F_a}{(R_e + 1) \left[\sum\limits_1^N C(n)\right]^2}$$ (59)

If an ideal (lossless) N port array were used with the same preamplifiers, the output SNR (SNR_{ideal}) would be,

$$SNR_{ideal} = \frac{NE_i^2}{KTBF_a} ,$$ (60)

It is then possible to define a signal-to-noise ratio factor (SNRF) as the ratio of the output SNR to that of an ideal beam-forming network:

$$SNRF = \frac{SNR_o}{SNR_{ideal}} \, . \tag{61}$$

Using the values found by equation 49 and 60 equation 61 becomes,

$$SNRF = \frac{G_a \left[\sum_1^N C(n) \right]^2 F_a}{N^2 \left[1 + \dfrac{R_e}{N} \sum_1^N C(n)^2 \right]} \, . \tag{62}$$

Solving for G_a in equation 43 and substituting equation 62 becomes,

$$SNRF = \frac{(R_e + 1) \left[\sum_1^N C(n) \right]^2}{N^2 \left[1 + \dfrac{R_e}{N} \sum_1^N C(n)^2 \right]} \, . \tag{63}$$

Comparing the value for the SNRF and the system noise factor (equation 59) it is seen that the system noise factor is simply,

$$F_S = \frac{F_a}{SNRF} \, . \tag{64}$$

providing that the conditions in the inequality (equation 58) are met.

2.10.3 Signal-to-noise Ratio Loss

From the preceding discussion it was seen that the noise figure of the system is increased by the SNR factor (SNRF $\leq$ 1) of the beam-forming networks. Therefore, it is important to maintain this ratio as near unity as possible. To evaluate the effect of R_e in maintaining the value of SNRF near unity several examples are given.

2.10.3.1 $R_e = 0$

To evaluate the effect of R_e upon the SNRF the first extreme,

$$R_e = 0 \quad \text{(no amplifiers)}$$

is illustrated. Substituting this value for R_e in equation 63 the SNR factor becomes

$$SNRF = \frac{\left[\sum_1^N C(n)\right]^2}{N^2} \ . \tag{65}$$

which is the power gain factor of the beam-forming networks.

The $C(n)$ contain, in these equations, the additional losses (with the exception of the $(1/N)$ loss) of the beam-forming networks. If the power losses are represented by K, then

$$C(n) = \sqrt{K} \ Cw(n) \tag{66}$$

where $Cw(n)$ are the aperture weighting coefficients which are not constant element to element.

Then the SNR factor is further reduced as

$$SNRF = K \frac{\left[\sum_1^N Cw(n)\right]^2}{N^2} \qquad \text{(67)}$$

which is K times the power gain factor of the aperture weighting used.

Referring to Table 5, the power gain factor was found to be -16.68 to -16.92 dB at 30 MHz depending upon the number of beams used. With no insertion loss ($K = 1$), the noise figure of the system would be high even with reasonable amplifier noise figures. For example, using an amplifier noise figure of 4 dB, the system noise figure would be 21 dB.

2.10.3.2 Re = ∞

Assuming $Re = \infty$, then the SNR factor becomes

$$SNRF = \frac{\left[\sum_1^N C(n)\right]^2}{N \sum_1^N C(n)^2} \ , \tag{68}$$

and again using $C(n) = \sqrt{K} \ Cw(n)$ then,

$$SNRF = \frac{\left[\sum_1^N Cw(n)\right]^2}{N \sum_1^N Cw(n)^2} \tag{69}$$

(90)

Equation 69 shows with Re = ∞ , the SNR factor is independent of fixed loss and depends only upon the aperture weighting used.

Referring to the SNR factors summarized in Table 4, these were found to range from -7.83 to -7.93 dB at 30 MHz, depending upon the number of beams used. With the same amplifier assumed above, the best system noise figure would be 12 dB at 30 MHz for the assumed array.

2.10.3.3 R_e = Intermediate Values

From the preceding paragraphs, it was seen the SNR factor can vary from the full power gain factor of the array to the SNR factor of the aperture weighting function. To further illustrate the effect of Re upon an array the following values were chosen:

(a) SNR factor of the aperture weight = -7.90 dB,

(b) power gain factor of the aperture weighting = -16.66,

(c) A 4 dB noise figure amplifier with 30 dB of gain was chosen (Re = 2510), and

(d) K was selected to equal 1 (0 dB losses) and .01 (20 dB losses).

The system noise figure (assuming the amplifier noise figure is a constan) for various values of Re is shown in Table 7.

Table 7. System Noise Figure of an Array as a
Function of Excess Noise (Re) and Losses

Re	K = 1 (0 dB)	System Noise Figure (dB) K = .01 (-20 dB)
0	20.60	40.66
1	18.19	37.66
10	13.92	30.30
100	12.17	21.16
2510	11.91	13.04
∞	11.90	11.90

(91)

2.10.4 System Figure of Merit

Traditionally, the system designer will specify the antenna gain in dBi (gain above an isotropic antenna) and a system noise figure. In doing so, he has essentially defined the output signal-to-noise ratio for a given incident field at the antenna (regardless of how that field came into being) that he is willing to accept.

Ignoring external noise to the system, an isotropic antenna would have an output SNR of

$$SNR_1 = \frac{\in^2 \lambda^2}{4\pi \, (KTB)} \quad , \tag{70}$$

where $\in^2$ is the power density of the signal in space,

$\frac{\lambda^2}{4\pi}$ is the capture area of an isotropic antenna.

When the gain of the antenna (G_{ant}) and noise factor of the system (F_s) are specified, the output SNR in the same incident field becomes

$$SNR_a = \frac{G_{ant} \in^2 \lambda^2}{4\pi \, KTR \, F_s} \quad , \tag{71}$$

which is the SNR acceptable to the designer (or at least the value he believes is achievable).

The system output SNR when referenced to the SNR form from an isotropic antenna would represent a system figure of merit (SFM) which is simply:

$$SFM = \frac{G_{ant}}{F_s} \quad . \tag{72}$$

The SFM for the array with embedded preamplifiers is

$$SFM = \frac{(R_e + 1) \, G_e \left[\sum\limits_{1}^{N} C(n) \right]^2}{N \left[1 + \frac{R_e}{N} \sum\limits_{1}^{N} C(n)^2 \right] F_a} \tag{73}$$

or

$$SFM = \frac{N\,Ge}{F_a}\,(SNRF),\qquad\qquad(74)$$

where Ge is the gain of an antenna element as previously defined.

Use of this SFM would allow the system designer flexibility in the selection of gains and noise figures, particularly if these parameters are a function of frequency. For an example, if the gain of the antenna decreases with decreasing frequency (below design specifications), the equivalent performance could be achieved by reducing the noise factor. Therefore, SFM is offered as a system criterion in place of using both values separately.

2.11 EXTERNAL NOISE

The previous paragraphs have described the design of low sidelobe arrays and methods for the calculation and maintenance of low noise figure active arrays. This work used only the internal noise, and since many sources believe HF systems are primarily externally noise limited, this topic should be investigated. The following is a limited examination of the problem.

2.11.1 Directivity and Array Gain

Given an antenna pattern $E^2(\phi, \theta)$ with the peak of the main lobe occurring in the direction (ϕ_o, θ_o), the "directivity gain" D of the pattern is defined as

$$D = \frac{4\pi\,E^2(\phi_o,\theta_o)}{\displaystyle\int E^2(\phi,\theta)\,d\Omega}\qquad\qquad(75)$$

where ϕ = the vertical angle of arrival

  θ = the azimuthal angle of arrival

  $d\Omega$ = the differential of solid angle [for the (ϕ, θ) coordinates employed, $d\Omega = \cos\phi\,d\phi\,d\theta$]

and the integral is to be taken over all 4π steradians of solid angle.

The "directive gain pattern" $P(\phi, \theta)$ with respect to an isotropic antenna is defined as

$$P(\phi,\theta) = \frac{D\,E^2(\phi,\theta)}{E^2(\phi_o,\theta_o)}\qquad\qquad(76)$$

(93)

It is easily seen that the function $P(\phi, \theta)$ satisfies the following conditions:

$$\int P(\phi, \theta) \, d\Omega = 4\pi \tag{77a}$$

$$P(\phi_o, \theta_o) = D. \tag{77b}$$

Note that if only the shape of the antenna pattern is known and represented by the function $f(\phi, \theta)$, then the directive gain pattern $P(\phi, \theta)$ is easily constructed by employing the normalization condition of equation 77a, namely,

$$P(\phi, \theta) = \frac{4\pi f(\phi, \theta)}{\int f(\phi, \theta) \, d\Omega} \tag{77c}$$

The "power gain function" $G(\phi, \theta)$ of an antenna, with respect to an isotropic antenna, is defined as

$$G(\phi, \theta) = \alpha P(\phi, \theta), \tag{78}$$

where α = the efficiency of the antenna.

If a signal arrives from the (ϕ_s, θ_s) direction, the output signal power is proportional to the value $G(\phi_s, \theta_s)$. The external noise signals arrive from all angles, and the output external noise power is therefore proportional to the integrated value of the product of $G(\phi, \theta)$ and the angular noise distribution $\psi(\phi, \theta)$.

2.11.2 Angular Noise Distribution

The external noise power P_N at the output of an antenna is obtained from

$$P_N = KTB \int G(\phi, \theta) \, \psi(\phi, \theta) \, d\Omega, \tag{79}$$

where $\psi(\phi, \theta)$ = the angular distribution of the external noise factor.

Traditionally, the external noise factor is taken as an isotropic distribution given by

$$\psi(\phi, \theta) = \frac{F_{CCIR}}{4\pi}, \tag{80}$$

where $KTB \, F_{CCIR}$ = the commonly used CCIR noise level at the antenna location (the CCIR measurements were made with a short vertical monopole over a good ground screen).

(94)

From equations 77a, 78, 79, and 80 it is seen that P_N is proportional to the antenna efficiency

$$P_N = \frac{(KTB) \ F_{CCIR}}{4 \pi} \int G(\phi, \theta) \ d\Omega = \alpha \ (KTB) F_{CCIR}. \tag{81}$$

2.11.3 Output Signal-to-Noise Ratio

The simple system of a single antenna driving a single receiver is considered first. When a radio signal arrives from the direction (ϕ_0, θ) of the main lobe with a power density $\in^2$, the "signal to internal (thermal) noise ratio" is given by

$$\text{Signal to internal noise ratio} = \frac{G(\phi_0, \theta_0) \ \left(\frac{\in^2 \lambda^2}{4 \pi}\right)}{KTB \ F_S} \tag{82}$$

where F_S = noise factor for the receiving system.

The "external noise to internal (thermal) noise ratio" is obtained by employing equation 79:

$$\text{External noise to internal noise ratio} = \frac{(KTB) \int G(\phi, \theta) \ \psi \ (\phi, \theta) \ d\Omega}{(KTB) \ F_S} \tag{83}$$

The total noise level against which background the signal is to be detected is the sum of the internal and external noises. The signal to total noise ratio (SNR) is then given by

$$\text{SNR} = \frac{\text{signal}}{\text{internal noise + external noise}} = \frac{\dfrac{\text{signal}}{\text{internal noise}}}{1 + \dfrac{\text{external noise}}{\text{internal noise}}} \tag{83a}$$

Substituting equations 82 and 83 into 83a, gives

$$\text{SNR} = \frac{G(\phi_0, \theta) \left(\dfrac{\in^2 \lambda^2}{4 \pi}\right)}{KTB \left[F_S + \int G(\phi, \theta) \ \psi \ (\phi, \theta) \ d\Omega\right]} \tag{84}$$

From equation 84, it is seen that if the antenna were 100% efficient $[G(\phi, \theta) = P(\phi, \theta)]$, if the noise were isotropic, and if the power density and the system noise factor were held constant, the only way to increase the SNR would be to increase the directivity gain (at the employed wavelength).

Equation 84 holds for the simple receiving system which consists of a single antenna driving a single receiver. For a receiving array containing N identical elements all aligned with the same spatial orientation (i.e., all pointing in the same direction), the gain of the array is $N\,G_e$ and

$$G(\phi_o, \theta_o) = N\,G_e,$$ (85)

where G_e = gain of individual antenna element.

(If $G_{ant}(\phi, \theta)$ is gain function for the individual antenna elements*,
then $G_{ant}(\phi_o, \theta_o) = G_e$)

It is also possible to write

$$G(\phi_o, \theta_o) = \alpha_a\,P(\phi_o, \theta_o) = \alpha_a\,D.$$ (86)

so that the efficiency of α_a of the antenna array system becomes

$$\alpha_a = \frac{N\,G_e}{D}.$$ (87)

The signal to total noise ratio for the antenna array system with a noise factor F_S as given by equation 55 is then

$$SNR = \frac{N\,G_e\left(\dfrac{\epsilon^2\,\lambda^2}{4\,\pi}\right)}{KTB\left[F_S + \dfrac{N\,G_e}{D}\int P(\phi, \theta)\,\psi(\phi, \theta)\,d\Omega\right]}.$$ (88)

*It is assumed that $G_{ant}(\phi, \theta)$ is the power gain function for an individual antenna element when it is immersed in the array so that all mutual couplings of the antenna element with its neighbors are automatically included in G_{ant}. It is further assumed that all antenna elements have the same $G_{ant}(\phi, \theta)$. If measurements should show that antenna elements near the edges of the array have power gain functions different from those of the elements near the middle of the array, then these calculations would have to be generalized to recognize those differences.

(96)

For equations 85 through 88, it has been assumed that the radio signal is arriving from the direction of the main lobe of the individual antenna elements and also that the signals all arrive in phase at the input ports of the summing junction, i.e. that the signal is also arriving on the boresight of the antenna array. To generalize equation 88 so as to treat signals which arrive from an arbitrary direction (ϕ_s, θ_s), let the power gain function for the individual antenna elements be $G_{ant}(\phi, \theta)$ and the beam-forming array factor be $AF(\phi, \theta)$. This "arraying factor" is defined in a manner similar to that used in defining "ideal arraying factor" in Section 2.7.1, namely

$$AF(\phi, \theta) = \frac{\left| \Sigma C_n \exp [i \, \psi_n (\phi, \theta)] \right|^2}{\left| \Sigma C_n \right|^2}, \tag{89}$$

where $\psi_n (\phi, \theta)$ = the phase angle of the signal which arrives at the nth input port of the summing junction when the signal is generated by a plane radio wave arriving from the (ϕ, θ) direction,

C_n = amplitude weighting coefficients as defined by the discussion which immediately follows Figure 47.

The power gain function $G_{ant} (\phi, \theta)$ for the individual antenna elements has a maximum value G_e, and the arraying factor has a maximum value of unity. The desired generalization of equation 88 is then

$$SNR_a = \frac{N \, G_{ant} (\phi_s, \theta_s) \, AF (\phi_s, \theta_s) \left(\dfrac{\epsilon^2 \lambda^2}{4 \pi} \right)}{KTB \left[F_S + \dfrac{N \, G_e}{D} \displaystyle\int P(\phi, \theta) \, \psi (\phi, \theta) \, d\Omega \right]}. \tag{90}$$

If the power gain function $G_{ant} (\phi, \theta)$ of the individual antennas in the array is known and if the arraying factor $AF (\phi, \theta)$ is also known, the directive gain pattern $P(\phi, \theta)$ and the directivity gain D can be calculated using equations 77b and 77c:

$$P(\phi, \theta) = \frac{4 \pi G_{ant} (\phi, \theta) \, AF (\phi, \theta)}{\displaystyle\int G_{ant} (\phi, \theta) \, AF (\phi, \theta) \, d\Omega} \; ; \tag{91}$$

$$D = \text{Maximum value of } P (\phi, \theta). \tag{92}$$

(97)

If the antenna elements are arrayed so that the maximum value (unity) of the arraying factor $AF\ (\phi, \theta)$ occurs in the direction of the main lobe of the individual antenna elements (as would usually be the case for a linear array if the array were not steered away from boresight)[*], then in place of equation 92,

$$D = \frac{4\pi G_e}{\int G_{ant}\ (\phi, \theta)\ AF\ (\phi, \theta)\ d\Omega} \tag{93}$$

Substituting equations 91 and 92 into equation 90 gives the somewhat simpler equation for an unsteered antenna array

$$SNR_a\ (unsteered)\ =\ \frac{N\ G_{ant}\ (\phi_s, \theta_s)\ AF\ (\phi_s, \theta_s)\left(\frac{\epsilon^2\ \lambda^2}{4\pi}\right)}{KTB\ [F_S + N \int G_{ant}\ (\phi, \theta)\ AF\ (\phi, \theta)\ \psi\ (\phi, \theta)\ d\Omega]} \tag{94}$$

If the arraying system is steered away from boresight, then the SNR must be calculated from the more general formulas 90, 91, and 92. In addition to the other undesirable effects which occur with a steered array, there will also be a reduction in SNR because the main lobe of the antenna element will not coincide with the main lobe of the arraying factor; there will be a consequent reduction of the directivity gain D.

It should also be noted that the concept of "system noise figure" is well defined by IEEE standards for electronic systems which have only one input port and one output port. However, for an antenna array which contains several input ports, the concept of "system noise figure" becomes less well defined, and a definition of system noise factor which is somewhat different from that given by equation 55 might be used. The basic equations 90 and 94 would have to be modified if an equation different from equation 55 were employed to define the system noise factor F_S.

From equation 90, it can be seen that the system will be limited by external noise of

$$F_S \ll \frac{N\ G_e}{D}\ \int P(\phi, \theta)\ \psi\ (\phi, \theta)\ d\Omega. \tag{95}$$

[*] Under these conditions, if a plane wave radio signal arrives from the boresight direction (ϕ_o, θ_o), equation 90 reduces to equation 88 as it should.

(98)

If this inequality is satisfied, then the SNR cannot be improved by reducing the internal thermal noise level of the amplifiers, etc. If inequality (95) is reversed, the system is internally noise limited; this situation could occur if for example the efficiency of the individual antenna elements were very low. If this were the case, then an improvement in SNR could be obtained by either reducing the internal noise level by using more efficient antenna elements*. The system could also become internally noise limited if the noise distribution $\psi(\phi, \theta)$ were highly directive and if the directive gain pattern $P(\phi, \theta)$ discriminated against those directions from which the main external noise signal were coming.

In any event, to ascertain system performance it is necessary to obtain a reasonable estimate of the angular noise distribution $\psi(\phi, \theta)$. Since the large aperture, low sidelobe array has a very directive pattern, it is possible that this directive pattern could exclude much of the CCIR noise at a given location if that noise were found to be originating primarily from directions outside of the main beam of the antenna array. Under such circumstances the external noise values applicable to the receiving system could possibly be well below the values given by CCIR.

*or by increasing the density of the inefficient elements (i.e., increase N)

(99)

3.0 SUMMARY AND CONCLUSIONS

From 1 May 1973 to 30 April 1974, GTE Sylvania Incorporated, ESG-WD, provided engineering field services in support of RADC's experimental HF FM/CW backscatter system in Dexter, New York. These experimental/theoretical investigations were primarily concerned with testing and evaluating the performance of the system and with the design of large aperture, low sidelobe arrays.

The measurement and analysis of the beam-forming networks and field components of the receiving array showed that

(a) an input cable (approximately 1000 feet) was short by one wavelength (at 30 MHz),

(b) large VSWRs were again present in the BFN as a result of loose mechanical connections,

(c) the new phasing and delay cables were incorrectly installed,

(d) manual signal measurements are not sufficiently reliable for accurate BFN calculations, even those measurements using semiautomatic measuring techniques.

As a result of this latter activity, it is recommended that fully automatic BFN measuring equipment, including a permanently installed field calibration system be installed.

Computer software for the RADC CDC 1700 (located at the DRC) should be redesigned and implemented for detailed analysis of the BFN measurements. The difficulties encountered during extensive computation on the CDC 1700 computer and the subsequent discovery of the deficiency of the "float point" software make further work of this type on the CDC 1700 unadvisable. It is recommended that these programs be translated, from the CDC 1700 Fortran to the new AN/GYK-26 being installed at the DRC.

It is recommended that the statistical development for beam-forming network design for sidelobe control and prediction be continued for multiple beam and planar arrays to include element patterns if possible.

(100)

A computer model of the beverage element used at Dexter should be developed. The major difficulty encountered was the limitation of the HIS 6000 Timesharing was inadequate to finish the work. It is recommended this development be continued using the CDC 1700 or the AN/GYK-26 located at the DRC.

A limited analysis of the effect of external noise on the output SNR was performed With the use of the array at Dexter, a study should be made to evaluate the effect of directivity in reducing the effect of external noise.

APPENDIX

RME OVERSEAS SITE
TRIP REPORT

14 July to 9 August 1973

H-1

1.0   INTRODUCTION.

The following report covers the trip made to the RME overseas site during the period 14 July to 9 August 1973. The trip was made primarily to investigate two major problem areas:

1)   the cause of the high Minimum Discernible Signal (MDS) experienced by the RME system, and

2)   the cause of the "synchronization problem" between the receiver and transmitter sites with the alleged loss of accurate timing with respect to world time standards.

In addition to the above problems, the following problem and general areas were to be observed:

1)   the "connector problem",

2)   general maintenance procedures and level of performance,

3)   general operational procedures, and

4)   any general areas where system performance could be improved.

Because of limited time available, a further stipulation was not to engage in any maintenance or repairs of the RME system or tests of auxiliary equipment, unless directly related to the definition of the immediate problems.

To accomplish the above tasks the investigation was done in two parts:

1)   complete testing of the RME receiver system and auxiliary receiving equipment used by the system (e. g. , multicouplers, amplifiers, etc.) and the transmitter equipment. These tests were conducted to determine if problem was hardware induced; and

1.0   --Continued.

2)   if no hardware problems are found, then on-air tests
to observe the noise sources causing high MDS read-
ings and if any found, determine if they are independent
or signal-related.

I would like to express my appreciation to all the unit personnel
for the excellent cooperation and assistance received during the trip and
particularly to:

SQN. LDR. C. I. Johnson

SGT. S. Weller

JT B. Ward

Without their help the tests would never have been accomplished.

2.0   CONCLUSIONS.

An overall conclusion made from this trip is that all unit personnel
are making a dedicated and professional effort to operate, analyze/report
and maintain the system for peak performance. The following specific
conclusions cover the areas of interest.

2.1   High MDS.

1)   The equipment is in generally good to excellent condition
and is now operating with specified or better performance
(with one major and some minor reservations, none of
which directly relate to the MDS problem).

2)   The level of ground wave at the receiver site can limit
system performance simply by rising to a level which
exceeds the available receiver dynamic range. In
addition, it presently increases the probability of inter-
modulation distortion and cross-modulation products.

A2

2.1   --Continued.

The ground wave averages approximately -50 dBm with recorded peak values of -30 dBm during the summer. Since the transmitted broadband noise floor is 100 dB or greater below the transmitted signal, the inband noise floor, at operational ranges, is set by the receiver to approximately 102 dB below the strongest received signal in the preselector bandwidth. Therefore, under normal operating conditions the average value (-50 dBm) would limit the MDS to -152 dBm. While the peak value (-30 dBm) would limit the MDS to -132 dBm, the previous data collected on ground wave strength would indicate this peak level is very rarely attained.

3)   An external, non-system related noise which could limit the system performance was observed at -130 to -135 dBm signal levels. While this noise was found to be external to the system, no statistical data, other than the limited numbers below, were collected during the short time available.

The source of this noise is unknown. However, it does appear to be an OTH noise source, since it has a short term cyclic period of .5 to 2 minutes with a much longer period superimposed upon this (period not identified) and was not observed on frequencies which were 8 to 10 MHz above the 3000 KM MUF. This noise, during the on-air testing performed, restricted the MDS to values above -140 dBm.

4)   A signal related noise was observed with a relative time delay centered at 150 KM, which, in conjunction with a large ground wave signal, could cause problems within the receiver. However, no evidence of this noise causing

A3

2.1   --Continued.

problems at operational ranges was found during the
limited testing done.

5)   A further source of noise which could set a lower limit
        in achievable MDS is the spurious responses generated
        in the transmitter due to blower motors, etc. The e
        spurious are not at integer values of 50 Hz and thus
        tend to cause a peaking of the noise between PRF lines,
        which, since the fax recorder responds to peak values,
        results in a corresponding increase in displayed noise.
        However, the measured level of this spurious is such
        that they are not considered to be the cause of the high
        MDS values reported.

6)   Local noise may become a problem in the near future,
        as new construction would indicate the city is expanding
        in the direction of the site. Since local noise is generated
        in the near vicinity of the receive antenna, the noise
        signal is propagated as a "Surface Wave". The effect of
        ground is to reduce the received signal strength below
        free space propagation loss. This reduction becomes
        negligible and independent of polarization as the height
        of the two antennas approaches one wave length above
        the ground. The present antenna system is 2 to 4 wave-
        lengths above ground and will be more susceptible to
        this threat than a low profile antenna.

2.2   Synchronization Problem.

1)   The severity of the problem was not found to be as great
        as pre-trip briefings had indicated. These estimates
        were that the time code generator was typically up to
        several seconds in error with respect to world time
        standards.

Presently, each operating shift checks the Time Code Generator against a world standard time signal. The maximum deviation, personally observed, was 40 milli-seconds (one PRF period at 25 Hz operation).

2) There is a hardware problem which at present does require a small slewing of the Time Code Generator to compensate. Unfortunately, the action of the advance/ retard controls on the Time Code Generator is somewhat misleading and operators under pressure to complete QSYs quickly, occasionally slew the clock the wrong way, thereby compounding the sync problem. Standardized operating procedures and modifying the advance/ retard controls should do much to alleviate the problem.

2.3 General Areas.

1) No connector problems were encountered during this trip. Site personnel indicated that only three (3) connectors had exhibited the described symptoms. It was recommended that cold solder joints should be considered as a possible problem before extensive connector relocation or replacement be undertaken.

2) No observations of the general maintenance procedures were made, as the testing done during this trip disrupted any normal maintenance schedules. However, considering the fact that receiver oscillations below 15 MHz were found, this would indicate the system has not bee periodically checked.

The receiver IF instability found would indicate additional checks, besides off-air MDS readings, are required to

2.3   --Continued.

verify the more subtle system parameters (e. g. , IMD product levels).

3)   No observations of the general operating procedures were made, as the testing done during this trip disturbed the normal operating schedules. The one operational and maintenance procedure observed (and tested) was reliance on the Lorch receiver to:

a)   check clear channels,

b)   detect interference on the operational frequency, and

c)   in conjunction with the Saicor analyzer and a fax recorder test the antenna for IMD and cross-modulation.

Unfortunately, due to the Lorch receiver performance degradation, this procedure resulted in:

a)   many unnecessary and time consuming QSYs, and

b)   extensive antenna maintenance which may or may not have been necessary.

3.0   RECOMMENDATIONS.

3.1   High MDS.

1)   Reduce the large ground wave signal level present, with all the attendant problems by decoupling the sites to a much greater extent than they are presently. This greater decoupling could be achieved by either moving one site or through antenna design.

2) To reduce the OTH noise, the receiver site must be capable of discriminating against unwanted signals. This can only be accomplished through the reduction of the antenna sidelobe structure to an acceptable level, provided the noise source is not located in the target area. Assuming the noise is entering the system through the sidelobe structure of the array, the side-lobes will require a 20 dB minimum reduction from the present levels.

3) Further identification and characterization in terms of amplitude, spectrum and frequency of occurrence of the signal-related noise should be performed.

4) The spurious lines in the transmitters should be reduced, at least to the levels found during the original acceptance tests on the equipment. Additional on-air spectrums should be made at various frequencies to verify the results obtained at the single frequency tested.

3.2 Synchronization Problem.

1) Determine the source of the hardware problem. The investigation into this problem has already commenced.

2) Institute the different synchronization procedures to reduce the effects of the hardware problem until it is found. Such procedures were started by the unit, but some diligence will be required until these become routine.

3) To alleviate some operator confusion, make a minor modification to the Time Code Generator to standardize the function of the ADVANCE/RETARD controls.

3.2   --Continued.

In the Demodulator controller the switch has the common
use that ADVANCE, for example, does indeed advance
the Local Oscillator timing in range.

In the Time Code Generator, unfortunately, ADVANCE
means to retard the Time Code Generator. (This is
standard TCG Logic. The theory being that the World
Time Standard Pulse, as seen on an oscilloscope
synchronized to the TCG 1PPS output, is ADVANCED
by retarding the TCG, hence, the inverse logic.) Even
though it is explainable, it does cause operator confusion.

3.3   General Areas.

1)   Inspect the three (3) connectors for loose or cold solder
        joint connections. This will require removing the in-
        sulation from the connection and the wire from the
        connector, to install new insulation. This would be a
        minor operation to determine if the changing or relocating
        of the connectors is actually required.

2)   After the receiver IF is realigned, the tests made during
        this trip should be redone and curves (see system test)
        generated. These curves could then become a base line
        reference to which periodic tests could be compared.
        In this manner gain, noise figure, and IMD performance
        degradation could easily be identified.

3)   Greater reliance on the MDS readings and RME fax
        display, in conjunction with the interference monitor,
        should be used, not the Lorch receiver, before starting
        a QSY. In addition, the Lorch receiver should be repaired
        or replaced before being used for any further antenna
        testing.

A8

3.3   --Continued.

4)   The Rockland Synthesizer should be returned for repair
      as it is understood that Rockland has admitted to a
      design flaw. The site has developed a reasonable sub-
      stitute for the calibrator by using the Display Parameter
      in the system software. By adjusting the DP level to
      obtain a uniform shade of grey, a close correlation to
      MDS can be made. This technique can be used until the
      synthesizer is returned.

5)   Some provision should be made to cool the preamplifier
      during the summer. The temperature was high during
      the tests, which apparently degraded the preamplifier
      performance. If the performance were to deteriorate
      even further during hotter days, this could present a
      problem with intermodulation and cross-modulation
      products.

6)   The rf switch and directional coupler on the calibrator
      chassis should be relocated. The new location should
      be in the vicinity of the receiver input. This would have
      the additional advantage that the rf input cable is not
      routed through an extra cabinet.

7)   The patch panel connections for the various systems
      should be tested for cross-coupling on critical cables.

4.0   SYSTEM TESTS.

While the cause of the high MDS was the primary concern, the
equipment was fully tested to determine if the cause could be equipment
induced. The results of these tests show the equipment to be in good to
excellent condition (with some exceptions, which did not affect this inves-
tigation). Only under very high signal levels would the system be limited

4. 0   --Continued.

by the hardware.   The groundwave which was found to be quite high during
the present investigation (-50 to -60 dBm) was not limiting.   However,
levels reported in the past, up to -30 dBm, would degrade system per-
formance.

The general system parameters found are as follows:

1)   Two-tone dynamic range 104 dB (1 Hz).

2)   Receiver noise figure (including multicoupler) 14 to 16 dB.

3)   IMD products (in-band to IF) 69 to 84 dB below maximum
        useable output.

        (Note: This is an area where the system was not
        operating normally due to IF amplifier instability. Talks
        with the receiver designer indicate this may be an
        amplifier termination problem due to the recent field
        installation of the new IF Bandpass filters. The
        designer will be on site to install the new receiver and
        will correct this problem. The IMD products should
        then be greater than 80 dB below the maximum useable
        output.)

4)   Power Gain (with new video amplifier) 67 dB (at zero
        dB IF attenuation) which represents a 6 dB loss from
        the gain measured during acceptance testing .

5)   Cable loss and coupling consistent with type and length
        indicating no deterioration.

6)   The preamplifier was found to have:

        a)   Noise figure -- apparently near specification (5 dB)

        b)   Gain of 10 dB (11 dB specification)

        c)   Third order intercept +28 dBm (specification is
                +50 dBm). This deterioration probably can be

A10

4.0 --Continued.

attributed to heating of the unit. The amplifier was found to be sensitive to heat during the original installation tests. and an attempt to heat sink the unit was made at that time.

7) Receiver antenna array -- in excellent electrical condition, no indication of noise or IMD generation at levels up to 0 dBm input.

8) Transmitter purity

a) Wideband noise base greater than 100 dB down (and falling) beyond ±200 Hz.

b) Spurious output high, causing the noise between PRF lines to have a "peaking" characteristic which appears darker on the system Fax recorder.

c) Narrow-band noise (±12.5 Hz) 80 to 85 dB down (would limit the system clutter to noise ratio (at 25 Hz PRF) to this range in area of strong ground backscatter).

9) Transmitter antenna array -- appears to be in excellent electrical condition, as on-air spectrum is duplicate of transmitter spectrum.

4.1 System Calibrator.

The receiver checks had to be delayed until the system calibrator was corrected. It was found the calibrator output was dependent upon whether the chassis was in or out of the rack. Either condition is equally likely as the switch for on-air/off-air operation is located inside the chassis as opposed to on the front panel. Two sources of this feed through were found.

4.1   --Continued.

The first and most variable was traced to the r-f switch (which selects either the on-air signal or a 50 ohm load for off-air). The +28 VDC power line was not bypassed and picked-up sufficient calibrator signal to feed through the switch at the -145 to -150 dBm level, dependent upon chassis location. This problem was temporarily corrected by placing a capacitor between the +28 VDC input to the switch and the switch ground.

The second source was cable coupling between the r-f input to the receiver and the calibrator output from the local oscillator. The output of the local oscillator is at -10 dBm while the input to the receiver is expected to reach -157 to -160 dBm. These cables were laced tightly together for a distance of 6 to 8 feet. The coupling was down 145 dB resulting in a -155 dBm feed through level. The solution to this was to cut the lacings and re-route the r-f line to a safer location.

A more permanent solution to these problems would be to re-locate the r-f switch and directional coupler to a location nearer the receiver input. This would have the added advantage of eliminating the routing of the input r-f lead in and out of an extra cabinet where stray signals can be picked up. This is desirable since the r-f input is the input to the system and should be maintained as clean as possible. In addition, the calibrator signal, in the vicinity of the receiver input, would be at low levels consistent with the r-f level.

4.2   Receiver Checks.

The receiver checks were made using the test set-up shown in Figure 1.
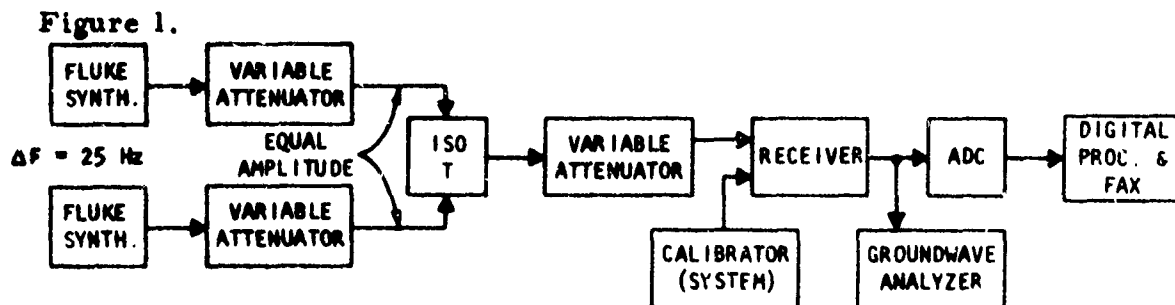

Figure 1.   Block Diagram of Test Set-Up Used to Make Receiver Checks.

4.2   --Continued.

The test procedure, after eliminating feed-through around the input attenuators, is to increase the signal input level in successive steps. At each step, the wave analyzer was used to measure the signal level, of each tone, the noise output, and the IMD product level. In addition, the system calibrator was used and site personnel made an MDS check on the fax.

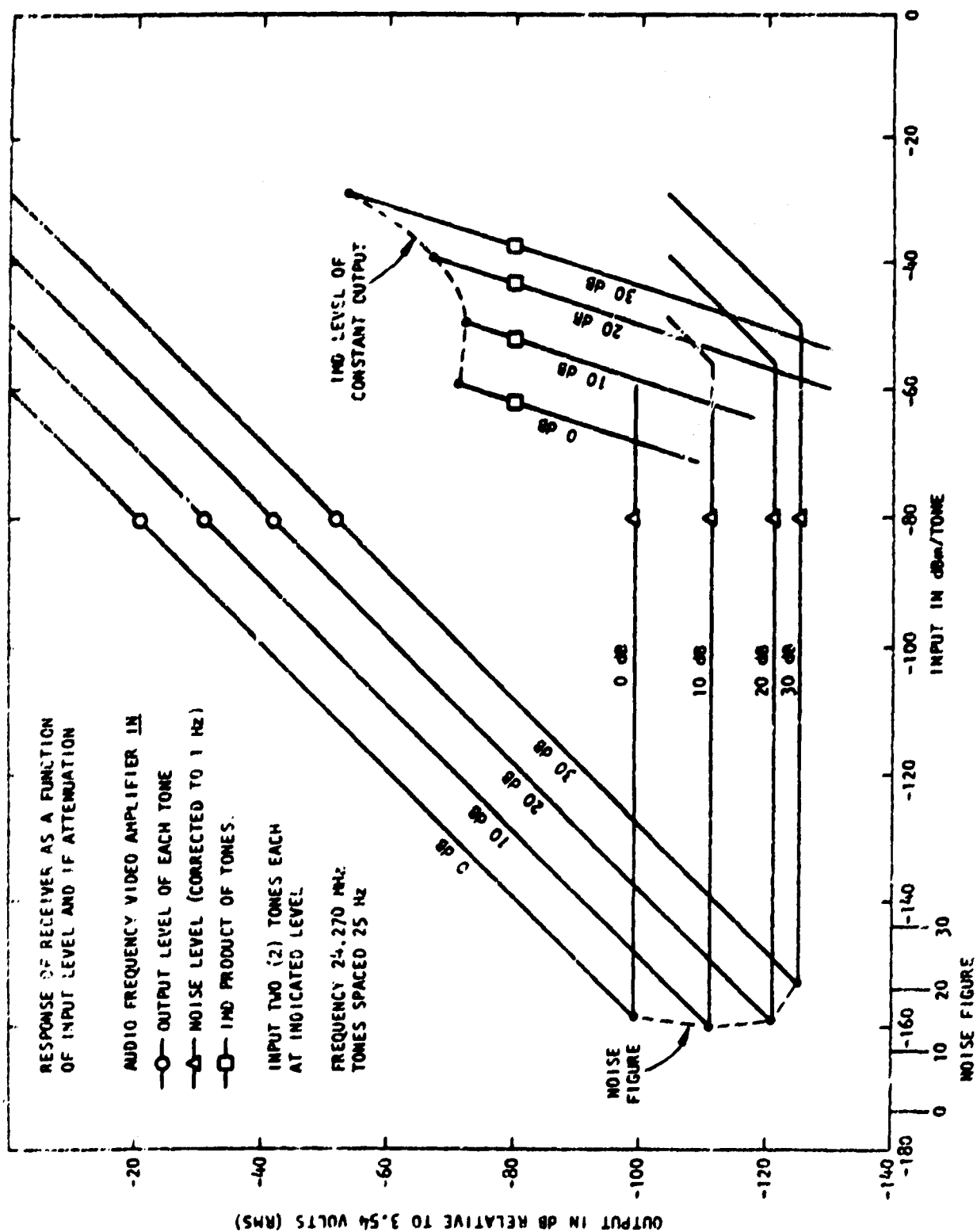The results of these tests are shown in the following figures:

Figure (2) -- is the composite performance of the receiver at 24.270 MHz without the new audio amplifier.

Figure (3) -- is the composite performance of the receiver at 24.270 MHz with the new audio amplifier.

Figure (4) -- is the summary of the data shown in figures (2) and (3) including the MDS data taken from the fax in CW and FM/CW mode. For the IMD products, two curves are shown:

a)   the IMD ratio (signal output level to IMD product level) at maximum output level (ADC saturation level), and

b)   the IMD ratio at the maximum dynamic range level, the level at which no further signal-to-noise ratio improvement is achieved. Limit established in the first mixer by L.O. noise.

From the results of these tests, it was recommended the audio amplifier be left in permanently and the IF attenuation be left at 10 dB, and use the R-F attenuator to prevent receiver overloading at an output of ±4.0 Vpp (this leaves an overload margin of 8 dB for peak values while retaining the full system capability). This choice was the best compromise between IMD products, sensitivity (MDS) and the analog to digital converter dynamic range. This recommendation was accepted and implemented.

Figure 2. Composite Performance of the Receiver at 24.270 MHz Without the New Amplifier

A14

Figure 3. Composite Performance of the Receiver at 24.270 MHz With the New Amplifier.
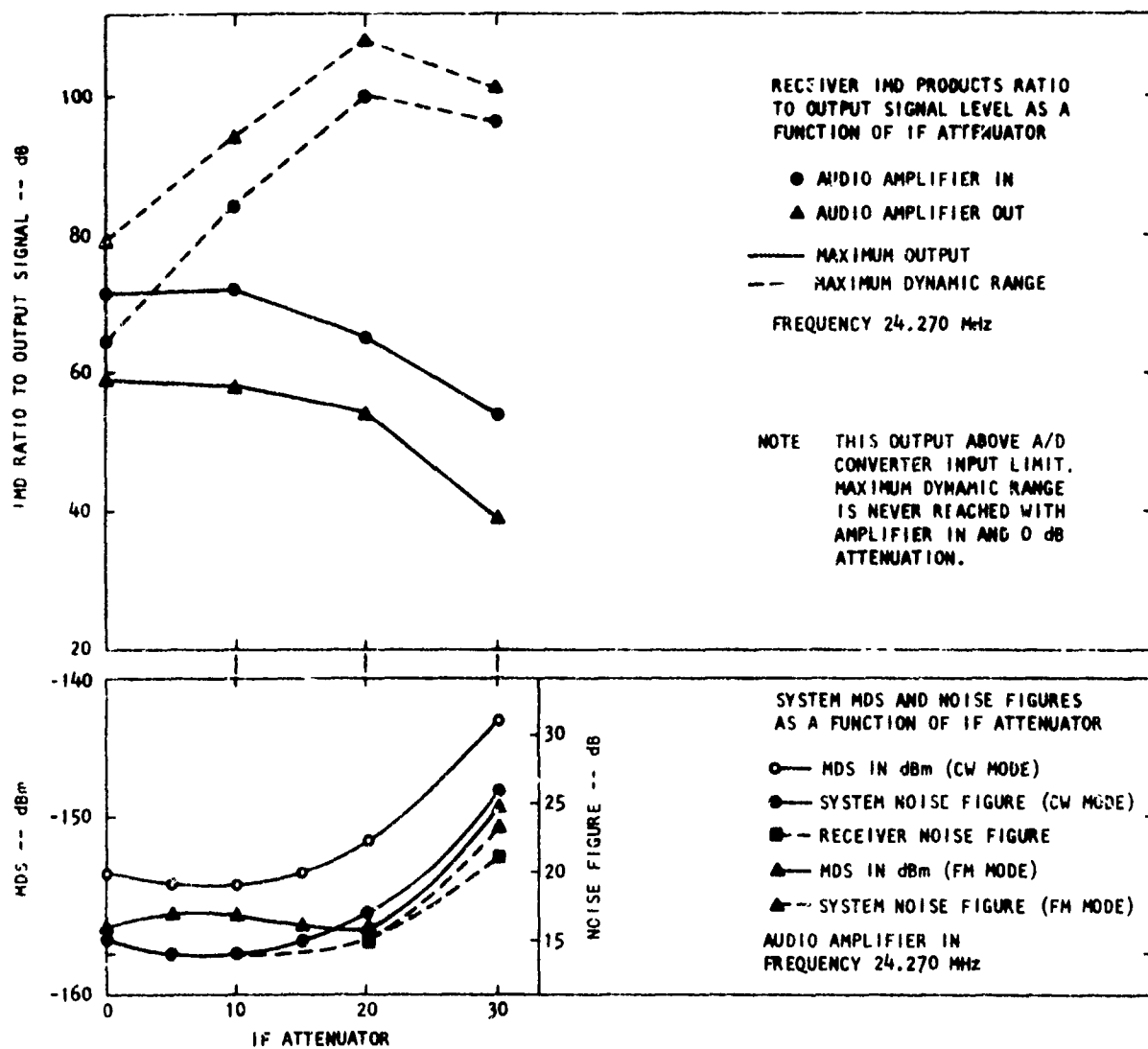
A15

Figure 4.   Summary of Data Shown in Figures 2 and 3.

Examination of Figures (2), (3), and (4) shows the IMD products for the IF attenuation of 0, 10, 20 dB are still generated by the IF amplifier. No evidence of the output amplifier or the new audio amplifier producing IMD products was found. The IMD products found using 30 dB of IF attenuation are mostly the composite of IF and RF and further increases would switch completely to the RF section generating the products.

The receiver was tested against 20.270 MHz and the results shown in Figure (5) and summarized in Figure (6). These results show the system to operate in a much worse condition than 24.270 MHz. Particularly in respect to the IMD products. In fact, at maximum dynamic range output with 10 dB of IF attenuation, the IMD ratio is 15 dB worse.

In light of these results, the recommendation for receiver operation is still valid, as this performance was found to be the result of IF amplifier instability. This instability is the tendency of the IF amplifier to oscillate, depending upon the r-f frequency to which the receiver is tuned. Since this is an abnormal condition, it is recommended this condition be corrected instead of tolerated. This recommendation is further strengthened, since the receiver IF was found to oscillate at any and all frequencies below 15 MHz. Hence, no tests were made in this band of operation. The oscillation is a typical spurious type oscillation:

a)   no fixed frequency or amplitude,

b)   dependent upon where external loading (a hand for example) is placed, or

c)   dependent upon component position.

The apparent cause of this instability (or at least the units without which oscillation ceases) are the new IF bandpass filters. The subject was not pursued any further since, major maintenance was not the intent of this trip, except where required to test the system. In addition, the receiver design engineer is expected within a few weeks and this seemed an appropriate problem for him to tackle.
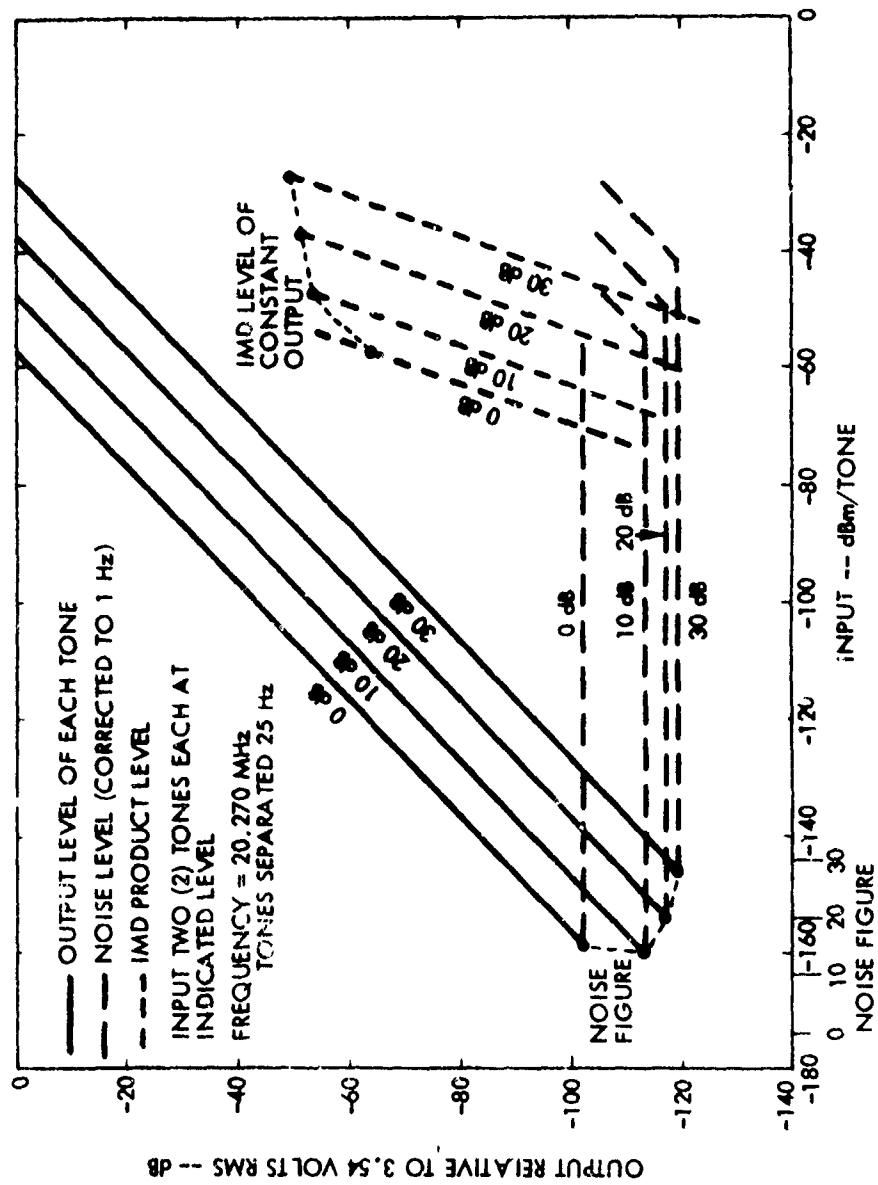
Figure 5. Response of Receiver as a Function of Input Level and IF Attenuation.

RECEIVER IMD PRODUCTS RATIO
TO OUTPUT SIGNAL LEVEL AS A
FUNCTION OF IF ATTENUATOR

AUDIO AMPLIFIER IN

●———MAXIMUM OUTPUT

●---MAXIMUM DYNAMIC RANGE

FREQUENCY 20.270

RECEIVER NOISE FIGURE AS A
FUNCTION OF IF ATTENUATOR.
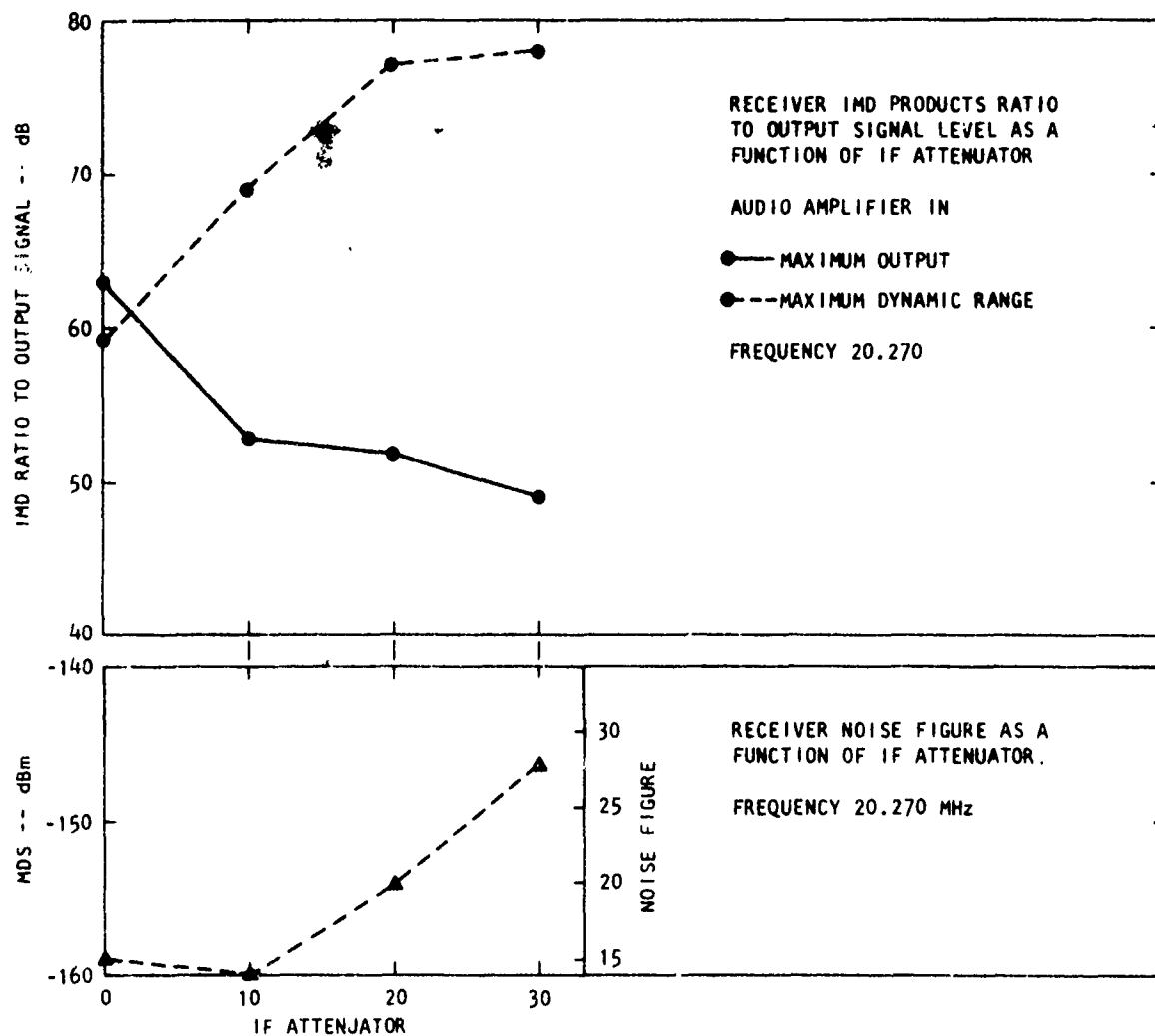
FREQUENCY 20.270 MHz

Figure 6.   Summary of Receiver Tests Against 20.270 MHz.

A19

4.2.1 Summary.

The receiver was found to have excellent characteristics and to be in general good repair. (With the one exception that oscillations, highly visible on the fax, were present below 15 MHz operation.) That the site personnel were unaware of this condition is most likely explained by the fact that with no nighttime operation, no frequencies below 15 MHz were used.

As seen in Figure (3), the receiver noise figure remains good at 20 dB IF attenuation; the system noise figure increases slightly. This rise is caused by the combination noise figure of the digital processor and the reduction of receiver gain. The noise figure of the digital processors are approximately: (a) 61 dB for the CW processor, and (b) 56 dB for the FM/CW processor. Once the receiver was checked, then it was used as test equipment to verify the performance of the remaining equipment.

4.3 Multicouplers.

The performance of the multicouplers was tested using the test configuration shown in Figure (7).
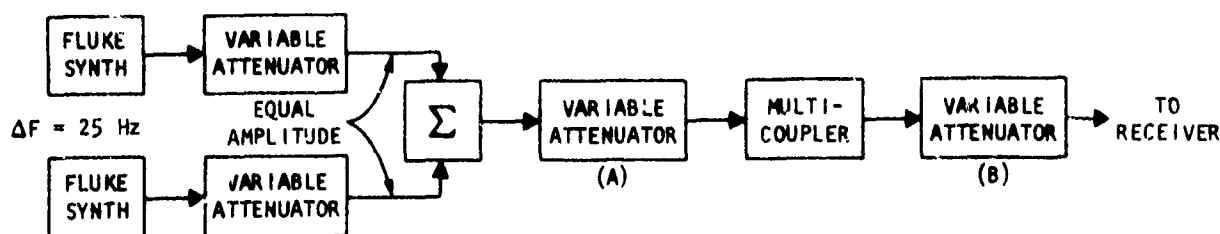
(a) TEST CONFIGURATION FOR IMD, NOISE FIGURE AND GAIN TEST AT 24,270 MHz
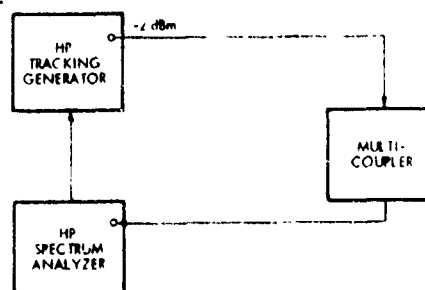
(b) TEST CONFIGURATION FOR GAIN AS A FUNCTION OF FREQUENCY

Figure 7. Block Diagram of Multicoupler Tests.

4.3   --Continued.

In each case, Figure (7a) and (7b), the test configuration was tested using a short connection in place of the multicoupler (a barrel adaptor). Then a multicoupler was inserted and tested.

The procedure in testing for noise figure and IMD products was:

1)   Set the output of the iso-T (Σ) to -5 dBm;

2)   Put 80 dB attenuation in attenuator (A);

3)   Put 0 dB attenuation in attenuator (B); and

4)   Using the wave analyzer, determine the signal output level, noise level and IMD products, if any. At this point, the noise level and signal level are compared to determine the change, if any, of the noise figure of the combination;

5)   Remove 10 dB attenuation from attenuator (A);

6)   Put 10 dB attenuation in attenuator (B), which keeps the input to the receiver a constant while increasing the input to the multicouplers;

7)   Using the wave analyzer, observe the change in gain and IMD products.

The above procedure was continued until -5 dBm input to the multicoupler was reached. No change in gain or IMD products, from -80 dBm to -5 dBm, were observed.

The procedure used in the tests to obtain the gain as a function of frequency was to replace the multicoupler (Figure 7b) with a barrel adaptor and photograph the output of the H. P. Spectrum Analyzer over the frequency range of 0 to 50 MHz. This photograph is then the calibration of the test cables used. A multicoupler is then inserted and another photograph taken. The difference between these photographs is the gain as a function of frequency of the multicouplers. The results of these tests are summarized in Table I.

A21

TABLE   I

MULTICOUPLER   PERFORMANCE

FREQ.	INPUT -2 Dbm TEST CABLE LOSS (Db)	INPUT Dbm	HIGH-BAND OUTPUT Dbm	GAIN Db	LOW-BAND OUTPUT Dbm	GAIN Db
5	0.4	-2.4	-1.1	1.3	-1.1	1.3
10	0.8	-2.8	-1.5	1.3	-1.5	1.3
15	1.2	-3.2	-1.8	1.4	-1.8	1.4
20	1.5	-3.5	-1.9	1.6	-1.9	1.6
25	1.7	-3.7	-2.1	1.6	-2.2	1.5
30	1.9	-3.9	-2.3	1.6	-2.6	1.3
MEAN				1.5		1.4

No noticable effect on system noise figure, therefore,
specification NF of 8 Db, with measured gains is
reasonable.   No discernable IMD products at -5 Dbm input.

4.3   --Continued.

During the tests using Figure (7a), indications of coupling between multicouplers were observed. Therefore, Figure (7b) was modified to use the Tracking Generator to drive the low-band multicoupler and the output of the high-band multicoupler was observed on the spectrum analyzer (all unused inputs or outputs were terminated). The coupling was found to be greater than 75 to 80 dB and deemed to be no problem.

4.4   Patch Panel.

Since the original tests had shown a definite coupling, the problem was found in the patch panel. The output of each multicoupler (High-Band and Low-Band) for use with the system were contained within the same panel block (vertically). The coupling here was approximately 40 dB and definitely presented problems. This was corrected, immediately, by moving the high-band output to another patch panel port where the isolation was tested to be greater than 80 dB.

Since any further checks would have been outside the frame of reference for these tests, no further pursuit of patch panel coupling was made. However, it was recommended a similar check of patch panels be made for the other systems in use.

Before the tests using the H. P. Spectrum Analyzer were made, it was determined the analyzer was out-of-calibration and adjustment. This condition was known by site personnel and a calibration chart was in the process of being made. Instead, the unit was calibrated and adjusted and a short training demonstration was given for site personnel.

4.5   Cable Loss and Amplifier Performance.

The cable loss from the beamforming buildings and the main building were then measured using the configuration shown in Figure (8).

A23

4.5   --Continued.
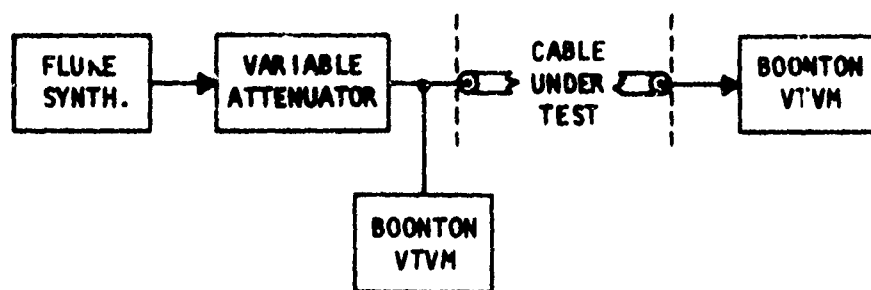
(a) ONLY CABLE LOSSES
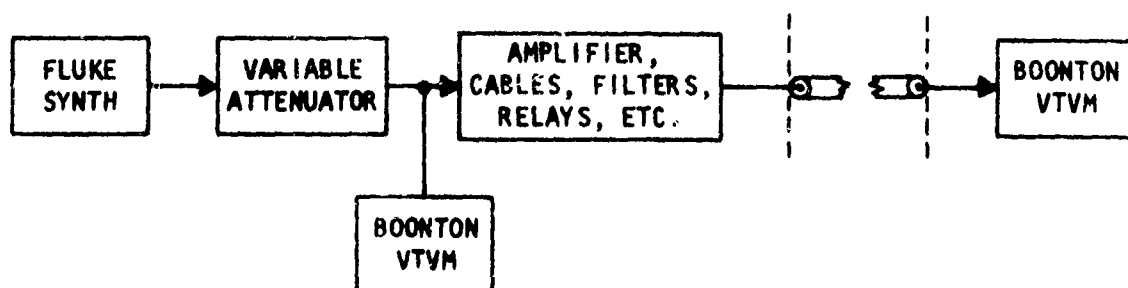
(b)   ALL LOSSES OR GAINS

Figure 8.   Test Configuration to Measure the Gains or Losses
from Beamforming Building to Main Building.

The procedure was to use the Boonton VTVM in the beamformer
building to maintain a constant input (0 dBm for the cable, -10 dBm for
the amplifier) to the circuit under test as the frequency was changed. The
Boonton in the main building was used to record the output. The two Boon-
tons were then calibrated using a common   source to obtain the correction
factor for the readings. It should be noted for any future tests, the Boonton
VTVM's read differently for the same input signal depending on whether 50

4.5   --Continued.

or 60 Hz power is used. Therefore, the correction factor should be ob-
tained for the appropriate line frequency used during the test.

The cable losses measured as a function of frequency are shown
in Figure (9). The summary of cable losses, amplifier gain and overall
gain/loss from the beamformer output to the multicoupler input are tabu-
lated in Table II.

The amplifier noise figure and IMD products were checked using
the configuration used for the multicoupler (Figure 7a) except for moving
the set-up to the beamforming building and using the cable back to the
receiver.

The noise figure for the system was measured at 13 dB (24,270
MHz). The input of the system being taken as the output of the final 4-way
combiner in the beamformer.

This noise figure, when combined with the measured gain through
to the receiver and the receiver noise figure, shows the amplifier noise
figure could be as low as 3 dB but probably not above 8 dB. The published
noise figure is 5 dB.

The published third order intercept point is +50 dBm; the measured
intercept was found to be +28 dBm. This represents a 22 dB decrease. In
any event, the +28 dBm intercept will have IMD products below the system
generated products until the signal level is sufficient, that the amplifier
can be safely switched out. This presents little or no problem unless strong
out-of-band signals are present (the High Pass Filters, in use, exclude the
broadcast bands, which are equal to or stronger than our own. At least one
signal was monitored which was certainly equal to the desired one.

While the equipment was configured for these tests, the cross-
coupling between the high-band and low-band cables (which are adjacent for
hundreds of feet) was checked. This consisted of driving the high-band cable
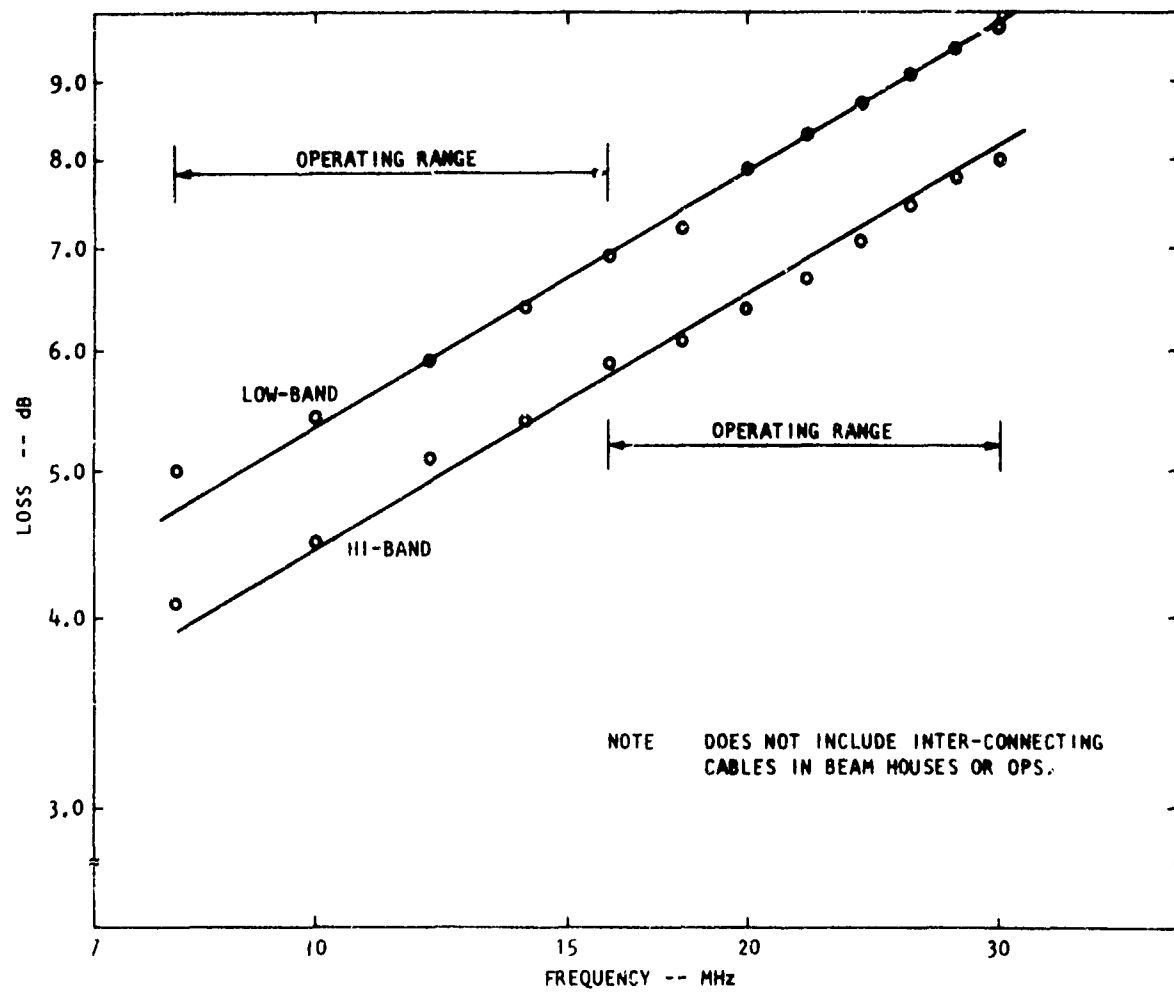with 0 dBm signals and using the receiver to measure the level of received

Figure 9.   Cable Loss as a Function of Frequency.

TABLE 11. PREAMPLIFIER GAIN.

FREQUENCY	LOW-BAND			HIGH-BAND		
	MEASURED GAIN	CABLE LOSS	AMPLIFIER GAIN	MEASURED GAIN (dB)	CABLE LOSS (dB)	AMPLIFIER GAIN (dB)
8	4.9	5.0	9.9		BELOW CUT-OFF OF HIGH	
10	4.7	5.4	10.1		PASS	
12	4.0	5.9	9.9		FILTER	
14	3.5	6.4	9.9	4.4	5.4	9.8
16	3.0	6.9	9.9	4.3	5.9	10.2
18	2.6	7.2	9.8	3.8	6.1	9.9
20	2.1	7.9	10.0	3.4	6.4	9.8
22	1.7	8.3	10.0	3.1	6.7	9.8
24	1.2	8.7	9.9	2.7	7.1	9.8
26	0.8	9.1	9.9	2.4	7.5	9.9
28	0.3	9.5	9.8	2.1	7.8	9.9
30	-0.1	9.8	9.7	1.8	8.0	9.8
MEAN		9.9				9.9

3RD ORDER INTERCEPT +28 dBm

NOISE FIGURE   5 dB (SPECIFICATION)

USING THE AMPLIFIER, THE SYSTEM NOISE FIGURE WOULD BE

$$NF_s = 10 \text{ LOG} \left\{ \text{ANTI-LOG } (5) + \frac{\text{ANTI-LOG } (1.5)-1}{\text{ANTI-LOG } (.27)} \right\}$$

- 12.9 dB (13 dB MEASURED VALUE)

A27

4. 5   --Continued.

signals from the low-band cable.   During this test, all unused input and
outputs and were terminated by 50 ohm loads.   The result of this test was
the coupling between cables in excess of 88 dB at 24. 270 MHz.   Since this
can be considered a traveling wave coupling (i. e. , non-resonant system),
the coupling will decrease for lower frequencies and raise only slightly at
30 MHz.

The correction factors for the MDS are taken on the receiver fax
to translate this to an MDS at the beamformer output were calculated and
shown in Figure (10).   The mean value of the dB values (the geometric mean)
of the correction factors are shown which if used for all frequencies will
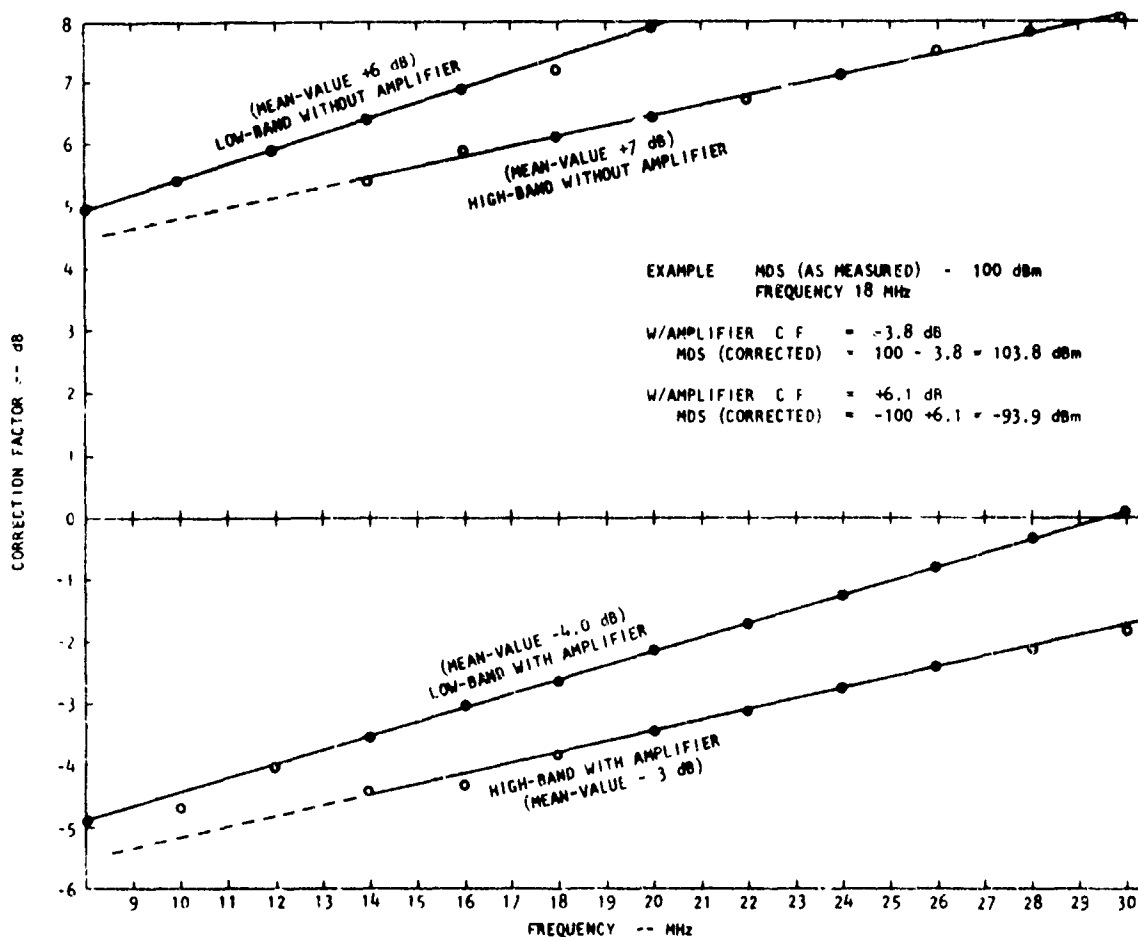provide MDS values within ±1 dB across the band.

Figure 10.   Correction Factor to MDS, as Measured at the Receiver,
for the High-Band and Low-Band Arrays With and Without
Pre-amplifier in Beam Huts as a Function of Frequency.

A28

4.6   Antenna Elements.

There was a great deal of concern that the antenna array elements were causing IMD products in the system. These were quite evident from the data taken and by listening to the received signal (CW) with earphones, it being generally conceded that the transmitted carrier does not contain music, as the received signal quite often did.

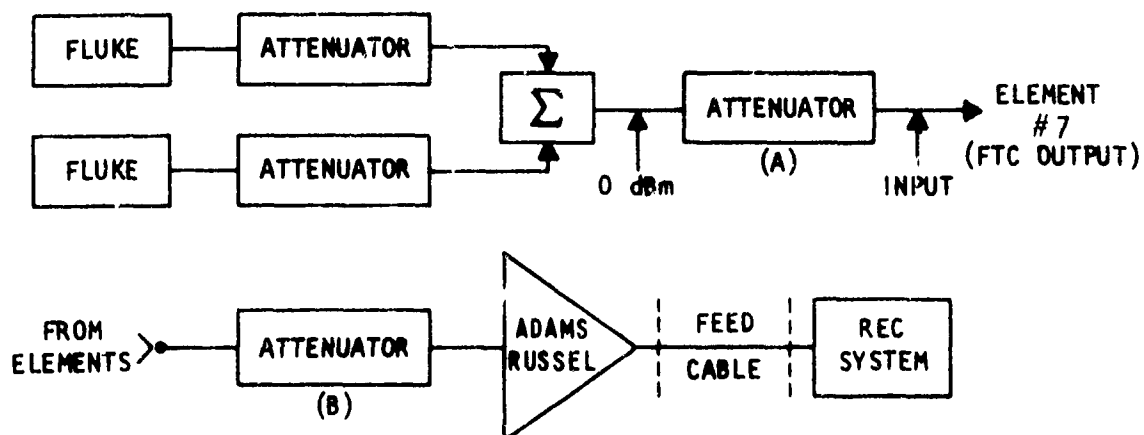To test the elements for IMD products, the configuration shown in Figure (11) was used.

Figure 11.   Block Diagram of the Test Configuration
for Antenna Element IMD Product Generation.

A29

4. 6   --Continued.

The procedure was to set attenuator (B) for zero dB attenuation then adjust attenuator (A) until a signal near -80 dBm was seen at the system input (input to Adams-Russell amplifier as measured by the receiver). The noise level and signal levels were recorded (input and output). The input was to the reverse field balun of element 7 (buck-off element) and the output was the normal output of the element under test.

The procedure was then to remove all attenuation from attenuator (A) and put the equivalent into attenuator (B). Thus, the input to the test equipment (receiving system) was kept a constant, while the input was raised to 0 dBm, resulting in readings shown in Table III.

The loss in dB also represents the output in dBm when the input was raised to 0 dBm. With the possible exception of two elements, these levels represent larger signals than normally received.

In all cases, no evidence of IMD product generation was found, of any kind.

Since IMD from on-air signals had been observed and heard by site personnel and myself, an additional test was performed to determine if such IMD was caused by the transmitters. For this test an independent CW transmission was monitored simultaneously by CW system and on the RME system. The side-by-side fax recordings taken during the test are shown in Figures (12) and (13).

From these there is little doubt the trouble did not lie in the antenna array. The IMD products and cross-modulation products were traced directly to the Lorch receiver being used for the CW. Based upon past records, the receiver has been in this condition for an undetermined but substantial period of time.

During the test an attenuator was inserted between the receiver and the antenna and the attenuation increased until the cross-modulation products could not be heard in the earphones, only the normal sounds usually associated

A30

TABLE 111. ELEMENT PERFORMANCE.

ELEMENT	BUCK-OFF ELEMENT INPUT (dBm)	ELEMENT OUTPUT (dBm)	LOSS (dB)	LOSS (W.R T.#7)
1	-45	-82	-37	-22
2	-40	-86	-46	-31
3	-50	-83	-33	-18
4	-40	-84	-44	-29
5	-60	-83	-23	- 8
6	-55	-90	-35	-20
7	-75	-90	-15	0
8	-60	-83	-23	- 8

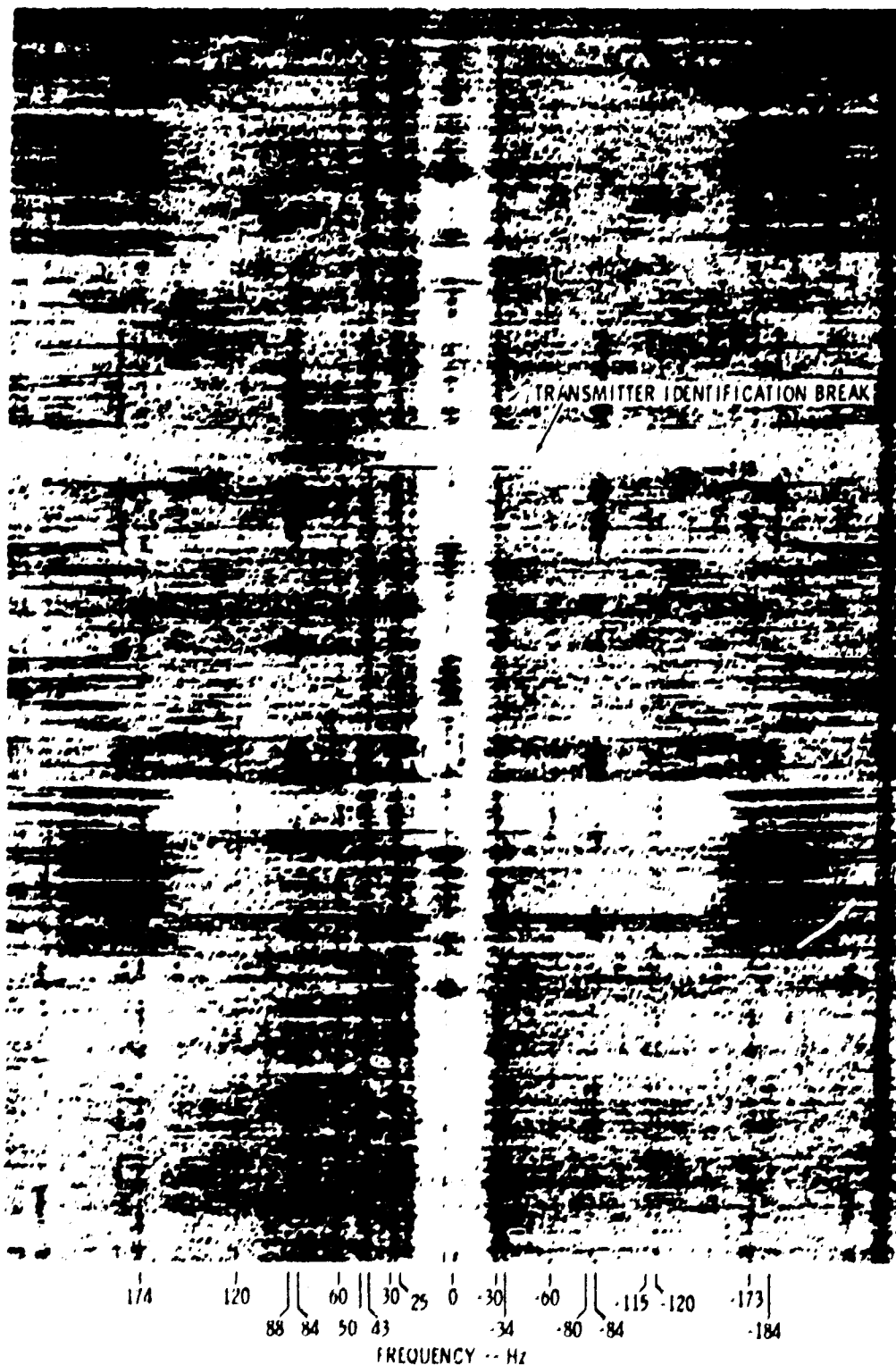TRANSMITTER IDENTIFICATION BREAK

FREQUENCY -- Hz

Figure 12. Fax Recording Made from an On-Air CW Signal Using the Old CW System in Parallel with the RME System. The Test was to Observe IMD and Cross-Modulation Products.
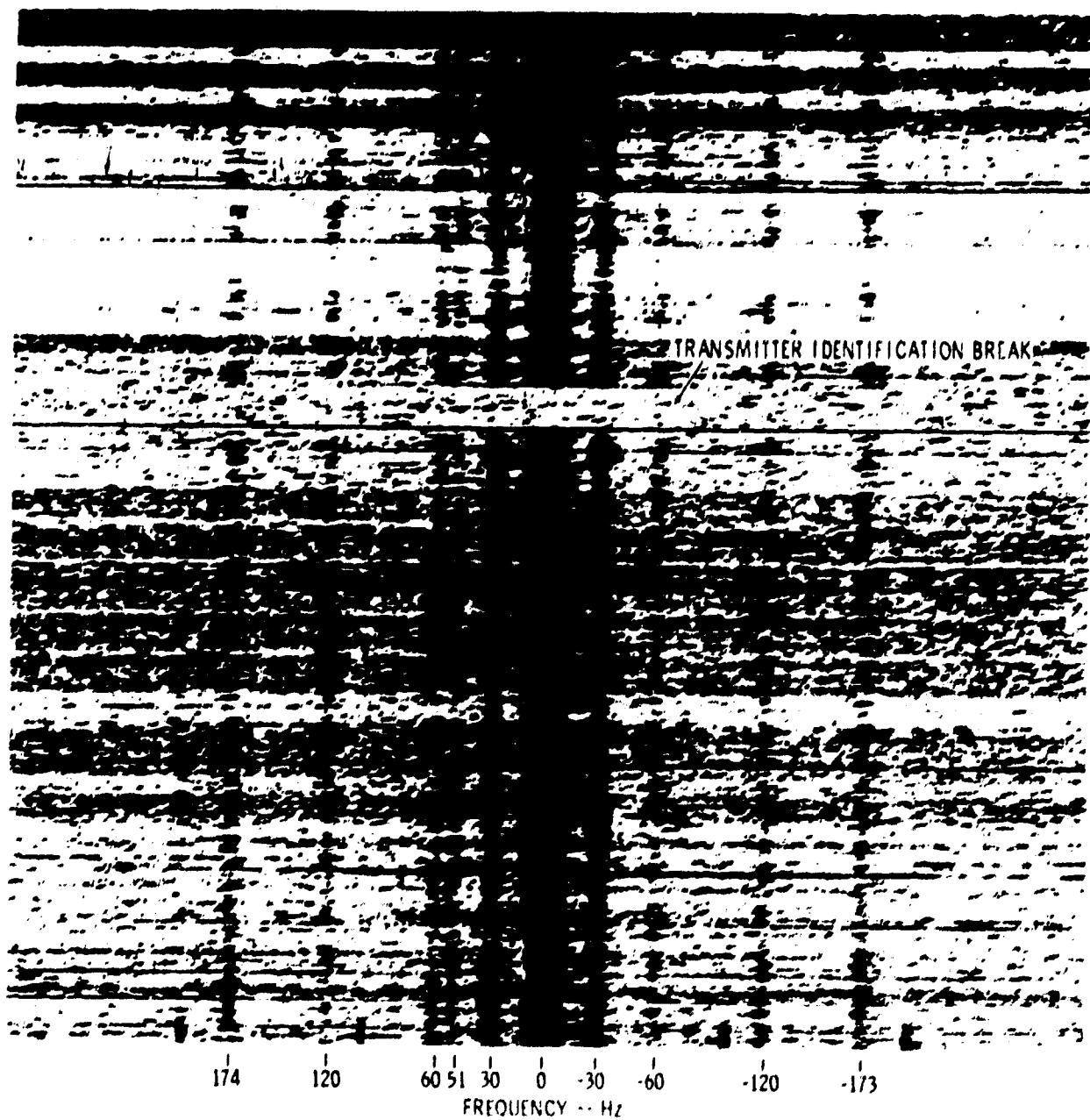
A32

Figure 13. Fax Recording Made from an On-Air CW Signal Using the RME System in Parallel with the Old CW System. The Test was to Observe IMD and Cross-Modulation Products.

4.6 --Continued.

with atmospheric noise. However, at this level there was apparently insufficient signal from the Lorch as no recording on the fax recorder could be made.

This is an unfortunate case of personnel believing an "old reliable friend" and blaming the antenna. Since this again was outside of the original frame of reference, no further tests were made to determine just how bad the receiver really is at this point in time.

Although it was not a part of this investigation, it does provide an interesting example of what can happen when operators "forget" about the large signals which notch filters (or time delay and bandpass filters) remove from the displays, but which nevertheless can cause problems in the front end of the receiver.

In summation, the antennas appear to be in excellent electrical condition due to extensive maintenance performed recently. The physical condition of some hardware (that which was still available) would indicate there is certainly a corrosion problem. Unfortunately, there is no evidence, in light of the receiver problem, which was the basic measuring instrument, as to whether or not these parts were indeed causing any electrical problems. (No comment on the structural soundness of the array is implied or intended.)

Undoubtedly, there are hardware components which have caused trouble in the past and will again in the future. Therefore, the antenna maintenance programs must be continued but it is hoped a jaundiced eye is maintained on the test set-up and equipment in the future.

4.7 Transmitter Site.

Prior to the visit to the transmitter site, it had been reported that the noise floor of the transmitter was 80 to 85 dB down. Since the noise on the received signal had been measured at approximately the same level, it had been concluded that at high levels of received ground wave (i.e., in

4.7   --Continued.

excess of -70 dBm) the transmitted noise floor rather than ambient noise would limit system sensitivity. This conclusion was shaken during the visit when measurements taken at the point where the transmitter feeder leaves the building revealed that although the noise floor at ±30 to 40 Hz was 80 to 85 dB, and it dropped to below 100 dB at ±200 Hz. Indeed from addition to spurious lines (slower motors, etc.) and a degradation of approximately 10 dB, the transmitter faithfully reproduces the exciter spectrum. The personnel, however, maintained that after radiation from the system antennas the noise floor was uniform at -80 to -85 dB.

To check for antenna induced noise, the transmitters were brought up after dark (a condition not normally encountered recently) and the arrays visibly inspected for arcs and/or corona effects. The results of these tests were negative, no visible arcs or corona were observed. In view of this, it was difficult to believe the antennas could themselves introduce noise, yet certainly not inconceivable since the levels measured represent only milliwatts of power. In interest of thoroughness, on-air wave analyzer records to complete the tests were made.

A wave analyzer run made on the newly installed horizontal dipole (for receiving time standard transmissions indeed showed noise approximately 85 dB down. The wind was blowing and concern about receive antenna motion was expressed. Sqn. Ldr. C. I. Johnson went to the roof and "wiggled" the antenna. The noise floor rose approximately 30 dB. Therefore, the results concerning transmitted noise level were inconclusive. The same results for noise level were found using the vertical sounder antenna. Again, however, using an antenna designed to look straight up, seemed hardly conclusive. Finally, tests were made using the new oblique sounder antenna, not available to previous investigators.

This antenna is a horizontal, large conductor antenna looking directly toward the transmitter array. Wave analyzer records made from this antenna show the transmitted spectrum from the array to be an exact replica of the one taken directly from the transmitter.

A35

4.7   --Continued.

While a receive antenna may degrade the transmitted spectrum, no receive antenna will improve the transmitted spectrum. Therefore, the transmitted spectrum is indeed clean down to 100 dB (beyond ±200 Hz) and falling.

It should be noticed, however, that these tests were done at one frequency only. Therefore, now that a means of recording the transmitted spectrum is available, it is recommended this be done at many other frequencies.

4.8   On-Air Tests.

Unfortunately, during all the on-air tests, the calibrator was not available to make MDS reading from the fax recorder. The Rockland Synthesizer was unserviceable at the time. During the equipment tests, however, some experience was gained in correlating Wave Analyzer records with MDS readings. Therefore, an estimate of these can be made.

For many of the on-air tests, there was a 2 to 6 dB difference in the displayed noise level on the fax between transmitters on and off. Simultaneous measurements taken with the wave analyzer revealed that there was no change in the basic noise floor received, whether the transmitter was on or off; however, some spurious responses were observed between PRF lines with the transmitter on (blower motor, spurs, etc.). It is believed that these spurious responses are the cause of the reduction in displayed MDS since the effect is only noticeable when the spurious signals and noise are interacting or the spurious is above the noise. However, this reduction in displayed MDS although readily apparent on the fax is not, in itself, of sufficient value to account for the high MDS problem.

Many on-air CW wave analyzer records were taken, and have been taken in the past. These records invariably showed a noise increase above the transmitter level which varied in magnitude run to run. This noise level had been attributed to the on-air transmitted signal, in fact, a Feed Through

A36

4.8   --Continued.

Canceller (FTC) was obtained to reduce the effect of this transmitted signal, particularly in the region of the carrier. However, on-air tests at the transmitter site showed the transmitted spectrum to be clean down to -85 dB (±25 Hz) and -100 dB and greater beyond ±200 Hz. In an effort to separate the ground wave signal (GW) received from the transmitter, the system was operated in the FM/CW mode and centered on the GW. In all cases the transmitted spectrum was reproduced by the receiver down to ambient noise. Therefore, another source for this noise must be found.

The apparent OTH noise level is approximately 10 to 20 dB higher, with a much greater standard deviation, than the ambient noise. During the course of a wave analyzer run (10 minutes) this OTH noise dropped from 20 dB above at the beginning back to ambient level at the end. To determine if this was a reproducible frequency (or range related) effect, a repeat run was made, but this time the noise remained at ambient. This type of run-down noise 10 to 20 dB above ambient with a high standard deviation was seen in the records a number of times.

Another noise source was observed only once during the tests on 1 August. The noise ambient was quite variable in CW mode varying from -150 dBm to areas of -136 dBm, while noise around the carrier was varying from -95 to -106 dBm (extending from 10 to 30 Hz). This close in noise represented only -30 to -40 dB down from the carrier.

In the FM mode, the ambient noise was -150 dBm in the maximum delay region and in the region between +50 to +250 Hz, then the noise rose sharply to -115 dBm, 10 Hz before the 112.5 km range line during one wave analyzer run. During this run, the system was operating at 100 Hz PRF and 37.5 km resolution. Thus, the 112.5 km range line was 300 Hz from the GW.

The sharp increase in noise was also observed on the fax recorder. In order to prevent this return from being a double period (a return from

A37

1612.5 km), the parameters were changed to 50 Hz PRF and 37.5 km range resolution. The noise stayed in place with respect to range, not frequency, moving to in frequency of 150 Hz away from the GW. The ambient noise levels are the same as previously found. The high noise, now -120 dBm, was observed between 10 Hz before the 112.5 km range line and 10 Hz beyond the 187.5 km range line. During this time, the disturbance as seen on the fax recorder appeared to be diminishing.

A wave analyzer run at the 1500 km range showed the ambient noise to average -145 dBm (2000 Hz from the GW) with a ±5 dB variation.

During the time this disturbance was seen on the FM/CW system, the normal one milli-second pulse ranging was being observed. This disturbance appeared as a shoulder (no real separation) on the GW pulse. Remarks were made at this time that this had been seen before, but had been taken as a time constant problem associated with the GW pulse. Site personnel then checked with photographs of the pulse ranging to see if it had been recorded before. The results were affirmative that it appears "often", however no estimate of frequency.

For those interested, 1 August was listed as a "Bad E-layer Day" and the ranges observed were consistent with the E-layer height above the sites.

From the recorded GW levels and in view of the GW level from the back-looking element, the GW coupling between sites is excessively high. The only protection the system has against this signal is the front-to-back ratio of the array. Since it has an end-fire spacing, the front-to-back ratio is going to vary as a function of frequency.

If a strong GW and a signal such as seen on 1 August were to reach high signal levels, the receiver would cross-modulate this noise to other signals contained in the r-f bandwidth. This would happen regardless, if the signals are band passed filtered later to remove this large signals so they

A38

4. 8   --Continued.

do not appear on the display. Since they do not appear on the display, the
receiver would be operated at maximum sensitivity (many instances have
been observed where 10 dB (or more) of r-f attenuation was required to
prevent the GW (CW or FM/CW) from saturating the Analog to Digital Con-
verter). When the range gate was moved out, the received signal being
displayed (fax and time domain scope) dropped to back scatter values and
the receiver was then brought back to maximum sensitivity. Granted a
signal only 10 dB above maximum sensitivity would not produce high MDS
values, since the major IMD products are produced in the IF amplifier and
the IF band pass filters exclude the high level signals.

4. 9   Synchronization Problem.

The following are hardware symptoms observed which produce a
synchronization loss. The only controls which are designed to have an effect
on the system synchronization are:

1)   the ADVANCE/RETARD CONTROL of the Time Code
        Generator (TCG), and

2)   the SYNC ENABLE of the Demodulator Controller.

The one pulse-per-second (1 PPS) from the TCG was observed for
relatively long periods of time (at the receiver site) against the World Time
Standard. The drift of the TCG is negligible compared to the synchronization
loss times.

The SYNC ENABLE was tested, in excess of 100 trials and never
failed to return the system reset pulse to the same location. This location
was one of five time slots centered on the trailing edge of the 1 PPS pulse.
The time slots were -20, -10, 0, +10, and +20 microseconds. The actual
time slot the SYNC ENABLE always returned to appeared to be random and
was selected by the initial SYNC ENABLE performed after a MODE ENABLE
was performed.

4.9   --Continued.

The MODE ENABLE control while not designed to have any effect on system synchronization (except alternating mode) did indeed exhibit this characteristics.

The MODE ENABLE had the effect to blank the system reset pulse for at least one PRF period, at least 70 to 80 percent of the operations. If the reset pulse was blanked, there was an 80 to 90 percent probability the pulse would be out of synchronization with the TCG. This results in a 50 to 70 percent probability the system will be out of synchronization after a mode change.

The standard procedure was to press the SYNC ENABLE, then the MODE ENABLE (even if there was no mode change required) which would account for many of the synchronization failures. The new procedures are:

1)   If there is a mode change required, depress the MODE ENABLE and wait 10 seconds, then

2)   Depress the SYNC ENABLE, and

3)   If no mode change is required, depress ONLY the SYNC ENABLE.

These procedures should help to reduce the effect of the hardware problem, when no mode change is involved, until it is located.

MISSION
of
Rome Air Development Center

RADC is the principal AFSC organization charged with planning and executing the USAF exploratory and advanced development programs for electromagnetic intelligence techniques, reliability and compatibility techniques for electronic systems, electromagnetic transmission and reception, ground based surveillance, ground communications, information displays and information processing. This Center provides technical or management assistance in support of studies, analyses, development planning activities, acquisition, test, evaluation, modification, and operation of aerospace systems and related equipment.

Source AFSCR 23-50, 11 May 70

A 41